Investigating New Lattice Approaches to the Momentum and Spin Structure of the Nucleon

DISSERTATION

zur Erlangung des akademischen Grades

doctor rerum naturalium
(Dr. rer. nat.)

im Fach Physik
Spezialisierung: Theoretische Physik

eingereicht an der
Mathematisch-Naturwissenschaflichen Fakultät
der Humboldt-Universität zu Berlin

von
Herrn M.Sc. Christian Wiese

Präsident der Humboldt-Universität zu Berlin
Prof. Dr. Jan-Hendrik Olbertz

Dekan der Mathematisch-Naturwissenschaftlichen Fakultät
Prof. Dr. Elmar Kulke

Gutachter/innen: 1. Prof. Dr. Ulrich Wolff
2. Dr. habil. Karl Jansen
3. PD Dr. Markus Diehl

Tag der mündlichen Prüfung: 13. Mai 2016

In memory of my father Friedrich (1958-2014)

Abstract

This thesis deals with the theoretical computation of nucleon structure observables as they can be experimentally obtained from inclusive and semi-inclusive scattering experiments. I present two exploratory studies on spin and momentum structure observables of the nucleon in the framework of lattice QCD. Throughout this work, I use the twisted mass formalism with dynamical fermions at maximal twist, which ensures an improved continuum limit scaling for the relevant quantities.

In the first part, I investigate the feasibility of a lattice calculation of the gluons' average momentum fraction in the nucleon $\langle x \rangle_g$, a quantity that is rarely studied in lattice QCD. For this purpose, I study two different methods, namely the Feynman-Hellman theorem, which enables an indirect computation of $\langle x \rangle_g$ by variation of the action, and the direct computation of the relevant form factor. Applying the latter method and combining it with several steps of stout gauge link smearing, I obtain a statistically significant signal, yielding $\langle x \rangle_g = 0.309(25)$ for a pion mass of $m_{\mathrm{PS}} \approx 370\,\mathrm{MeV}$ and $\langle x \rangle_g = 0.28(4)$ for a physical value of the pion mass. In order to obtain these renormalized values, the results of a perturbative computation are applied.

The second study is concerned with the direct computation of the full momentum and spin distribution of quarks and antiquarks within the nucleon. I investigate the feasibility of a recently published approach proposing the computation of a purely spatial quasi-distribution that can be related to the physical distribution. I test the influence of gauge link smearing and different nucleon momentum boosts on the lattice data. Ultimately, I obtain quark distributions featuring a good qualitative agreement to quark distributions acquired from phenomenological fits and can reproduce crucial features, for example the asymmetry between quark and antiquark distributions. Finally, I present the resulting iso-vector quark distributions for the unpolarized and the polarized case.

As a key result of this work, I demonstrate that the demanding calculation of $\langle x \rangle_g$ and the novel approach of computing quark distributions directly within lattice QCD are feasible in principle, although significantly more effort has to be invested into obtaining accurate results with reliable uncertainties, in particular concerning systematic effects.

Zusammenfassung

Diese Arbeit beschäftigt sich mit der Berechnung von für die Struktur des Nukleons relevanten Observablen, die experimentell durch inklusive und semi-inklusive Streuexperimente bestimmt werden können. Es werden zwei Pilotstudien erörtert, welche die Spin- und Impulsstruktur des Nukleons mithilfe von Gitter-QCD untersuchen. Hierfür werden dynamische Fermionen mit einem chiral rotierten Massenterm verwendet (Twisted-Mass-Formalismus), um sicherzustellen, dass die untersuchten Größen einen verbesserten Kontinuumslimes aufweisen.

Der erste Teil dieser Arbeit untersucht die Umsetzbarkeit einer Rechnung, die sich mit dem durchschnittlichen Impulsanteil der Gluonen im Nukleon $\langle x \rangle_g$ auseinandersetzt. Diese Größe wurde bisher kaum im Rahmen der Gitter-QCD behandelt. In diesem Zusammenhang werden zwei verschiedene Gittermethoden untersucht: das Feynman-Hellman-Theorem, das über die Variation eines Parameters der Wirkung indirekt eine Berechnung von $\langle x \rangle_g$ zulässt, sowie die direkte Berechnung der relevanten Formfaktoren. Mithilfe der zweiten Methode und mehreren Iterationen des Schmierens der Eichlinks ist es möglich, ein statistisch aussagekräftiges Resultat zu erzielen: $\langle x \rangle_g = 0.309(25)$ für eine Pionmasse von $m_{\mathrm{PS}} \approx 370\,\mathrm{MeV}$ und $\langle x \rangle_g = 0.28(4)$ für eine physikalische Pionmasse. Um diese Werte zu erhalten, wurde eine perturbative Renormierung vorgenommen.

Die zweite Studie beschäftigt sich mit der direkten Berechnung der vollständigen Impuls- und Spinverteilung von Quarks und Antiquarks im Nukleon. Hierfür wird untersucht, ob eine kürzlich publizierte Methode praktikabel ist, nach der eine räumliche Quasiverteilung zu berechnen und aus dieser die physikalische Verteilung abzuleiten ist. In diesem Zusammenhang wird der Einfluß des Schmierens der Eichlinks und unterschiedlicher Impulsboosts des Nukleons auf die Gitterdaten erprobt. Die anschließend berechneten Quarkverteilungen weisen eine gute qualitative Übereinstimmung mit Verteilungen auf, die mithilfe von phänomenologischen Analysen experimenteller Daten bestimmt wurden und können wichtige phänomenologische Eigenschaften wie die Quark-Antiquark-Asymmetrie reproduzieren. Hierbei werden die Isovektor-Quarkverteilungen sowohl für den unpolarisierten als auch für den polarisierten Fall erörtert.

Zentrale Erkenntnis dieser Arbeit ist der Nachweis, dass es auf dem Gitter prinzipiell möglich ist, die anspruchsvolle Berechnung von $\langle x \rangle_g$ auf einem quantitativ signifikanten Niveau durchzuführen und die Quarkverteilung mithilfe einer neuen Vorgehensweise direkt zu berechnen. Nichtsdestotrotz muss noch erheblich mehr Arbeit aufgewendet werden, um verlässliche Resultate für diese Größen zu erhalten, insbesondere in Hinblick auf systematische Unsicherheiten.

Contents

1. Introduction

Ever since the discovery of the proton and the neutron as the essential building blocks of the atomic nucleus, both their properties and structure have been one of the most important research topics of particle physics. In order to make observations on such a small scale, scattering experiments were conducted, which turned out to be a crucial tool to explore the nature of nucleons. Soon, these experiments suggested the existence of an inner structure. Yet, the components and characteristics of such a structure remained unknown. In fact, while early experiments focused on properties like the radius and the charge distribution of the proton, *cf.* [1] for example, only later on, with increasing scattering energies, a possible internal structure of the nucleon started to draw attention.

The vast amount of hadronic states that were produced in these high-energy scattering experiments were puzzling and indicated that more fundamental building blocks might exist. In 1964, it was Gell-Mann who first proposed quarks as the fundamental constituents of the nucleon and other hadrons [2] in order to arrange and classify the large amount of newly discovered mesons and baryons[1].

Triggered by these theoretical developments, further experiments were designed in the hope to unravel this inner structure. As a matter of fact, the first experimental evidence for fundamental particles inside the proton was found in high-energy scattering experiments at the Stanford linear accelerator (SLAC) in 1969 [4, 5]. The observed structure functions that are used to parametrize the scattering cross-section, were basically flat over a large range of Q^2, in contrast to the proton elastic form factors, which show a strong Q^2 dependence in the same energy range. Q^2 is proportional to the momentum of the injected particles. Early measurements of this feature are shown in Fig. 1.1.

This scaling behavior was first predicted by Bjorken [7] and explained in detail by Feynman's formulation of the parton model [8], which assumes that the proton is composed of point-like objects called partons. While it was clear that Gell-Mann's quarks could be identified as partons, it was soon discovered that quarks alone do not generate the complete proton momentum. This was determined by the measurement of the quark momentum fraction from scattering data. The momentum fraction did

[1] In the same year, Zweig independently proposed aces as fundamental buildings blocks [3].

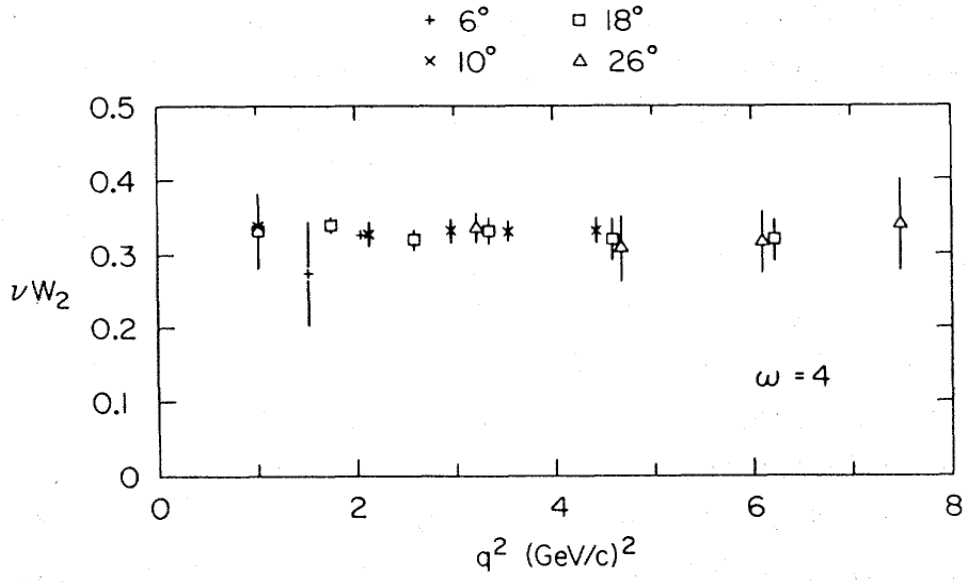

Figure 1.1: Results for νW_2, which can be related to the proton's structure function, as a function of $q^2 = -Q^2$ for several scattering angles. ω is the inverse of the Bjorken variable x and will be defined in Section 2.2. Figure is taken from Ref. [6].

not add up to one, as the momentum sum rule for partons predicts, *cf.* Eq. (2.21).

This inconsistency could finally be explained by the formulation of quantum chromodynamics (QCD), a non-abelian SU(3) gauge theory that introduces gluons as exchange particles between quarks, inducing the corresponding strong force. Many works contributed to this discovery, for instance Refs. [9, 10, 11, 12, 13]. In 2004, the Nobel Prize in Physics was awarded to Gross, Politzer and Wilczek for their work on this topic.

The presence of interacting quarks, however, is a fundamental extension to Feynman's parton model, since the model is only valid for non-interacting constituents and thus does not include gluons. Nevertheless, the predictions of the parton model were quite accurate. This could be explained by the discovery of asymptotic freedom [12], which predicts quasi-free behavior of quarks for large energies and, correspondingly, small distances. Yet, free quarks are a sufficient approximation only for certain energy ranges, thus a QCD improved parton model is certainly necessary to explain the hadron structure for arbitrary scales. In principle, this can be done by applying the operator product expansion (OPE) to the corresponding hadronic currents [14], which enables a perturbative QCD analysis of the parton model.

In practice, a universal quantity that can be used to characterize the internal structure of hadrons was found to be helpful. In his work on the parton model, Feynman already introduced parton distribution functions (PDFs). These are universal functions providing the momentum distribution for all partons in the parent

hadron for different energy scales. Only much later, these PDFs were generalized to functions that contain many more quantities, such as the spin distribution and transverse momentum distributions, among others. These functions, which today are most commonly known as generalized parton distributions (GPDs), were first studied in detail in Ref. [15]. A comprehensive review on this topic can be found in Ref. [16].

Consequently, it would be highly desirable to obtain these distributions or respectively their moments directly from the equations of QCD. However, an analytic determination is not possible due to the nature of QCD as a strong interacting theory. Thus, the most common method to extract parton distributions is the phenomenological analysis of experimental scattering data. Latest analyses are presented in Refs. [17, 18, 19, 20], for instance. Nevertheless, these results strongly depend on the included scattering data and on the employed analysis, therefore an independent extraction from first principles would be ideal.

An alternative fundamental approach to compute quantities from QCD is through lattice gauge theories, which were introduced by Wilson in 1974 [21]. This approach consists of the discretization of QCD on a four-dimensional space-time lattice and the numerical calculation of the necessary Feynman integrals by Monte-Carlo methods. Lattice QCD is, in contrast to perturbation theory, able to make predictions in a large energy range from low to high energy regimes. Thus, it can be utilized for the computation of matrix elements of local operators, which are necessary for hadron structure studies. In fact, lattice QCD has successfully been applied to compute several hadronic form factors, including the moments of parton distributions. An extensive review of these calculations can be found in Ref. [22], while most recent results are presented in Ref. [23], for example.

Nevertheless, other hadron structure observables are rather hard to access on the lattice and have therefore rarely been studied up to now. In this thesis, I will study two particular quantities, namely the gluons' average momentum fraction $\langle x \rangle_g$ and the full iso-vector quark distribution, each for the nucleon. Both are fundamental quantities and obtaining an *ab initio* estimate from lattice QCD could provide valuable information on the interaction of quarks and gluons. The gluon momentum fraction furthermore contributes to the computation of the gluon spin and thus could be utilized to study the nucleon spin puzzle [24]. However, the gluon momentum fraction suffers from a poor noise-to-signal ratio and has so far only been computed with a quenched setup, where no dynamical fermions are present [25, 26, 27]. Recent improvements of lattice algorithms though enabled the generation of large gauge ensembles with dynamical fermions, including ensembles with a physical pion mass. Consequently, this thesis will focus on further studying $\langle x \rangle_g$ in the named setup.

A determination of the quark distributions from lattice QCD could be directly confronted with experimental scattering data and thus provide a crucial test of QCD without the involvement of a phenomenological step. However, the direct computa-

tion of PDFs is generally not possible in the framework of lattice QCD, since the evaluation of the corresponding matrix elements requires light-cone dynamics, which cannot be implemented on a Euclidean lattice. A possible solution was pointed out recently in Ref. [28], where the author suggests the computation of a purely spatial quasi-distribution, which can be related to the physical PDF by a perturbative matching procedure in the large momentum limit. This proposal has already been tested in Ref. [29] and will be further explored in this thesis.

Before discussing the actual research that has been done to study the gluon momentum fraction and the quark distribution, I will give a brief summary on the theory of hadron structure in Chapter 2. In this context, it is important to point out the significance of deep inelastic scattering results on exploring the structure of the nucleon. I will introduce the PDFs through the parton model, discuss their relation to the structure functions and outline how they can be obtained.

In Chapter 3, I will give a brief overview of lattice QCD, twisted mass fermions and the question of how observables can be computed when using the lattice discretization. In particular, it will be explained how hadron structure observables can be extracted from lattice QCD calculation. Finally, I will give a short review on present results for three important nucleon structure observables g_A, $\langle x \rangle_{u-d}$ and $\langle x \rangle_{\Delta u - \Delta d}$.

The lattice study of the first moment of the gluon distribution will be presented in Chapter 4. I will outline and compare two different methods that can be used for the calculation. The influence of gauge link smearing on the noise-to-signal ratio will be studied and results for the gluon momentum fraction from two different gauge ensembles will be presented. For this purpose, the necessary renormalization factors were computed recently in lattice perturbation theory to one-loop order and will be utilized in this work.

In the last part of this thesis, Chapter 5, I will study the possibility of computing the full quark distribution of the nucleon from lattice QCD. I will present the necessary matrix elements for three different lattice momenta in order to study the large momentum behavior. I will apply multiple steps of gauge link smearing to the operator and try to estimate the influence of renormalization by comparing the resulting matrix elements. I will discuss and apply necessary corrections to the resulting quasi-distribution in order to restore the physical quark distribution. Finally, I will present and discuss results for the iso-vector quark distribution and also show first results for the polarized distribution.

2. The basic principles of hadron structure

This chapter is intended as a preface to my actual work on hadron structure in the framework of lattice QCD. I will give a very brief history of deep inelastic scattering experiments, explain the parton model of the nucleon and sketch the theory behind parton distribution functions. I would like to stress the importance of these distributions as well as their moments, among others in modern collider experiments and point out important relations that can later be used in lattice QCD computations in order to extract those quantities.

Refs. [30, 31] were used as guidelines for this chapter.

2.1 Introduction to deep inelastic scattering

Scattering experiments have always been an important tool to explore the structure of the nucleon. First conclusions about an internal structure of the proton were made from high energy proton-hadron collisions with more than 10 GeV, *e.g.* in Ref. [32]. They were found to produce a large number of pions, however little transverse momentum transfer was observed. It was thus assumed that the proton was not fundamental, but consisted of many loosely bound constituents.

In order to test this assumption, proton-electron scattering experiments with large center of mass energy were performed at the SLAC linear collider in the late 1960s [4, 5]. These collisions were excellent tests of hadron structure due to the fact that on a basic level they can be described as the electromagnetic scattering of an electron with the proton, or its constituents respectively, which is well understood in the framework of quantum electrodynamics (QED).

Surprisingly, the cross section of hard-scattered electrons at a large deflection angle was large, which was inconsistent with the expected results from a complex composite nucleon with softly bound constituents. Instead, the observed cross section was comparable to elastic scattering at a point-like charged particle, *e.g.* electron-muon scattering. However, the proton is certainly not a point-like object and rarely a single proton emerged from these scatterings.

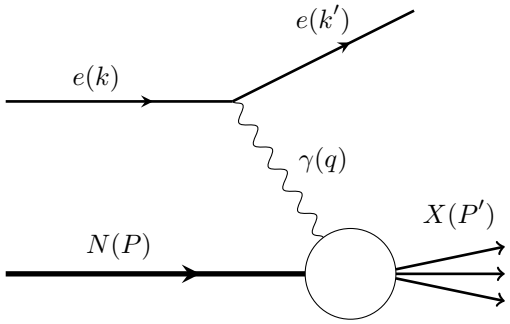

Figure 2.1: Schematic diagram of nucleon-electron scattering.

Moreover, for a large momentum transfer ($1 < Q^2 < 10\,\mathrm{GeV}^2$) and fixed $x \propto Q^2$ (*cf.* Eq. (2.5)), the proton's structure functions showed little to no influence on Q^2, which is in contradiction to elastic scattering form factors of the proton. This behavior in the deep inelastic scattering region is known as Bjorken scaling and was predicted by Bjorken in 1969 [7]. Feynman extended this work, which led to his formulation of the parton model [8]. This model states that the proton is a compound of point-like constituents. These partons are fundamental particles able to exchange large momenta q^2 with each other through strong interactions and are partly capable of electromagnetic interactions, *e.g.* with an electron.

In the next few sections, I will briefly sketch the important theoretical aspects of these scattering experiments, the implications of the parton model and its limitations, namely scaling violation.

2.2 Nucleon-electron scattering

Before studying the scattering process in detail, the relevant parameters of this two-body scattering should be established. The nucleon-electron scattering is described by the initial and final states

$$e(k) + N(P) \to e(k') + X(P')\,, \tag{2.1}$$

as sketched in Fig. 2.1, with the electron state e, the nucleon N and the final hadronic state X. Here, the content of X determines the nature of the scattering process. If the intact nucleon is found in the final state, *i.e.* $X = N$, the scattering is elastic. If the nucleon is shattered during the scattering and thus X denotes various hadronic states, the process is inelastic.

A virtual vector boson γ acts as the exchange particle and has the four-momentum

$$q = k - k'. \tag{2.2}$$

In addition, when studying these scattering processes it is helpful to introduce the following Lorenz invariant quantities,

$$s = (P + k)^2, \tag{2.3}$$

$$Q^2 = -q^2, \tag{2.4}$$

$$x = \frac{Q^2}{2Pq}. \tag{2.5}$$

The latter is called Bjorken x and is a crucial quantity in the following sections.

In case of elastic nucleon-electron scattering, it can be derived that $x = 1$ with the premise that the nucleon mass is conserved throughout the process,

$$P^2 = (P')^2 = (P + q)^2 = P^2 + 2Pq + q^2 \tag{2.6}$$

$$\Rightarrow 0 = 2Pq + q^2 \Rightarrow \frac{Q^2}{2Pq} = 1\,. \tag{2.7}$$

However, the elastic scattering region is not the point of interest if one wants to explore the structure of the nucleon. Instead, the experiments were designed to probe the inelastic region where the nucleon is not intact after the scattering process. Consequently, no nucleons were tagged in the final state of these experiments.

Thus, in order to make predictions for the expected cross section, one has to study the theory behind inelastic nucleon-electron scattering.

2.3 The structure functions of inelastic scattering

Therefore, it is important to understand the internal structure of the scattering process. For this purpose, one can express the cross section in terms of the leptonic and hadronic tensor,

$$d\sigma \propto L^e_{\mu\nu} W^{\mu\nu}\,. \tag{2.8}$$

These tensors can be related to the two vertices at which the photon interacts with the electron and the hadron.

The structure of the leptonic tensor $L^e_{\mu\nu}$ is well-known, because the electromagnetic current is known from QED and the interaction can be described as point-like. The structure of the hadronic tensor $W^{\mu\nu}$ is not that simple, because it is a composite object with no well-defined vertex. However, it can be decomposed into six independent Lorenz invariant tensor objects

$$\begin{aligned} W^{\mu\nu} = &- g^{\mu\nu} W_1 + p^\mu p^\nu \frac{W_2}{m^2} - i\epsilon^{\mu\nu\sigma\rho} p_\sigma p_\rho \frac{W_3}{2m^2} + q^\mu q^\nu \frac{W_4}{m^2} \\ &+ (p^\mu q^\nu + q^\mu p^\nu) \frac{W_5}{m^2} + i(p^\mu q^\nu - q^\mu p^\nu) \frac{W_6}{2m^2}\,. \end{aligned} \tag{2.9}$$

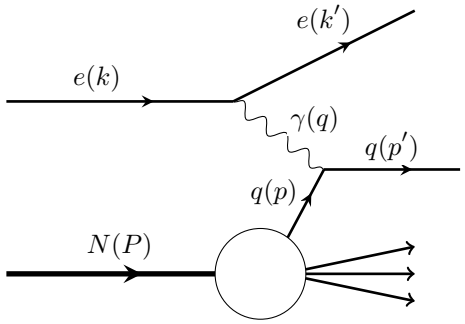

Figure 2.2: Schematic diagram of the scattering of an electron with a parton from the nucleon.

The coefficients of these terms are the real scalar functions W_1 - W_6, which are called structure functions. When taking into account current conservation of the electron-nucleon scattering and requiring a symmetric tensor, one can simplify the hadronic tensor to

$$W^{\mu\nu} = W_1(\frac{q^\mu q^\nu}{q^2} - g^{\mu\nu}) + \frac{W_2}{m^2}(p^\mu - \frac{pq}{q^2}q^\mu)(p^\nu - \frac{pq}{q^2}q^\nu)\,. \tag{2.10}$$

The differential cross section for the electron-nucleon scattering can now be written as

$$\frac{d^2\sigma}{dxdy} = \frac{2\pi\alpha^2 s}{xQ^4}\big((1+(1-y)^2)F_2(x,Q^2) - y^2F_L(x,Q^2)\big)\,, \tag{2.11}$$

where $F_1 = W_1$, $F_2 = W_2 pq/m^2$ and $F_L = F_2 - 2xF_1$.

In general, these structure functions will strongly depend on Q^2. This, however, contradicts the deep inelastic scattering experiments [4, 5], where the structure functions have shown barely any influence on Q^2.

2.4 The quark-parton model

Since the observed scattering cross section and the Q^2 independence of the structure functions cannot fully be explained by inelastic proton-electron scattering, a more elaborate model has to be found.

It was mentioned earlier that the observed deep inelastic scattering cross sections showed a similar behavior to those of elastic scattering of an electron with a fundamental point-like object. Thus, as a coherent approach, one can assume that the nucleon itself is made up of fundamental point-like charged particles, called partons, which are able to exchange momentum by the means of strong interaction. The nucleon-electron scattering can then be described as parton-electron scattering as depicted in Fig. 2.2. The parton momentum p can be expressed as a fraction of the total nucleon momentum $p = \xi P$, where $0 < \xi < 1$. If one repeats the calculation

shown in Eq. (2.7) for parton-electron scattering and consistently replaces P with $p = \xi P$ one finds,

$$\frac{Q^2}{2Pq} = \xi. \tag{2.12}$$

Thus, the momentum fraction ξ can be identified with the Bjorken x. From now on, x will be used for both quantities.

It is assumed that the total scattering cross section can be written as an incoherent sum over single parton-electron scattering cross sections $\sum_q \sigma\big(eq \to eq\big)$, where $\sum_q$ is the sum over all possible partons in the nucleon. This, however, is only possible if the momentum fraction the partons carry is known. It thus seems necessary to define a function $f_q(x)$, which provides the probability density of finding a parton q to have a momentum fraction x of the parent hadron's momentum. These functions are known as parton distribution functions (PDFs). The cross section of the nucleon-electron scattering can eventually be expressed as

$$\sigma\big(e(k)N(P) \to e(k')X(P')\big) = \int_0^1 dx \sum_q f_q(x)\, \sigma\big(e(k)q(xP) \to e(k')q(p')\big)\,. \tag{2.13}$$

Combined with the parton-electron scattering cross section known from elastic two-body scattering, one obtains the differential cross section for nucleon-electron scattering

$$\frac{d^2\sigma}{dxdy} = \left(\sum_q x f_q(x) Q_q^2\right) \frac{2\pi\alpha^2 s}{Q^4}\big(1 + (1-y)^2\big)\,, \tag{2.14}$$

where Q_q is the parton charge, α the fine-structure constant, and

$$y = \frac{Pq}{Pk}. \tag{2.15}$$

In order to relate this result to the structure functions, one can compare Eq. (2.11) with Eq. (2.14) and obtain the identities,

$$F_2(x, Q^2) = \sum_q x f_q(x) Q_q^2 \tag{2.16}$$

$$F_L(x, Q^2) = 0\,. \tag{2.17}$$

Thus, the structure functions do not depend on Q^2 anymore. This means that the Bjorken scaling observed in DIS experiments can be explained with a simple parton model, where the partons do not interact with each other. This is remarkable, because one would assume that the partons exchange gluons by means of strong interaction. This issue was resolved in 1973 with the discovery of asymptotic freedom [12]. It states that at large energies, *e.g.* in the deep inelastic scattering region, quarks can be seen as almost free particles.

Nevertheless, there is still a non-zero interaction between quarks in the nucleon, which yields to a scaling violation. This will be discussed in the next section.

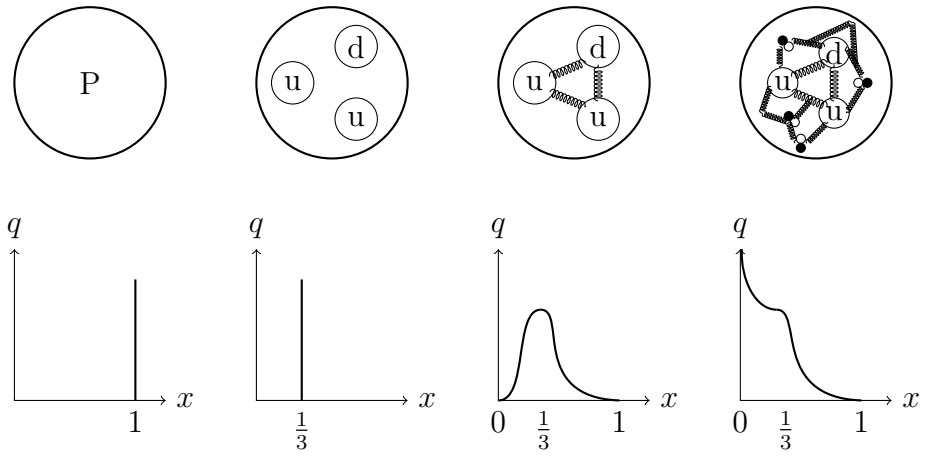

Figure 2.3: Schematic parton distributions for different parton models of the proton.

2.5 Obtaining parton distributions

In the previous section, the PDF was introduced as an important function to characterize the momentum distribution within the proton. In practice, it is highly desirable to acquire these PDFs. First of all, they are a fundamental property of the nucleon and can provide a deeper insight into its internal structure, as the schematic picture in Fig. 2.3 suggests. Secondly, because they are universal, they can be used for the evaluation of other scattering experiments, e.g. proton-proton scattering. In particular, during recent LHC experiments, PDFs provided an important input for the analysis of proton collisions.

Unfortunately, the PDFs cannot be directly measured in experiments. Thus, in order to extract them from scattering data, one has to identify the distributions with quantities that can be measured in these experiments, such as the structure functions. In case of the non-interacting parton model, this identity can be found in Eq. (2.16). For a precise determination of the PDFs, however, the naive parton model is not sufficient anymore, since the strong interaction of the quarks is not taken into account.

For the structure functions, for instance, one finds a slight dependence on Q^2 at a higher level of precision, which is known as scaling violation and is not predicted by the parton model. These corrections to the Bjorken scaling emerged from the fact that even in the DIS regime, where partons were supposed to be almost free particles, a non-vanishing strong interaction exists. Since these corrections are of the order α_s, a precise measurement of the deviation from the parton model can help with the determination of the strong coupling.

In order to make such predictions though, the theoretical corrections to the parton model have to be known. Thus, one has to take into account QCD effects, *e.g.* gluon exchange and quark pair production and use them to formulate a QCD

improved parton model. This cannot be done analytically to all orders anymore. Instead, perturbative methods have to be applied.

Using this QCD improved parton model, it is possible to obtain universal PDFs from the structure functions by making phenomenological assumptions for their parametrization, and to fit these to the QCD improved structure function relations. Also, other scattering experiments, for example neutrino induced DIS, provide access to additional structure functions of $W^{\mu\nu}$, which can be used to further constrain the PDF fit. A generic parametrization for an up-quark distribution might be

$$x f_u(x) = A_u x^{a_u} (1-x)^{b_u} P_u(x), \tag{2.18}$$

where $P_u(x)$ is a polynomial in x or $\sqrt{x}$ and A_u, a_u, b_u are free parameters, with A_u being determined by the flavor sum rules, *cf.* Eq. (2.19). The parametrization differs for other quarks and the gluons.

For the PDFs, there are other well-known constraints based on the number of valence quarks in the hadron. For the proton for example, one finds

$$\int_0^1 dx \left(f_u(x) - f_{\bar{u}}(x)\right) = 2, \quad \int_0^1 dx \left(f_d(x) - f_{\bar{d}}(x)\right) = 1\,, \tag{2.19}$$

on the basis of two up and one down quark in the proton. These identities already take into account the presence of quark-antiquark pairs in the sea.

A further important constraint makes use of the first moment of the PDFs, which is defined as

$$\langle x \rangle_q = \int_0^1 dx\, x \left(f_q(x) + f_{\bar{q}}(x)\right)\,. \tag{2.20}$$

This can be interpreted as the average momentum fraction x of the parton q. When adding the average momentum of all partons, one obtains the total momentum of the nucleon, thus the following identity should certainly hold for the momentum fraction

$$\int_0^1 dx\, x \big(f_u(x) + f_{\bar{u}}(x) + f_d(x) + f_{\bar{d}}(x) + f_g(x)\big) = 1\,, \tag{2.21}$$

where the strange and all heavier quarks were ignored.

2.6 Operator analysis of DIS

For a more general description of the nucleon-electron scattering, one can express the hadronic tensor in terms of hadronic currents, respectively their matrix elements.

$$W^{\mu\nu} = \frac{1}{4\pi} \int d^4z\, e^{iq\cdot z} \langle P|[J^\mu(z), J^\nu(0)]|P\rangle \tag{2.22}$$

The tensor can be related to the forward Compton amplitude, using the optical theorem,

$$W^{\mu\nu} = \frac{1}{2\pi}\mathrm{Im}\, T^{\mu\nu}\,, \tag{2.23}$$

where $T^{\mu\nu}$ can be written in terms of matrix elements of time-ordered currents

$$T^{\mu\nu} = i\int d^4z\, e^{iq\cdot z}\langle P|T\{J^\mu(z)J^\nu(0)\}|P\rangle. \tag{2.24}$$

It can be shown that in the Bjorken limit $Q^2 \to \infty$, the integral $\int d^4z$ is dominated by the region close to the light-cone, $z^2 \to 0$.

In this limit, one can use the formalism of the operator product expansion (OPE) to study the structure of the currents. Generally speaking, the OPE can relate the two currents that are separated by a light-like distance to a linear combination of singular coefficient functions (known as Wilson coefficients) multiplied with non-singular local operators. While the Wilson coefficients can be computed by the means of perturbation theory, the local operators have to be obtained by non-perturbative methods.

As one example, one can relate the matrix elements of a twist-2 operator to certain nucleon form factors, which can be identified with the moments of PDFs,

$$\langle P|\mathcal{O}_V^{\mu_1\cdots\mu_n}|P\rangle = 2A_{n0}P^{\{\mu_1}\cdots P^{\mu_n\}},\,, \tag{2.25}$$

with

$$\mathcal{O}_V^{\mu_1\cdots\mu_n} = \bar{q}i\gamma^{\{\mu_1}D^{\mu_2}\cdots D^{\mu_n\}}q\,, \tag{2.26}$$

where $|P\rangle$ denotes a nucleon state with momentum P and $\{\cdots\}$ is the index symmetrization and the subtraction of trace.

One can relate these moments of PDFs to the original distribution by a Mellin transformation. Thus, transforming Eq. 2.25 yields a formal definition of the quark distributions in the nucleon via matrix elements of the light-cone operator

$$f_q(x) = \frac{1}{4\pi}\int_{-\infty}^{\infty} d\xi^-\, e^{-ix\xi^-P^+}\langle P|\bar{\psi}(\xi^-)\gamma^+\exp\left(-ig\int_0^{\xi^-}A^+(\eta^-)\,d\eta^-\right)\psi(0)|P\rangle\,, \tag{2.27}$$

with the light-cone coordinates $\xi^\pm = {}^1\!/\!_{\sqrt{2}}(\xi^0 - \xi^3)$ and the gauge fields A^μ. In Chapter 5, I will show how to use this light-cone operator to compute parton distributions on the lattice.

Coming back to Eq.(2.25), the easiest possible operator can be used to extract the F_1 form factor, which is the conserved charge,

$$\langle P|\bar{q}\gamma^\mu q|P\rangle = \bar{u}(P)\gamma_\mu A_{10}(0)u(P)\,, \tag{2.28}$$

where one can identify $A_{10}(0) = F_1(0)$.

As a next step, operators with two indices μ, ν, more specifically the energy-momentum tensor of QCD, can be used to extract moments of PDFs

$$\langle P|T^{\{\mu\nu\}}|P\rangle = \bar{u}(P)A_{20}(0)\gamma^{\{\mu}P^{\nu\}}u(P)\,, \tag{2.29}$$

where the form factor $A_{20}(0)$ can be related to $\langle x\rangle$. With the proper choice of $T^{\mu\nu}$, several moments can be extracted. In Chapter 4, I will utilize this relation to compute the first moment of the gluon distribution $\langle x\rangle_g$.

3. Lattice QCD and twisted mass fermions

After having outlined the theory of hadron structure and deep inelastic scattering in the previous chapter, I would now like to give a short introduction to quantum chromodynamics (QCD) on a lattice. The lattice discretization of QCD used throughout this thesis, is a non-perturbative method which is able to make *ab initio* predictions for strongly interacting systems.

I will briefly explain the basics of lattice QCD, with a focus on the Wilson Twisted Mass formalism, which is a particular fermion discretization used in this thesis. I will outline how to obtain physical quantities by the computation of two- and three-point correlation functions and illustrate how to extract hadronic form factors from matrix elements of local operators. Finally, I will give a short review on the status of hadron structure on the lattice by presenting selected results.

An extensive guideline to lattice QCD can be found in Refs. [33, 34]. For additional information on hadron structure calculations on the lattice, see Ref. [22].

3.1 Quantum chromodynamics

The interaction of quarks and gluons are described by the principles of QCD. This is a SU(3) gauge invariant quantum field theory whose degrees of freedom are the fermion fields ψ, $\bar{\psi}$ and the gluon vector fields A^μ. The well-known QCD action is [1]

$$S_{QCD} = \int d^4x\, \bar{\psi}(x)\big(i\gamma_\mu D^\mu - m\big)\psi(x) - \frac{1}{4}F_a^{\mu\nu}(x)F^a_{\mu\nu}(x)\,. \tag{3.1}$$

Here, ψ and $\bar{\psi}$ are QCD spinors with an internal spin index $\alpha \in \{1\ldots4\}$ and color index $a \in \{1\ldots3\}$. D^μ is the covariant derivative given by

$$D^\mu = \partial^\mu - igA^\mu\,, \tag{3.2}$$

where $A^\mu(x) = T^a A^\mu_a(x)$ and T^a are the generators of the SU(3) gauge group. $A^\mu_a(x)$ is the gluon field in the adjoint representation and has the color index $a \in \{1\ldots8\}$.

[1] Following the conventions from Ref. [30] in Section 16.1.

$F_a^{\mu\nu}$ is the field-strength tensor in the adjoint representation defined as

$$F_a^{\mu\nu} = \partial^\mu A_a^\nu - \partial^\nu A_a^\mu + g f^{abc} A_b^\mu, A_c^\nu \,, \tag{3.3}$$

where g is the strong coupling constant and $if^{abc}T^c = [T^a, T^b]$. f^{abc} are called the structure constants of SU(3).

In principle, the nature of strong interaction can be derived from these equations. However, up to now, no analytic solution has been found for the group of non-abelian Yang-Mills theories in four dimensions, which QCD belongs to.

3.2 Discretization of QCD on a lattice

A well-known formalism that can make non-perturbative *ab initio* predictions of strong interactions is lattice QCD.

The basic principle of this formalism is to define QCD on a discrete Euclidean space-time lattice with a lattice spacing a and to consequently express the action in terms of discrete field variables

$$\psi(x) \to \psi_x \,, \quad \bar{\psi}(x) \to \bar{\psi}_x \,, \quad A_\mu(x) \to (A_\mu)_x \,. \tag{3.4}$$

For reasons of convenience, the form $\psi(x)$ will be kept throughout this work for discretized variables as well. Consequently, the integral $\int d^4x$ is replaced by a discrete sum $a^4 \sum_x$.

The transition to Euclidean space-time is necessary in order to obtain a real action in the weight factor of the Feynman integral Eq. (3.25), making it possible to perform numerical simulations. Yet, the transition does not provide a challenge, since Euclidean observables can usually be related to their Minkowski counterparts by a Wick rotation and vice versa.

In a lattice gauge theory, it is further necessary to write the gauge degrees of freedom as gauge links $U_\mu(x)$, which are defined as $U_\mu(x) = \exp(iagA_\mu(x))$, in order to conserve gauge invariance. These are also known as parallel transporters, because they can be seen as connecting links between two fermion fields at the lattice sites x and $x + \hat{e}_\mu$ due to their behavior under gauge transformation. $\hat{e}_\mu$ denotes one step on the lattice in the μ direction.

In order to define a lattice gauge action, it is helpful to define the plaquette term, which is a minimal non-trivial closed path of gauge links and written as

$$U_{\mu\nu}(x) = U_{\mu\nu}^{1\times1}(x) = U_\nu(x)^\dagger U_\mu(x+\hat{e}_\nu)^\dagger U_\nu(x+\hat{e}_\mu) U_\mu(x) \,. \tag{3.5}$$

This plaquette term can be related to the gluonic field strength tensor

$$U_{\mu\nu}(x) = \exp\bigl(iga^2 F_{\mu\nu} + O(a^3)\bigr) \,. \tag{3.6}$$

Thus, a simple gauge action can be constructed from plaquette terms in the following way

$$S_G[U] = \frac{\beta}{3} \sum_x \left(\sum_{\mu<\nu} \{1 - \text{Re Tr}(U_{\mu\nu}^{1\times1}(x))\} \right) . \tag{3.7}$$

This concept can also be extended to include a rectangular path of gauge links, which is denoted by $U_{\mu\nu}^{1\times2}(x)$. The improved gauge action is then written as

$$S_G[U] = \frac{\beta}{3} \sum_x \left(b_0 \sum_{\mu<\nu} \{1 - \text{Re Tr}(U_{\mu\nu}^{1\times1}(x))\} + b_1 \sum_{\mu,\nu} \{1 - \text{Re Tr}(U_{\mu\nu}^{1\times2}(x))\} \right) , \tag{3.8}$$

with the coefficients b_0 and b_1 being defined as $b_0 = 1 - 8b_1$ and $b_1 = 0$ for the unimproved case and $b_1 = -0.331$ for the Iwasaki gauge actions. The latter was proposed by Iwasaki in Ref. [35] and is used for current lattice simulations with four dynamical quark flavors in order to suppress unphysical short distant fluctuations which cause dislocation. The strong coupling constant g is related to β by $\beta = 6/g^2$.

One possible way to discretize the fermionic part of the action is the Wilson-Dirac action

$$S_F[\psi, \bar{\psi}, U] = a^4 \sum_x \bar{\psi} \left(D_W + m \right) \psi , \tag{3.9}$$

where the covariant derivative,

$$D_W = \frac{\gamma_\mu}{2} (\nabla_\mu + \nabla_\mu^*) + \frac{ar}{2} \nabla_\mu \nabla_\mu^* , \tag{3.10}$$

contains the Wilson term $\frac{ar}{2} \nabla_\mu \nabla_\mu^*$, which avoids fermion doubling, an unwanted effect of the naive discretization of QCD. The derivatives ∇_μ are defined as,

$$\nabla_\mu \psi(x) = \frac{1}{a} \left(U_\mu(x) \psi(x + \hat{e}_\mu) - \psi(x) \right) \tag{3.11}$$

$$\nabla_\mu^* \psi(x) = \frac{1}{a} \left(\psi(x) - U_\mu(x - \hat{e}_\mu)^\dagger \psi(x - \hat{e}_\mu) \right) . \tag{3.12}$$

For certain applications, it is useful to perform an expansion in powers of next-neighbor interaction. Therefore, the hopping parameter is introduced as

$$\kappa = \frac{1}{8r + 2m} . \tag{3.13}$$

The action from Eq. (3.9) can be written as

$$S_F[\psi, \bar{\psi}, U] = \frac{1}{2\kappa} \sum_{x,y} \bar{\psi}(x) Q(x, y) \psi(y) \tag{3.14}$$

where $Q(x,y)$ is an operator acting on the spinors $\psi(x)$. This operator can be split into a diagonal and an off-diagonal part as

$$Q(x,y) = \delta_{x,y}\mathbb{1} + \kappa\tilde{Q}(x,y)\,, \tag{3.15}$$

where the off-diagonal $\tilde{Q}$ contains only next-neighbor interactions. The additional factor in Eq. (3.14) can be removed by rescaling the fields by a factor of $\sqrt{1/2\kappa}$,

$$\psi(x) \to \sqrt{\frac{1}{2\kappa}}\psi(x)\,, \tag{3.16}$$

and likewise for $\bar{\psi}$.

In this form, a hopping parameter expansion can be performed, as it has been done in Ref. [36], for instance. Apart from this application, the parameter κ is still frequently used in current lattice QCD formulations.

3.3 Twisted mass lattice QCD

In order to avoid large cut-off effects, it is highly desirable to remove the $O(a)$ effect that was introduced by inserting the Wilson term into the action. One possible way to obtain an improved continuum limit scaling was pointed out in Ref. [37] and is called the twisted mass formalism.

For this formalism, a new set of spinor doublets $\chi, \bar{\chi}$ is introduced, which is related to the physical bases $\psi, \bar{\psi}$ by

$$\psi = \exp\left(i\frac{\omega}{2}\gamma_5\tau_3\right)\chi, \quad \bar{\psi} = \bar{\chi}\exp\left(i\frac{\omega}{2}\gamma_5\tau_3\right)\,. \tag{3.17}$$

The twist angle ω satisfies the relation

$$\tan\omega = \frac{\mu^R}{m^R}\,, \tag{3.18}$$

where μ^R and m^R are renormalized masses and τ_i are the Pauli matrices in flavor space. The renormalized mass is connected to the bare value by an additive mass renormalization m_{cr}

$$m_R = m_0 - m_{cr}\,. \tag{3.19}$$

For the light doublet, *i.e.* up- and down-quarks whose masses were chosen to be degenerate, the new action contains one additional term, namely the twisted mass term

$$S_{F,l}[\chi,\bar{\chi},U] = a^4\sum_x \bar{\chi}_l\left(D_W + m + i\mu\gamma_5\tau_3\right)\chi_l\,. \tag{3.20}$$

In case of $N_f = 2 + 1 + 1$ simulation where strange and charm quarks are present as well, one needs to insert two new terms into the action, taking into account the distinctly different masses of these quarks

$$S_{F,h}[\chi, \bar{\chi}, U] = a^4 \sum_x \bar{\chi}_h \left(D_W + m + i\mu_\sigma \gamma_5 \tau_1 + \tau_3 \mu_\delta \right) \chi_h \,, \tag{3.21}$$

where the renormalized strange and charm quark masses are defined as

$$m_{s,R} = Z_P^{-1} \left(\mu_h - \frac{Z_P}{Z_S} \mu_\delta \right) \quad m_{c,R} = \left(\mu_h + \frac{Z_P}{Z_S} \mu_\delta \right) , \tag{3.22}$$

where Z_P and Z_S are the renormalization constants of the pseudoscalar and scalar densities in a massless quark scheme.

In order to achieve an automatic $O(a)$ improvement, *i.e.* the operators being automatically improved, the bare mass m_0 needs to be tuned to the critical value m_{cr} so that the renormalized mass m_R vanishes. This is called maximal twist and is equivalent to a twist angle of $\omega = \pi/2$. In practice, this is carried out by measuring the PCAC mass, which is defined as

$$m_{\mathrm{PCAC}} = \frac{\sum_{\vec{x}} \langle \partial_0 A_0(\vec{x}, t) P(0) \rangle}{2 \sum_{\vec{x}} \langle P(\vec{x}, t) P(0) \rangle} \tag{3.23}$$

with

$$A_\mu(x) = \bar{\chi}(x) \gamma_\mu \gamma_5 \frac{\tau_1}{2} \chi(x) \quad P(x) = \bar{\chi}(x) \gamma_5 \frac{\tau_1}{2} \chi(x) \,, \tag{3.24}$$

and tuning κ to a critical value κ_{crit} so that $m_{\mathrm{PCAC}} \approx 0$. It can be shown that the thus obtained κ_{crit} can also be used for improvement of the heavy doublet [38].

Due to the use of twisted mass fermions, all quantities studied in this thesis are automatically $O(a)$ improved without any alteration of the used operators.

3.4 Computing observables in lattice QCD

After introducing the concept of lattice QCD and the associated action, one needs to find suitable method to extract physical quantities from these equations. For this purpose, Feynman's path integral formalism can be employed to compute expectation values of local operators denoted $\mathcal{O}$

$$\langle \Omega | \mathcal{O} | \Omega \rangle = \frac{1}{Z} \int D\chi D\bar{\chi} DU \; \mathcal{O} e^{-S_E[\chi, \bar{\chi}, U]} \,, \tag{3.25}$$

with $|\Omega\rangle$ being the vacuum state and

$$Z = \int D\chi D\bar{\chi} DU \; e^{-S_E[\chi, \bar{\chi}, U]} \,, \tag{3.26}$$

where $S_E[\chi, \bar{\chi}, U] = S_F[\chi, \bar{\chi}, U] + S_G[U]$ is the Euclidean action of the system, consisting of the fermionic part S_F and the gauge part S_G.

It is possible to relate these expectation values to physical observables by choosing appropriate local operators and combining them in the right way. Unfortunately, due to the nature of QCD and the high dimensionality of the integral, it is not possible to find an exact analytic solution. Instead numerical methods, *e.g.* important sampling, can be used to approximate the result.

In practice, a Monte Carlo simulation can be applied to produce a Markov chain of representative gauge field configurations. It is possible to utilize the Grassmann properties of the fermion fields $\chi, \bar{\chi}$ to write the fermion integral as the determinant of the Dirac operator Q, *cf.* Eq. (3.14),

$$\int D\chi D\bar{\chi}\, e^{-S_f[\chi,\bar{\chi},U]} = \det[Q(U)]\,, \tag{3.27}$$

where it is assumed that Q is positive definite. The determinant can further be related to the bosonic Gaussian integral

$$\det[Q] \propto \int D\phi\, e^{\phi^\dagger Q^{-1}\phi}\,, \tag{3.28}$$

where ϕ labels complex scalar fields that are referred to as pseudo fermionic fields. In this way, the fermions can be included in the weight factor for the Monte-Carlo algorithm. The integral is highly non-local though due to the inverse matrix Q^{-1}. Hence, modern lattice QCD algorithms use a Hybrid Monte Carlo (HMC) method, which is a powerful global algorithm including many improvements and being capable of simulating at small quark masses. In case of twisted mass lattice QCD, the underlying HMC algorithm is explained in detail in Ref. [39].

From the thus obtained gauge field configurations, the expectation value of an operator can now be computed as the average of the operator on this gauge ensemble

$$\frac{1}{N}\sum_{U_n} \mathcal{O}(U_n) \equiv \left\langle \mathcal{O} \right\rangle = \langle \Omega|\mathcal{O}|\Omega\rangle + O\left(\frac{1}{\sqrt{N}}\right)\,, \tag{3.29}$$

where a statistical error of the order $O(1/\sqrt{N})$ is expected for the standard Monte Carlo methods. From now on, the expression $\left\langle \mathcal{O} \right\rangle$ will be used to denote the average over gauge field configurations.

Although there are no fermion fields present in the ensemble, fermionic quantities can be computed by using the quark propagator which can be related to the inverse Dirac operator Q^{-1} through Wicks theorem

$$\left\langle \chi_A(x)\bar{\chi}_B(y) \right\rangle = Q^{-1}_{AB}(x,y)\,, \tag{3.30}$$

where A, B are spin and color indices.

3.4.1 Two-point correlation functions

As the next step, the expectation value of local operators has to be related to quantities that can be measured in experiments. For this purpose, one can employ the method of spectral decomposition on certain well-chosen combinations of operators.

A rather simple choice is the two-point correlation function which can be used to extract masses and decay constants of physical states, but is also needed for the proper normalization of matrix elements of operators later on. A typical two-point correlation function in position space is defined as

$$C^{\mathrm{2pt}}(x, x') = \langle \Omega | N(x) \overline{N}(x') | \Omega \rangle \,, \tag{3.31}$$

where Ω is the QCD vacuum state and $N(x)$ is an arbitrary hadronic state at position x. In general, this can be interpreted as a hadron propagator, *i.e.* the probability that a hadron propagates from space-time point x' to x. As pointed out earlier, this can generally be acquired in lattice QCD by computing the average value of this combination of operators on a gauge field ensemble, as defined in Eq. (3.25)

$$C^{\mathrm{2pt}}(x, x') = \left\langle N(x) \overline{N}(x') \right\rangle . \tag{3.32}$$

Since one is interested in states with a well-defined momentum, the momentum-projected two-point function can be defined by applying a Fourier transformation

$$C^{\mathrm{2pt}}(\mathbf{P}, t, t') = \sum_{\mathbf{x}} e^{-i\mathbf{P}(\mathbf{x}-\mathbf{x}')} \left\langle N(\mathbf{x}, t) \overline{N}(\mathbf{x}', t') \right\rangle , \tag{3.33}$$

where the source point x' is fixed. Instead of transforming the two-point function, one can equivalently transform the interpolating fields $N(P) = \sum_{\mathbf{x}} e^{-i\mathbf{P}\mathbf{x}} N(\mathbf{x}, t)$.

In order to extract physical observables from this two-point function, one can perform the spectral decomposition of Eq. (3.31) by inserting a set of eigenstates

$$C^{\mathrm{2pt}}(\mathbf{P}, t, t') = \sum_{n} \frac{e^{-E_n (t-t')}}{2E_n} \langle \Omega | N(P) | n \rangle \langle n | \overline{N}(P) | \Omega \rangle \,. \tag{3.34}$$

Here, for convenience, the momentum-projected version of the interpolating fields was used. By considering large time separations $t \gg t'$, the sum will be dominated by the ground state[2] $|0\rangle$ due to the fast decay of the coefficient $e^{-E_n(t-t')}$ for the condition $E_n < E_{n+1}$. One then obtains

$$C^{\mathrm{2pt}}(\mathbf{P}, t, t') \overset{t \gg t'}{=} \frac{e^{-E_0 (t-t')}}{2E_0} \langle \Omega | N(P) | 0 \rangle \langle 0 | \overline{N}(P) | \Omega \rangle \,. \tag{3.35}$$

[2] Not to be confused with the vacuum state $|\Omega\rangle$

As a result, one can use the two-point function to extract the ground state's energy E_0 by its exponential decay over time. Furthermore, its normalization can be used to compute the decay constant.

If one wants to study a particular hadron, the interpolating fields $N(x)$ have to be chosen in order to match the state's quantum numbers. For the proton, a possible form is

$$N_\alpha(x) = \epsilon^{abc} u^a_\alpha(x) \left(d^{b^T}(x) \mathcal{C}\gamma_5 u^c(x) \right) , \tag{3.36}$$

where $\mathcal{C} = i\gamma_0\gamma_2$ and $u(x)$, $d(x)$ are up- and down-quark fields. Since this spinor does not have a well-defined parity, one needs to project it with a suitable parity projector, *e.g.* $\Gamma = (1 + \gamma_4)/2$ for positive parity. Thus, one obtains the proton two-point function

$$C^{\text{2pt}}(\mathbf{P}, t, t') = \sum_{\mathbf{x}} e^{-i\mathbf{P}(\mathbf{x}-\mathbf{x}')} \Gamma_{\alpha\beta} \left\langle N_\alpha(\mathbf{x}, t) \overline{N}_\beta(\mathbf{x}', t') \right\rangle . \tag{3.37}$$

This two-point function can now be expressed in terms of quark propagators by performing the relevant Wick Contractions, *e.g.* $u(x)\bar{u}(x') = Q_u^{-1}(x, x')$, where Q_u^{-1} is the up component of the inverse Dirac operator, *cf.* Eq. (3.30). The latter can be computed on the provided gauge field configurations by solving the linear equation $Q\phi = \xi$, where ξ is a source that has to be chosen adequately.

Here, usually sources with a single entry in space-time $\xi(x) = \delta_{x\,x_0}$ are used, called point sources. One hereby obtains a point-to-all propagator, *i.e.* the propagator from a fixed lattice point x_0 to every other one.

3.4.2 Three-point correlation functions

If one is interested in hadron structure, it is not sufficient to only compute the two-point correlation function, because hadronic form factors cannot be accessed this way.

However, as seen in Eq. (2.25), the matrix elements of local operators can be related to these form factors. The operators can be interpreted as currents which are inserted into the hadronic correlation function in order to probe its structure. The hadronic matrix elements can be computed with a three-point correlation function,

$$C^{\text{3pt}}(x, y, x') = \langle \Omega | N(x) \mathcal{O}(y) \overline{N}(x') | \Omega \rangle , \tag{3.38}$$

where the operator $\mathcal{O}$ was inserted at space-time point $y = (\mathbf{y}, \tau)$. Again, in order to obtain a momentum projected three-point function, a Fourier transformation can be used

$$C^{\text{3pt}}(t, \tau, t'; \mathbf{P}, \mathbf{P}') = \sum_{\mathbf{x},\mathbf{y}} e^{-i\mathbf{P}(\mathbf{x}-\mathbf{y})} e^{-i\mathbf{P}'(\mathbf{y}-\mathbf{x}')} \langle \Omega | N(x) \mathcal{O}(y) \overline{N}(x') | \Omega \rangle , \tag{3.39}$$

where the difference $\mathbf{q} = \mathbf{P} - \mathbf{P}'$ can be interpreted as the momentum transfer at the operator insertion.

In this thesis, however, only matrix elements for zero momentum transfer will be computed. Thus, Eq. (3.39) simplifies to

$$C^{\text{3pt}}(t,\tau,t';\mathbf{P}) = \sum_{\mathbf{x},\mathbf{y}} e^{-i\mathbf{P}(\mathbf{x}-\mathbf{x}')} \langle\Omega|N(x)\mathcal{O}(y)\overline{N}(x')|\Omega\rangle\,. \tag{3.40}$$

The matrix elements can be isolated from this three-point function by inserting two sets of eigenstates

$$C^{\text{3pt}}(t,\tau,t';\mathbf{P}) = \sum_{n,m} \frac{e^{-E_n(t-\tau)}e^{-E_m(\tau-t')}}{2E_n 2E_m} \langle\Omega|N(P)|n\rangle\langle n|\mathcal{O}|m\rangle\langle m|\overline{N}(P)|\Omega\rangle\,. \tag{3.41}$$

Again, the momentum-projected hadron fields are used.

In order to extract the relevant form factors from this equation, one needs to perform a form factor decomposition of the matrix elements. For baryons, this is

$$\langle n,P|\mathcal{O}|m,P\rangle = \bar{u}(P)\mathcal{O}_{nm}u(P)\,, \tag{3.42}$$

where $\mathcal{O}_{nm}$ contains the form factors and u, $\bar{u}$ are the well-known spinor amplitudes.

In addition, the decomposition of the nucleon field matrix elements is needed

$$\langle\Omega|N_\alpha(P)|n,P\rangle = Z_n u_\alpha(P)\,. \tag{3.43}$$

Here, Z_n is the normalization of the state n and it is always assumed that only the states $|n\rangle$ and $|m\rangle$ with momentum P survive.

Finally, the spinor completeness relation can be applied,

$$\sum u_\alpha(P)\bar{u}_\beta(P) = (\not{P} + m)_{\alpha\beta}\,, \tag{3.44}$$

where $\not{P} = P_\mu\gamma^\mu$ and $\sum$ is the sum over the spin states, which were implicitly defined within the fields here. Combining the last four equations yields

$$C^{\text{3pt}}_{\alpha\beta}(t,\tau,t';\mathbf{P}) = \sum_{n,m} \frac{e^{-E_n(t-\tau)}e^{-E_m(\tau-t')}Z_nZ_m}{2E_n 2E_m} \left((\not{P}_n + m)\mathcal{O}_{nm}(\not{P}_m + m)\right)_{\alpha\beta}\,. \tag{3.45}$$

Again, the ground state form factors can be extracted by choosing large time separations

$$C^{\text{3pt}}_{\alpha\beta}(t,\tau,t';\mathbf{P}) \overset{t\gg\tau\gg t'}{=} \frac{e^{-E_0(t-t')}Z_0^2}{4E_0^2} \left((\not{P}_0 + m)\mathcal{O}_{00}(\not{P}_0 + m)\right)_{\alpha\beta}\,. \tag{3.46}$$

The open spinor indices imply that a suitable Γ needs to be defined equivalently to the two-point function in order to perform the parity projection

$$C_{\Gamma}^{3\mathrm{pt}}(t,\tau,t';\mathbf{P},\mathbf{P}) = \Gamma_{\beta\alpha} C_{\alpha\beta}^{3\mathrm{pt}}(t,\tau,t';\mathbf{P},\mathbf{P})\,. \tag{3.47}$$

The choice of this projector strongly depends on the operator that is used and the form factors one wants to extract. In Section 3.5, two examples for possible projectors will be given.

In practice, the three-point correlation function can be computed on the lattice by expressing the hadronic field in terms of quark fields and by finding the possible Wick contractions. The type of Wick contractions that can be performed strongly depends on the form of the inserted operator. There are three general types of diagrams that can be computed. They are shown in Fig. 3.1.

For operators of type $\mathcal{O} = \bar{\psi}\Lambda\tau_3\psi$, where Λ is an arbitrary γ structure, only the first type of diagrams occurs. In this case disconnected quark loops cancel due to the flavor structure of the operator. This type is referred to as connected diagrams.

If this cancellation is not present, *e.g.* for operators of type $\mathcal{O} = \bar{\psi}\Lambda\mathbb{1}\psi$, the second type of diagrams has to be considered in addition to the connected ones. This type is referred to as disconnected diagrams.

Lastly, the operator can consist only of gluonic quantities. Here, only the third type appears, since there is no possible connection between the quark fields in the hadron and the gluon fields in the operator. Consequently, the loop will be purely gluonic. This diagram type will be computed in Chapter 4 in order to obtain the gluon momentum fraction.

3.4.3 Extracting form factors

Up to now, every necessary step was taken to isolate the term $\mathcal{O}_{00}$, which contains the relevant form factors. However, it can still not be computed, because in particular the wave function renormalization constants Z are not known.

To solve this issue, it is helpful to perform the spectral decomposition of the two-point function by applying Eqs. (3.43) and (3.44) to Eq. (3.35).

$$C_{\Gamma}^{2\mathrm{pt}}(\mathbf{P},t,t') \overset{t\gg t'}{=} \mathrm{Tr}\left(\Gamma \frac{e^{-E_0(t-t')} Z_0^2}{2E_0}(\not{P}_0 + m)\right)\,. \tag{3.48}$$

Clearly, one can now remove the Z factors by computing the ratio of Eq. (3.46) with Eq. (3.48):

$$\frac{C_{\Gamma}^{3\mathrm{pt}}(t,\tau,t';\mathbf{P},\mathbf{P})}{C_{\Gamma'}^{2\mathrm{pt}}(t,t';\mathbf{P})} \overset{t\gg\tau\gg t'}{=} \frac{\mathrm{Tr}\left(\Gamma(\not{P}_0 + m)\mathcal{O}_{00}(\not{P}_0 + m)\right)}{2E\,\mathrm{Tr}\left(\Gamma'(\not{P}_0 + m)\right)}\,. \tag{3.49}$$

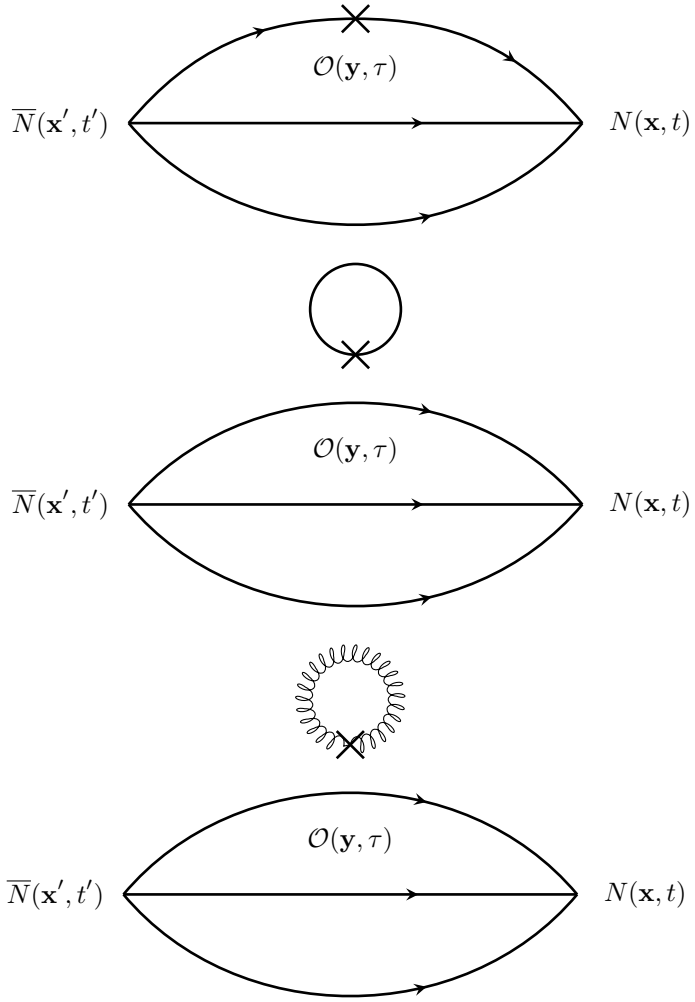

Figure 3.1: Schematic picture of possible Wick contractions of three-point functions. Each continuous line represents a quark propagator, while the curly line represents a gluon loop. **Top:** connected three-point function, **middle:** disconnected three-point function with a quark loop, **bottom:** disconnected three point function with a gluon loop.

To proceed here, the exact structure of $\mathcal{O}_{00}$ from Eq. (3.49) has to be known from the form factor decomposition. For a rather simple case, this can be the form factor multiplied with a combination of Dirac matrices Λ and momenta P.

$$\mathcal{O}_{00} = \Lambda f(P) A(0)\,, \tag{3.50}$$

where $f(P)$ is a function of the momenta and $A(0)$ is the form factor at zero momentum transfer. For non-vanishing momentum transfer or special operators, this can take a more complicated form though.

Finally, Eq. (3.49) can be evaluated by inserting Eq. (3.50), defining the projectors and eventually applying trace algebra. Usually one finds a kinematic factor K, which can be some function of P and relates the ratio with the form factor

$$\frac{C^{\mathrm{3pt}}_{\Gamma}(t,\tau,t';\mathbf{P},\mathbf{P})}{C^{\mathrm{2pt}}_{\Gamma'}(t,t';\mathbf{P})} \overset{t\gg\tau\gg t'}{=} K(P)A(0)\,. \tag{3.51}$$

Since this ratio is a frequently occurring quantity within this thesis, it is convenient to introduce the quantity $R(N(P);\mathcal{O};N(P))$, which is defined as the ratio of a three-point function with initial and final fields $N(P)$ and an inserted operator $\mathcal{O}$ with an appropriate two-point function

$$R_{\Gamma,\Gamma'}\big(N(P);\mathcal{O};N(P)\big) \overset{t\gg\tau\gg t'}{=} \frac{C^{\mathrm{3pt}}_{\Gamma}(t,\tau,t';\mathbf{P},\mathbf{P})}{C^{\mathrm{2pt}}_{\Gamma'}(t,t';\mathbf{P})}\,. \tag{3.52}$$

From now on, this ratio will be used whenever calculating nucleon structure form factors, meaning that both two- and three-point functions need to be provided in most of the cases.

In order to relate the obtained form factors from the lattice to the physical equivalents, an appropriate renormalization procedure has to be found. Yet, this issue will not be addressed in detail in this thesis.

3.5 The status of nucleon structure from lattice QCD

In the last section of this introduction to lattice QCD and hadron structure, I will give a short review on selected important nucleon structure quantities that have been computed using lattice QCD. The following results are taken from the latest European Twisted Mass Collaboration (ETMC) paper on nucleon structure [23], which includes the latest ETMC results from lattice simulation at a physical value of the pion mass, as well as results from other groups, employing different fermionic actions.

3.5.1 The nucleon axial charge g_A

The nucleon axial charge g_A is an important quantity for nucleon structure calculations on the lattice. First of all, it is an experimentally well-known quantity which can be determined from the β-decay of the neutron and is connected to the chiral structure of the nucleon. Secondly, it serves as an excellent benchmark quantity for lattice calculations, since it can be computed rather straightforwardly at zero momentum transfer.

The relevant operator inserted into the nucleon correlator is the axial-vector quark current

$$\mathcal{O}_A^\mu = \bar{\psi}\gamma_5\gamma^\mu\tau_3\psi\,, \tag{3.53}$$

where τ_3 is a Pauli matrix in flavor space and $\psi = (u, d)$, $\bar{\psi} = (\bar{u}, \bar{d})$.

From the relevant decomposition of its nucleon matrix elements, the axial form factor $\tilde{A}_{10}(0) = g_A$ can be extracted as

$$\langle P|\mathcal{O}_A^\mu|P\rangle = i\,\bar{u}(P)\tilde{A}_{10}(0)\gamma^\mu\gamma_5 u(P)\,. \tag{3.54}$$

Consequently, g_A can be extracted from the ratio of three- and two-point functions as defined in the previous section,

$$g_A = i\,R_{\Gamma_j}\big(N(0); \mathcal{O}_A^j; N(0)\big)\,, \tag{3.55}$$

where a special projector $\Gamma_j = i\gamma_j\gamma_5(1+\gamma_4)/2$ has to be used due to the γ_5 in the operator. In all cases, the parity plus projector $\Gamma_+ = (1+\gamma_4)/2$ will be used for the two-point function.

In recent years, different groups have put a lot of effort into computing g_A. Results for different pion masses and fermion actions are shown in Fig. 3.2.

In order to obtain these physical results, the bare lattice results have to be renormalized. In case of g_A, this is done with the renormalization constant of the axial current Z_A, which can be computed non-perturbatively on the lattice.

An important observation from Fig. 3.2 is the fact that most of the results tend to be lower than the experimental result $g_A = 1.272(2)$ [46][3]. Yet, the ETMC result at the physical point does agree with experiments, although its error still has to be reduced to make a better statement. In general, further calculations with a physical pion mass, in particular at different volumes and lattice spacings, are certainly necessary.

3.5.2 The quark momentum fraction $\langle x\rangle_{u-d}$

Considering other twist-2 operators, the next relevant quantity is the first moment of the iso-vector quark PDF, which can be interpreted as the average iso-vector quark

[3] Taken from the β decay parameters of the neutron review.

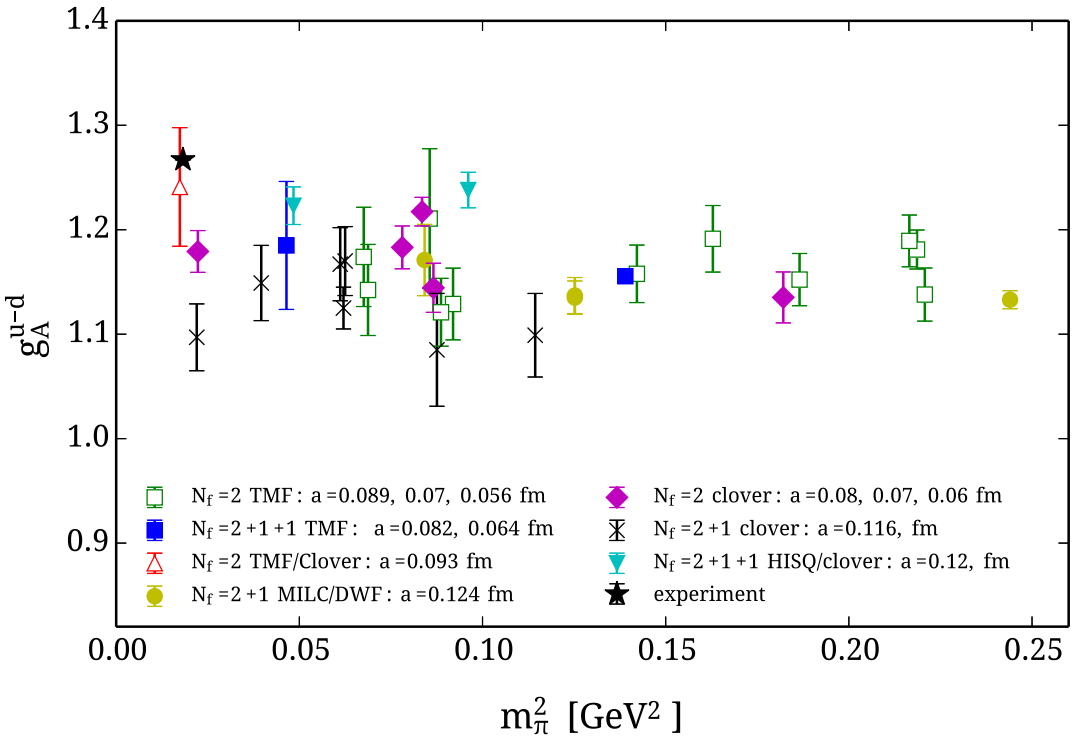

Figure 3.2: Results for the nucleon axial charge as a function of the pion mass for different fermion actions. Twisted mass fermion results are shown with open green squares for $N_f = 2$ ensembles [40], with filled blue squares for $N_f = 2+1+1$ [41] and with the open red triangle for the physical ensemble using the plateau value at ${}^{t_s}/_a = 14$ [23]. Results are also shown using $N_f = 2$ clover fermions (filled purple diamonds) [42]; $N_f = 2 + 1 + 1$ staggered sea and clover valence quarks (filled light blue inverted triangles) [43]; $N_f = 2 + 1$ with domain wall fermions (DWF) on a staggered sea (filled yellow circles) [44]; and $N_f = 2+1$ clover (black x-symbols) [45]; experimental result from Ref. [46]. The figure is taken from Ref. [23].

momentum fraction in the nucleon $\langle x \rangle_{u-d} = \int_0^1 dx\, x\, (f_u(x) + f_{\bar{u}}(x) - f_d(x) - f_{\bar{d}}(x))$. This quantity is particularly interesting for several reasons. Most importantly, as discussed in the previous chapter, the PDF and their moments cannot be directly measured in experiments. Instead, perturbation theory has to be applied and phenomenological assumptions have to be made in order to perform a fit to experimental data. Lattice QCD, on the other hand, can give a non-perturbative estimate of the moments and thus provide additional insight into the PDFs.

The operator used for the extraction of the momentum fraction can be related to Eq. (2.26) and involves a covariant derivative

$$\mathcal{O}_V^{\mu\nu} = \bar{\psi}\gamma^{\{\mu} D^{\nu\}} \tau_3 \psi \,. \tag{3.56}$$

Hence, the form factor decomposition of the nucleon matrix element at zero momentum transfer is

$$\langle P|\mathcal{O}_V^{\mu\nu}|P\rangle = \bar{u}(P) A_{20}(0) \gamma^{\{\mu} P^{\nu\}} u(P) \,. \tag{3.57}$$

Thus, the average momentum fraction can be extracted from the ratio

$$\langle x \rangle_{u-d} = A_{20}(0) = \frac{1}{m_N} R_{\Gamma_+}\left(N(0); \mathcal{O}_V^{44} - \frac{1}{3}\mathcal{O}_V^{kk}; N(0)\right) , \tag{3.58}$$

where m_N is the nucleon mass and the parity plus projector was used this time. Similar to g_A, the average momentum fraction has been computed by several groups in recent years, especially because the results for heavier pion masses were mostly in clear contradiction to the experimental results. A selection of different results can be seen in Fig. 3.3.

The average momentum fraction is renormalized with the vector derivative renormalization constant Z_{DV}, which is computed non-perturbatively and converted to the $\overline{\text{MS}}$ scheme at a scale of $\mu = 2\,\text{GeV}$.

From these results, which are close to the physical point, it seems that the deviation from the experimental result is decreasing. However, larger statistics and thus smaller errors, are certainly necessary to confirm this behavior. Here, the computation of the full PDF on the lattice could provide additional input to explain the deviation for larger quark masses. A first attempt to compute this distribution will be presented in Chapter 5. In addition, the lattice result for the singlet momentum fraction $\langle x \rangle_{u+d}$ can be extracted from the computation. This quantity needs to be included in the renormalization of the gluon momentum fraction, which will be addressed in the following chapter.

3.5.3 The quark helicity $\langle x \rangle_{\Delta u - \Delta d}$

Another twist-2 operator that can be studied is the axial-vector derivative operator which, like $\langle x \rangle_{u-d}$, is extracted for zero momentum transfer. It can be used to compute the first moment of the polarized PDF and can be interpreted as the average helicity of quarks in the nucleon.

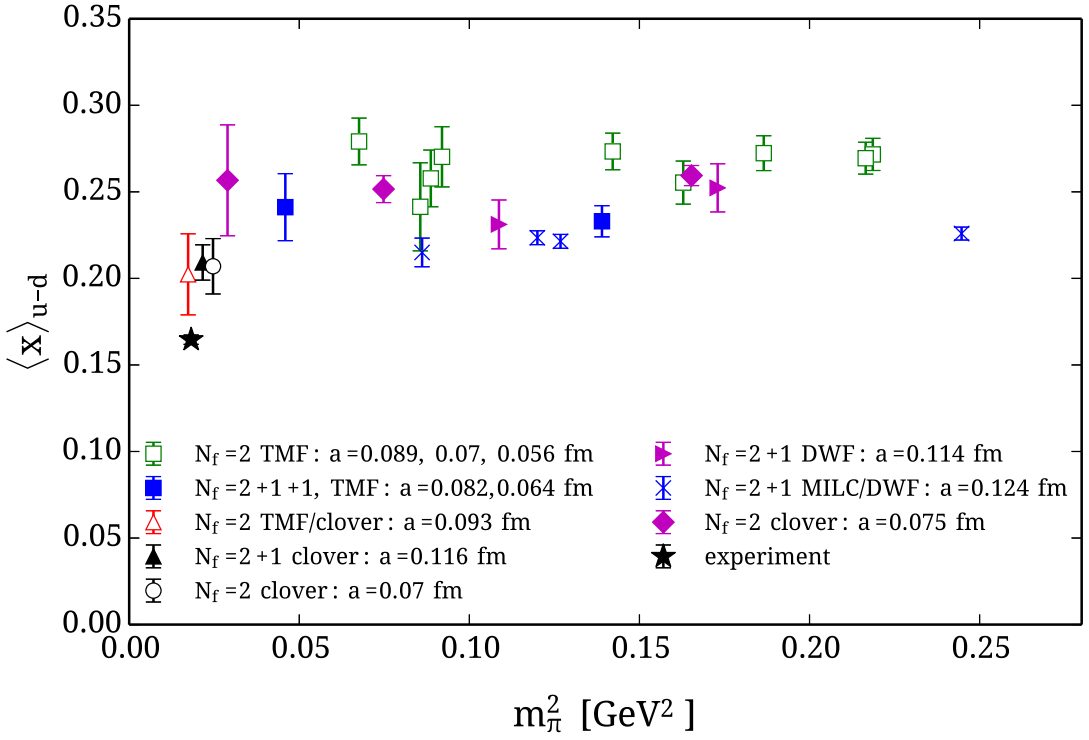

Figure 3.3: Iso-vector nucleon momentum fraction $\langle x \rangle_{u-d}$. Twisted mass fermion results are shown for $N_f = 2$ ensembles (open green squares), for two $N_f = 2+1+1$ ensembles (blue filled square) and for the physical ensemble with a clover term (open red triangle). Also shown are results from RBC-UKQCD using $N_f = 2+1$ DWF (magenta right pointing triangle) [47], from LHPC using DWF on $N_f = 2+1$ staggered sea (blue crosses) [44], QCDSF/UKQCD using $N_f = 2$ clover fermions (filled magenta diamonds) [48], LHPC using $N_f = 2+1$ clover with 2-HEX smearing (filled black triangles) [45] and $N_f = 2$ clover (open black circle) [49]. All values are extracted using the plateau method and $t_s \sim (1-1.2)$ fm, except the result at the physical point for which $t_s \sim 1.3$ fm was used; experimental result from Ref. [50]. The figure is taken from Ref. [23].

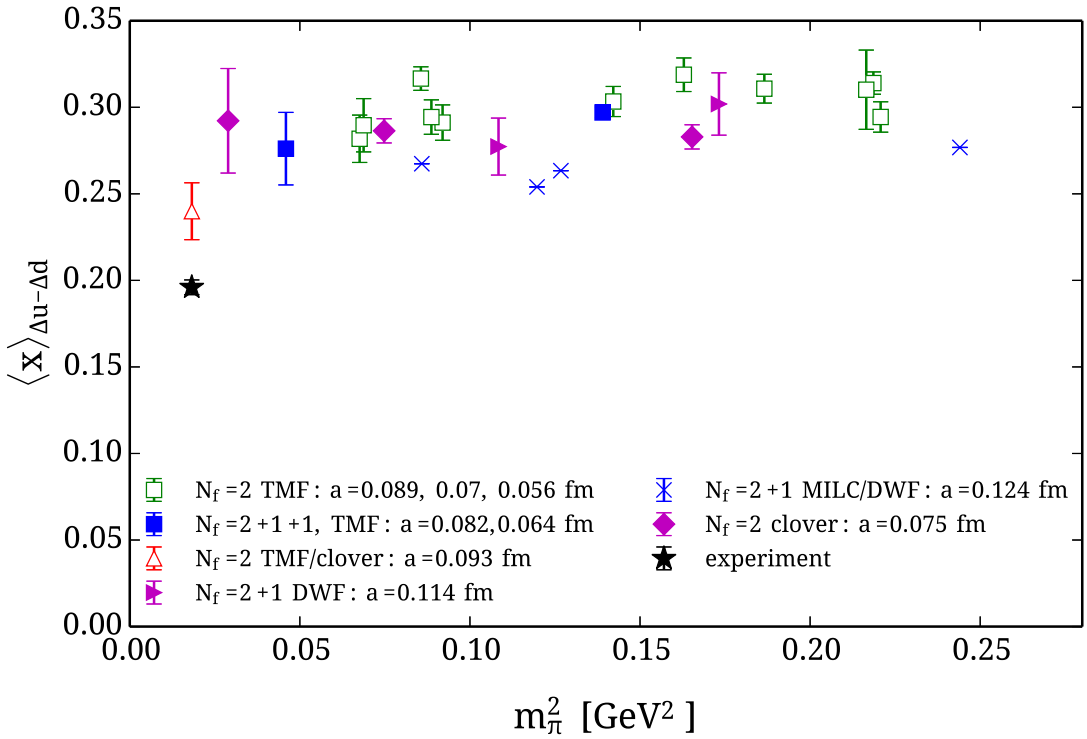

Figure 3.4: Nucleon helicity $\langle x \rangle_{\Delta u - \Delta d}$. Symbols are identical to Fig. 3.3; experimental result from Ref. [51] and figure is taken from Ref. [23].

Again, the operator involves a covariant derivative and has an additional γ_5 matrix in contrast to the vector derivative operator

$$\mathcal{O}_A^{\mu\nu} = \bar{\psi}\gamma^5\gamma^{\{\mu}D^{\nu\}}\tau_3\psi\,. \tag{3.59}$$

From the nucleon matrix element decomposition

$$\langle P|\mathcal{O}_A^{\mu\nu}|P\rangle = i\,\bar{u}(P)\tilde{A}_{20}(0)\gamma_5\gamma^{\{\mu}P^{\nu\}}u(P)\,, \tag{3.60}$$

one can derive

$$\langle x \rangle_{\Delta u - \Delta d} = \tilde{A}_{20}(0) = \frac{i}{m_N} R_{\Gamma_j}\big(N(0); \mathcal{O}_A^{j4}; N(0)\big)\,, \tag{3.61}$$

for the helicity, where Γ_j is the same projector as in the computation of g_A. The physical results are renormalized with the axial-vector derivative renormalization constant Z_{DA} and are shown in Fig. 3.4.

In general, most of the lattice results are significantly larger than the result obtained from phenomenology. Even for the ETMC result that is computed at a physical value of the pion mass, there is still a slight discrepancy present. Again, in order to understand this deviation, the full computation of the polarized PDF will provide valuable information, *cf.* Chapter 5.

4. The gluon content of the nucleon from lattice QCD

Following the introduction to lattice QCD and the short review on latest hadron structure results from the lattice, I will now move on to current research within the ETM collaboration that I contributed to.

This chapter will deal with the calculation of the gluons' average momentum fraction within the nucleon, which can be identified with the first moment of the gluon distribution

$$\langle x \rangle_g = \int dx\, x f_g(x)\,. \tag{4.1}$$

For various reasons, this is an interesting quantity to study, as I will discuss in the following. Since the gluons themselves are partons contributing to the total momentum of the nucleon, their momentum fraction certainly has to be considered in the momentum sum rule, *cf.* Eq. (2.21)

$$\sum_q \langle x \rangle_q + \langle x \rangle_g = 1\,, \tag{4.2}$$

where $\sum_q$ is the sum over all quarks.

The analysis of phenomenological PDF data [19] suggests that at a scale of $Q^2 = 6.25\,\mathrm{GeV}^2$ for example, all quarks only contribute about 57 percent to the total nucleon momentum fraction. This implies that the gluons carry an essential amount of the nucleon momentum so that the momentum sum rule is satisfied.

A further topic that can be studied by the calculation of the gluons' average momentum fraction is the spin structure of the nucleon. According to Ref. [52], the nucleon spin can be decomposed as a gauge invariant sum of the total angular momentum of the gluons and the total angular momentum of the quarks, which itself can be written as a sum of the quarks' spin and orbital angular momentum. This gauge invariant decomposition of the nucleon spin is known as Ji's sum rule and is usually written as

$$\frac{1}{2}\Delta\Sigma_q + L_q + J_g = \frac{1}{2}\,. \tag{4.3}$$

In this sum rule, the gluon's angular momentum can be written in terms of gluon form factors as

$$J_g = \frac{1}{2}(A^g_{20}(0) + B^g_{20}(0))\,. \tag{4.4}$$

The A^g_{20} form factor at zero momentum transfer gives the gluons' average momentum fraction and thus will be available thanks to the computation done in this thesis. In order to obtain the B^g_{20} form factor however, additional calculations with non-zero momentum transfer at the operator have to be performed. Studying the spin structure of the nucleon is particularly interesting because of the nucleon spin puzzle, which states that the quark spin only contributes a surprisingly small fraction to the total nucleon spin [24]. Thus, the remaining fraction must be provided by the gluons or an orbital angular momentum. For a more extensive discussion of the spin puzzle, see Section 4 of Ref. [41] and the references therein.

Therefore, a non-perturbative computation of $\langle x\rangle_g$ can help to understand the momentum and spin structure of the nucleon and confirm the gluons' significant momentum contribution. Yet, despite the fact that there are plenty of results from lattice QCD for the quark structure of the nucleon (see e.g. Refs. [23, 41, 49]), there are currently just a few results for the gluon structure [25, 26, 27]. Moreover, these results are only obtained from quenched computations. In a quenched setup, one neglects the influence of dynamical fermions when generating the gauge field configurations by omitting the fermion determinant, *cf.* Eq. (3.28), in the calculation.

This is why this study aims at giving a first estimate for the gluon content using gauge configurations with dynamical fermions and testing the feasibility of different methods. It is not intended to give a precise value with all systematic effects considered. In the following sections, I will first discuss the theoretical setup employed for the computations. I will introduce two possible methods that can be applied to extract $\langle x\rangle_g$ and compare the feasibility of both methods. I will briefly cover the complicated renormalization pattern of this quantity and finally present results for two different gauge ensembles, one of them at a physical value of the pion mass.

4.1 Theoretical setup

The gluon momentum fraction $\langle x\rangle_g$ can be identified with the $A^g_{20}(0)$ form factor that can be extracted from matrix elements of the gluon operator, which is the gauge part of the QCD energy momentum tensor, as pointed out in Ref. [53]

$$\langle P|T_g^{\{\mu\nu\}}|P\rangle = 2A^g_{20}(0)P^{\{\mu}P^{\nu\}}\,, \tag{4.5}$$

where the normalization $\langle P|P\rangle = 2E$ was used and $\{\cdots\}$ is again symmetrization and subtraction of the trace, *cf.* Eq. (2.25).

The gluonic energy momentum tensor is defined as

$$T_g^{\{\mu\nu\}} = \frac{1}{4} g^{\mu\nu} F_{\alpha\beta} F^{\alpha\beta} - F^{\mu\sigma} F_{\sigma}{}^{\nu}, \tag{4.6}$$

where $F_{\mu\nu} = T^a F^a_{\mu\nu}$ which is given in Section 3.1. Here and in the following equations, a trace over the implicit color indices of the field strength tensor and later also the plaquette term is present.

Following the conventions used in Refs. [25, 26], one can now construct the following Euclidean operator from the gluon field strength tensor,

$$\mathcal{O}_{\mu\nu} = -F_{\mu\sigma} F_{\nu\sigma} \,. \tag{4.7}$$

From this tensor operator, one can define the following vector and scalar operators

$$\mathcal{O}_{Ai} = \mathcal{O}_{i4} \tag{4.8}$$

$$\mathcal{O}_B = \mathcal{O}_{44} - \frac{1}{3} \mathcal{O}_{jj} \,. \tag{4.9}$$

With the help of Eq. (4.5), the matrix elements of these operators can be directly related to $\langle x \rangle_g$ as

$$\langle P | \mathcal{O}_{Ai} | P \rangle = -2iEP_i \langle x \rangle_g \tag{4.10}$$

$$\langle P | \mathcal{O}_B | P \rangle = 2(E^2 - \frac{1}{3}\mathbf{P}^2) \langle x \rangle_g \,. \tag{4.11}$$

Eq. (4.10) indicates that in order to extract the gluon momentum fraction from matrix elements of $\mathcal{O}_A$, a non-zero momentum for the nucleon fields is required, whereas the kinematic factor for operator $\mathcal{O}_B$ stays finite for zero momentum. Since nucleon fields with zero momentum are known to feature a better signal-to-noise ratio than boosted nucleon fields, the first choice for the operator will be $\mathcal{O}_B$. Extracting $\langle x \rangle_g$ from $\mathcal{O}_A$ to study the quality of the signal and compare it to $\mathcal{O}_B$ would certainly be an interesting task for future research.

As explained earlier, the zero momentum form factors can be extracted on the lattice by computing

$$R\big(N(0); \mathcal{O}_B; N(0)\big) = m_N \langle x \rangle_g \,, \tag{4.12}$$

where the definition of R is given in Eq. (3.52).

One can now utilize Eq. (4.7) in order to express the operator in terms of the field strength tensor

$$\mathcal{O}_B = \frac{2}{3} \sum_i \sum_{j<k} \left(F^2_{jk} - F^2_{4i} \right) \,. \tag{4.13}$$

On the lattice, the field strength tensor can be related to the plaquette terms in the following way, *cf.* Eq. (3.6)

$$U_{\mu\nu}(x) = \exp\big(iga^2 F_{\mu\nu} + \mathcal{O}(a^3) \big) \,. \tag{4.14}$$

When performing a Taylor expansion of the right-hand side, one finds that the field strength tensor can eventually be isolated by computing

$$\mathrm{Re}(1 - U_{\mu\nu}(x)) = \frac{1}{2} g^2 a^4 F_{\mu\nu}^2 = \frac{3}{\beta} a^4 F_{\mu\nu}^2 \,. \tag{4.15}$$

Consequently, the $\mathcal{O}_B$ operator can be written by means of plaquette terms as

$$\mathcal{O}_B = \frac{2}{9} \frac{\beta}{a^4} \left(\sum_i \mathrm{Re}(U_{i4}) - \sum_{i<j} \mathrm{Re}(U_{ij}) \right) . \tag{4.16}$$

The crucial part when calculating the operator is the subtraction of the plaquettes. Here, two large quantities which are yet very similar in magnitude have to be subtracted. Hence, the precision of the result will depend on the correlation of the two terms. Nevertheless, precise measurements are certainly required to calculate the form factors.

The next challenge is to find a suitable method to compute the left-hand side of Eq. (4.12) on the lattice. In following sections, two possible methods to do so will be presented.

4.2 The Feynman-Hellmann theorem

One possible approach to extract $\langle x \rangle_g$ can be found in Ref. [26]. Here, an Euclidean lattice version of the Feynman-Hellmann theorem is employed. The original quantum mechanical form of this theorem was for example proposed by Feynman in Ref. [54].

Furthermore, the Feynman-Hellmann theorem has already been used on the lattice, for example to calculate the axial charge g_A [55] or the pion-nucleon sigma term [56].

The theorem states that if one includes a λ dependent operator $\lambda\mathcal{O}$ into the action of the system, the operator's nucleon form factors can be related to the derivative of the nucleon energy with respect to λ. Naturally, this can be extended to any hadronic state.

A convenient approach to show this relation is to compute the derivative of the zero momentum nucleon two-point correlation function with respect to λ. When starting at the path integral representation of the two-point correlation function, *cf.* Eq. (3.25), one obtains

$$\frac{\partial}{\partial\lambda} \big\langle N(t)\overline{N}(0) \big\rangle = \big\langle N(t) \frac{\partial S(\lambda)}{\partial\lambda} \overline{N}(0) \big\rangle - \big\langle N(t)\overline{N}(0) \big\rangle \big\langle \frac{\partial S(\lambda)}{\partial\lambda} \big\rangle \,. \tag{4.17}$$

For simplicity $\sum_{\mathbf{x}} \big\langle N(x)\overline{N}(x') \big\rangle$ is written here as $\big\langle N(t)\overline{N}(0) \big\rangle$.

On the other hand, one can express the two-point correlation function by the spectral decomposition like in Eq. (3.35)

$$\big\langle N(t)\overline{N}(0)\big\rangle = A_N(\lambda)e^{-E_N(\lambda)t}\,, \tag{4.18}$$

where the derivative of this expression is

$$\frac{\partial}{\partial\lambda}\big\langle N(t)\overline{N}(0)\big\rangle = -\frac{\partial E_N(\lambda)}{\lambda}\,t\,A_N(\lambda)e^{-E_N(\lambda)t} + \frac{\partial A_N(\lambda)}{\partial\lambda}e^{-E_N(\lambda)t}\,. \tag{4.19}$$

For large time separations t, only the first term has to be considered and the equation can be rewritten as

$$\frac{\partial}{\partial\lambda}\big\langle N(t)\overline{N}(0)\big\rangle = -\frac{\partial E_N(\lambda)}{\lambda}\,t\,\big\langle N(t)\overline{N}(0)\big\rangle\,. \tag{4.20}$$

To proceed further, one can now compare the right-hand sides of Eq. (4.17) and Eq. (4.19) to obtain

$$-\frac{\partial E_N(\lambda)}{\lambda}\,t = \frac{\big\langle N(t)\frac{\partial S(\lambda)}{\partial\lambda}\overline{N}(0)\big\rangle}{\big\langle N(t)\overline{N}(0)\big\rangle} - \big\langle\frac{\partial S(\lambda)}{\partial\lambda}\big\rangle\,. \tag{4.21}$$

Here, the operator $\partial S(\lambda)/\partial\lambda$ contains an implicit sum over the insertion time τ due to the nature of the action. From the application of the summation method, *e.g.* see in Ref. [57], it is known that

$$\sum_{\tau=0}^{t} R\big(N(P);\mathcal{O}(\tau);N(P)\big) = tR\big(N(P);\mathcal{O}(\tau);N(P)\big)\,. \tag{4.22}$$

Applying this relation to Eq. (4.21) thus yields

$$\frac{\partial E_N(\lambda)}{\partial\lambda} = R\big(N(P);\frac{\partial S(\lambda,\tau)}{\partial\lambda};N(P)\big) - \big\langle\frac{\partial S(\lambda,\tau)}{\partial\lambda}\big\rangle\,. \tag{4.23}$$

The second term is the vacuum expectation value of the operator which has to be subtracted.

Hence, in order to extract the gluon momentum fraction, is it helpful to alter the Wilson gauge action in the following way

$$S(\lambda) = \frac{\beta}{3}\sum_x\left((1+\lambda)\sum_i \mathrm{Re}(1-U_{i4}(x)) + (1-\lambda)\sum_{i<j}\mathrm{Re}(1-U_{ij}(x))\right)\,, \tag{4.24}$$

where $\lambda = 0$ corresponds to the standard Wilson plaquette action. The reason of this modification can be understood when looking at the derivative of the action appearing in Eq. (4.23)

$$\frac{\partial S(\lambda)}{\partial\lambda} = \frac{\beta}{3}\sum_x\left(\sum_{i<j}\mathrm{Re}(U_{ij}(x)) - \sum_i \mathrm{Re}(U_{i4}(x))\right)\,, \tag{4.25}$$

which can be related to $\mathcal{O}_B$ by Eq. (4.16). Consequently, one can relate the left-hand side of Eq. (4.23) to $\langle x \rangle_g$ by using Eq. (4.11) and finds

$$\frac{\partial E_N}{\partial \lambda}\Big|_{\lambda=0} = -\frac{3}{2}\left(E_N - \frac{\mathbf{P}^2}{3E_N}\right)\langle x \rangle_g \,. \tag{4.26}$$

This relation only holds if the vacuum expectation value of the operator vanishes $\langle \Omega | \mathcal{O}_B | \Omega \rangle = 0$. In the present setup, this is certainly the case due to rotational symmetry on the lattice, which implies that the vacuum expectation value of temporal and spatial plaquettes is equal.

When considering the nucleon at rest, one can simplify Eq. (4.26) and compute the gluon momentum fraction as

$$\langle x \rangle_g = \frac{2}{3m_N}\frac{\partial m_N}{\partial \lambda}\Big|_{\lambda=0} \,. \tag{4.27}$$

Next, in order to compute the derivative at $\lambda = 0$, several values for the nucleon mass at different λ values are required. It is assumed that for λ close to zero, $m_N(\lambda)$ can be approximated by a linear function so that the derivative at $\lambda = 0$ can be extracted from the slope of a linear fit.

In order to compute the nucleon mass for non-zero λ values of the action, new gauge ensembles have to be generated. This, however, induces certain difficulties, because due to the change of the action the hopping parameter κ has to be re-tuned to its critical value κ_{cr} for each ensemble in order to regain the automatic $O(a)$ improvement, *cf.* Section 3.3.

To explore the feasibility of this method an initial test was conducted on a small lattice with rather heavy quark masses to keep the computational cost affordable. The simulations are carried out on $24^3 \times 48$ lattices with $N_f = 2 + 1 + 1$ flavors of maximally twisted mass fermions. The coupling is set to $\beta = 1.95$ corresponding to a lattice spacing of $a \approx 0.082\,\text{fm}$. The twisted mass parameter is chosen to be $a\mu = 0.085$, which amounts to a pion mass of $m_{PS} \approx 490$ MeV. As gauge action the Iwasaki action [35] is used. However, only the Wilson part, *i.e.* the pure plaquette part, is multiplied with $1 \pm \lambda$ as in Eq. (4.24). The rectangular plaquettes remained untouched. The results for three different λ values on ~ 200 gauge configurations and the nucleon mass at $\lambda = 0$ which is taken from Ref. [58], are shown in Fig. 4.1.

In order to extract $\langle x \rangle_g$, a linear fit in λ is applied to the data. The fact that the data shows a λ dependence suggests that one can obtain a non-zero signal for the gluon moment. From the result for the slope, one can extract the following bare lattice result

$$\langle x \rangle_g^{bare} = 0.46(14) \,. \tag{4.28}$$

The statistical error of the result is rather large, but the systematic error is probably even larger, because it is not fully clear in which λ region a linear fit is justified. To study this systematic effect, one has to compute the nucleon mass with a better

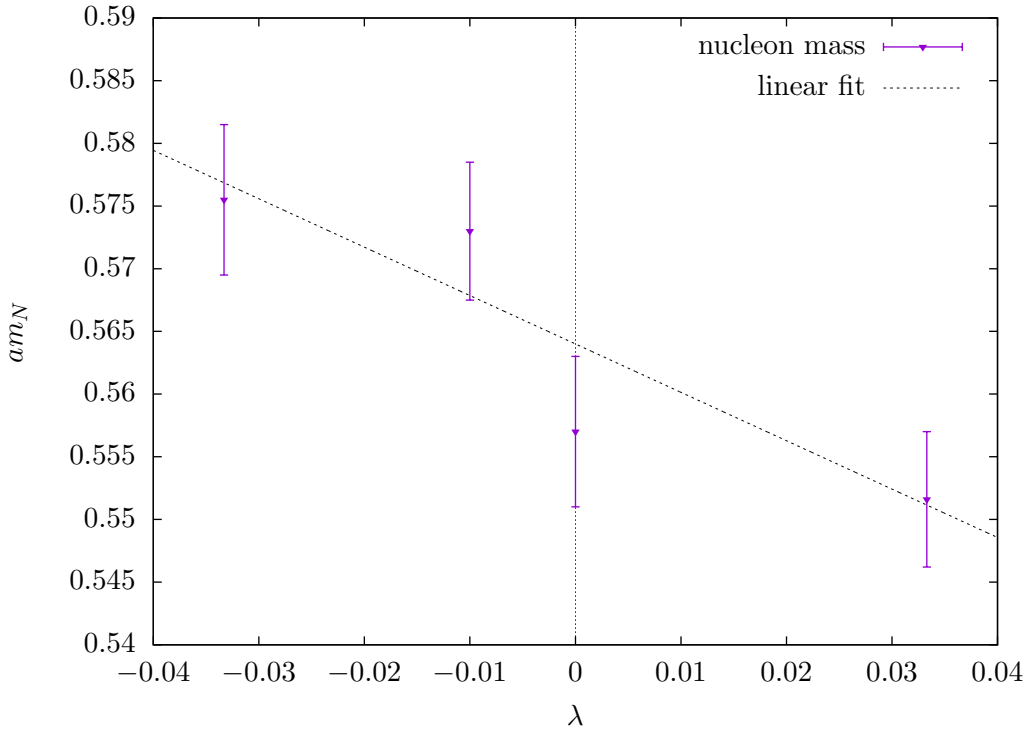

Figure 4.1: Results for the nucleon mass as a function of λ. Linear fit parameters: $am_N = -0.39(12)\lambda + 0.563(3)$. The nucleon mass at $\lambda = 0$ is taken from Ref. [58].

precision for more λ points than used here. Furthermore, the plateau fit that is used to extract the nucleon masses introduces yet another uncertainty.

All in all, it is possible to employ the Feynman-Hellmann theorem to extract the gluon momentum fraction. However, there are rather large systematic uncertainties and the method is quite costly, especially for twisted mass fermions where the action has to be re-tuned to maximal twist for each new λ. Therefore, the method seems quite unfeasible, in particular for large lattices and pion masses close to the physical point.

4.3 Direct operator approach

Since the application of the Feynman-Hellmann theorem has proved to be rather cumbersome, an alternative, more straightforward method is tested in this work. It involves the direct computation of the right-hand side of Eq. (4.12), *i.e.* the computation of relevant three- and two-point functions in terms of quark propagators and gluon loops as well as the extraction of the form factors as it was explained in the previous chapter. The gluon content can be extracted as

$$\langle x \rangle_g = \frac{1}{m_N} R\left(N(0); \mathcal{O}_B; N(0)\right) . \tag{4.29}$$

For this purpose, the relevant unprojected three-point function is the expectation value of two nucleon fields and the operator $\mathcal{O}_B$

$$C^{3\mathrm{pt}}(t, \tau, t'; \mathbf{P} = 0) = \frac{2}{9}\beta \sum_{\mathbf{x},\mathbf{y}} \left\langle N(x) \left(\sum_{i<j} \mathrm{Re}(U_{ij}(y)) - \sum_i \mathrm{Re}(U_{i4}(y)) \right) \overline{N}(x') \right\rangle . \tag{4.30}$$

The definition of the nucleon operator in terms of quark fields can be found in Eq. (3.36), while the operator can be written by means of plaquette terms as shown in Eq. (4.16). Thus, because there are no quark fields in the operator, performing the Wick contractions in the three-point function is a trivial task, as there are no possible contractions between the gluon operator and the interpolating fields of the nucleon. The three-point function can in fact be written as the expectation value of a product of nucleon correlators with a gauge link dependent operator. A schematic image of the resulting diagram was shown in the previous chapter at the bottom part of Fig. 3.1.

The advantage of this method is that existing two-point functions can be re-used and only the gluon operator has to be calculated on the very same configurations by computing the plaquette terms from the gauge links. This can be done with rather small computational effort. Since this is a disconnected diagram, the subtraction of the expectation value of $\mathcal{O}_B$ from the ratio R generally has to be performed. Technically, this is not necessary in this setup, because the vacuum expectation

	N_f	β	$L/a, T/a$	c_{sw}	κ	$a\mu$	m_{PS} [MeV]	a [fm]
B55.32	2+1+1	1.95	32,64	0	0.161236	0.0055	370	0.082
cA2.09.48	2	2.1	48,96	1.57551	0.13729	0.0009	130	0.093

Table 4.1: Parameters of two different gauge ensembles that were used in the computation of the gluon moment.

value of the operator is supposed to vanish as was explained earlier. Nevertheless, the expectation value of the operator is rather noisy. Hence, it is beneficial to subtract the term in this case.

4.4 Lattice setup

The results shown in this work are computed on two different gauge ensembles. The first being a $32^3 \times 64$ lattice from an ETMC (European Twisted Mass Collaboration) production ensemble [59] labeled **B55.32**. It features $N_f = 2 + 1 + 1$ flavors of maximally twisted mass fermions, *i.e.* two degenerate light quarks and non-degenerate strange and charm quarks. The ensemble has a bare coupling corresponding to $\beta = 1.95$, which yields a lattice spacing of $a \approx 0.082\,\mathrm{fm}$ [60] and the twisted mass parameter $a\mu = 0.0055$, corresponding to a pion mass of $m_{PS} \approx 370\,\mathrm{MeV}$. The two-point correlation functions were provided by the ETMC as well and computed with 15 different source positions on each of the 2298 gauge field configurations. This sums up to 34470 measurements each, for proton and neutron and two different time directions, which all can be averaged. Admittedly, these measurements are slightly correlated, yet, several tests suggest an error scaling close to $1/\sqrt{N}$.

A second ensemble labeled **cA2.09.48** that has recently been generated is used to compute $\langle x \rangle_g$ as well and has the feature of a physical value of the pion mass [61]. Here, $N_f = 2$ flavors of maximally twisted mass fermions are employed, together with a clover term and $c_{sw} = 1.57551$ on a $48^3 \times 96$ lattice. The bare coupling corresponds to $\beta = 2.1$, which is a lattice spacing of $a \approx 0.093\,\mathrm{fm}$ set with the nucleon mass. The twisted mass parameter is set to $a\mu = 0.0009$, which corresponds, within errors, to a setup with physical pion masses. The analysis is done on 1558 configurations with 100 different source positions each, which amounts to a total of 155800 measurements.

For the quark fields that make up the nucleon interpolating field, standard smearing methods (Gaussian and APE) were used, which are known to increase the overlap of the fields with the nucleon ground state while decreasing the overlap with excited states and thus improving the results for nucleon spectroscopy and structure, *cf.*

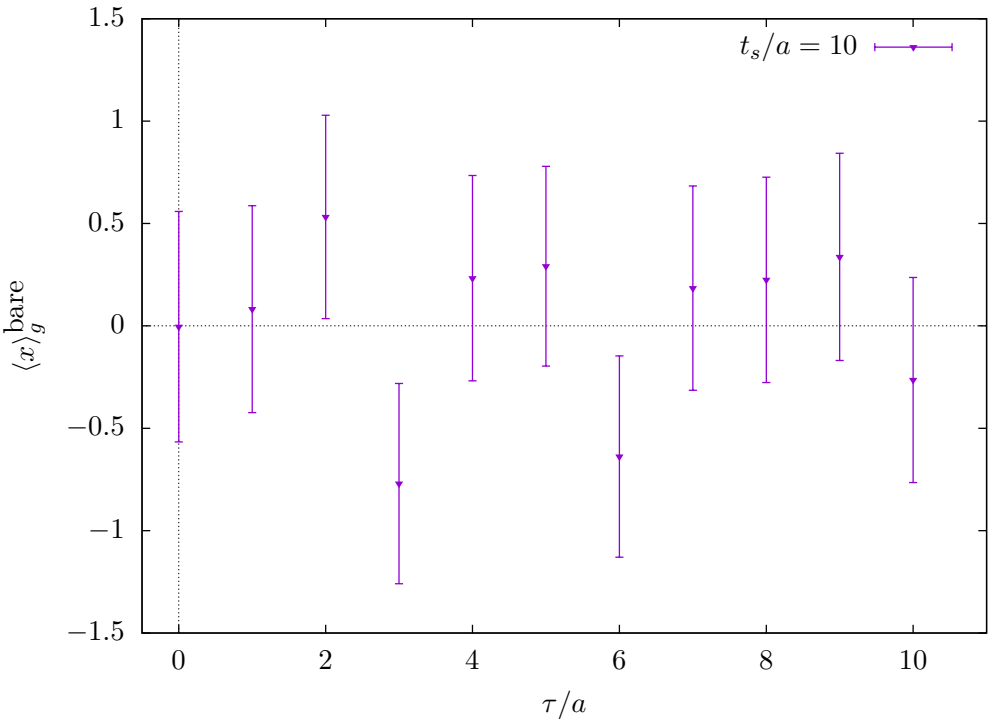

Figure 4.2: Results for the effective gluon momentum fraction as a function of the operator insertion time with 34470 measurements on the B55.32 ensemble, *cf.* Tab. 4.1. No smearing was applied to the operator.

Ref. [41] and references therein. In fact, 50 steps of Gaussian smearing with $\alpha = 4$ were applied to the quark fields while the gauge fields that were used for this purpose are smeared with 20 steps of APE smearing with $\alpha = 0.5$.

4.5 Results and stout smearing

Initial results for the effective gluon momentum fraction are shown in Fig. 4.2. The effective gluon momentum fraction denotes the τ dependent result of Eq. (4.29) where $\langle x \rangle_g$ can be extracted from a constant fit to an existing plateau. Unfortunately, the thus obtained signal is too noisy to extract any significant result.

One possible solution for this problem can be found in [62], where it is suggested to use HYP smearing [63] for the links in the gluon operator. Initial tests with up to five steps of HYP smearing with parameters from [63] were successful, however this smearing is not well suited for the purpose of renormalization by a perturbative lattice calculation. Since HYP smearing cannot be expressed as an analytic function and the gauge links need to be re-projected to SU(3) after each step of smearing, the perturbative lattice calculation is not feasible due to the enormous computational

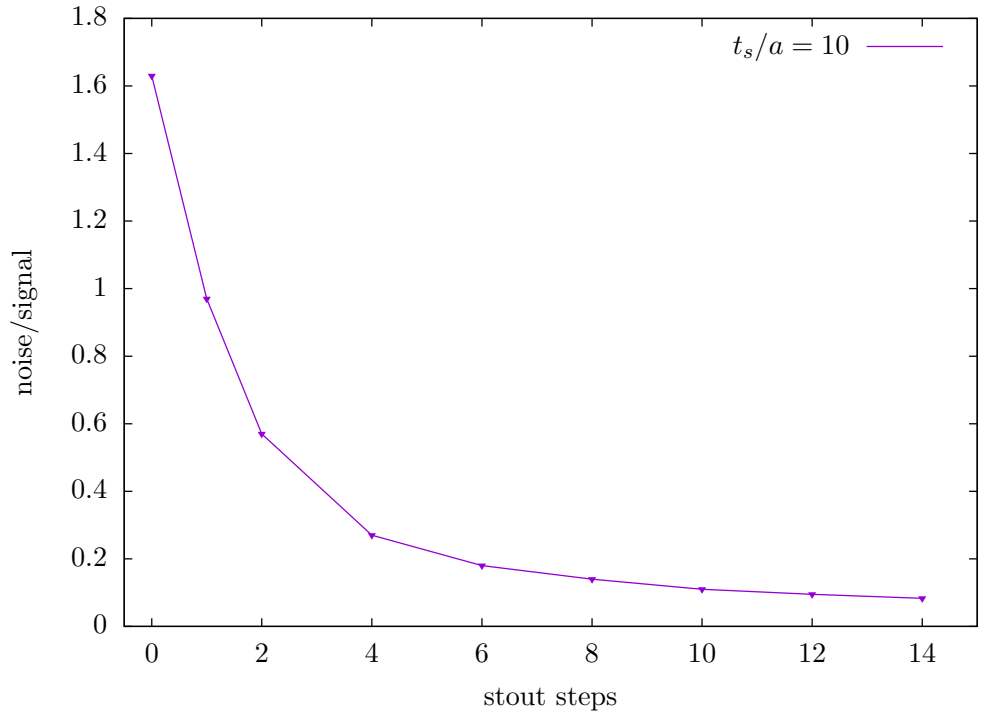

Figure 4.3: Noise-to-signal ratio as a function of the number of stout smearing steps. Noise-to-signal ratio is the average error of plateau values divided by result of a plateau fit for 10 steps of smearing. B55.32 ensemble was used, *cf.* Tab. 4.1.

effort it involves.

Instead, stout smearing of the gauge links as introduced in Ref. [64] is used in this work. This is an analytic link smearing method where the gauge links are smeared according to

$$U_\mu^{(n+1)} = \exp\left(iQ_\mu^{(n)}\right) U_\mu^{(n)}\,, \tag{4.31}$$

where Q_μ is a particular linear combination of perpendicular gauge link staples that are weighted with the factor[1] ω, *cf.* Ref. [64] for details. In this work, the isotropic four-dimensional scheme is used and ω is tuned so that the plaquette reaches a maximal value. Up to 14 steps of stout smearing were applied and the noise-to-signal ratio of the result was determined, by computing the average error of the plateau values and weighting it with a generic plateau value that was extracted using 10 steps of smearing. The noise-to-signal ratio as a function of the number of stout smearing steps is shown in Fig. 4.3.

A significant reduction of the resulting noise with an increasing number of stout smearing steps can be observed from this analysis. While the improvement for a

[1] This parameter is called ρ in the original work, but in recent works and in this thesis is labeled as ω.

	$\langle x \rangle_g^{\text{bare}}$	Z_{gg}	Z_{gq}	$\langle x \rangle_{u+d}^{\text{bare}}$	$\langle x \rangle_g$
B55.32	0.300(25)	1.0134	0.0084	0.677(5)	0.309(25)
cA2.09.48	0.28(4)	0.9590	0.0218	0.522(16)	0.28(4)

Table 4.2: Bare and renormalized lattice results for the gluon moment along with the perturbatively computed Z factors at $\mu = 2\,\text{GeV}$ in the $\overline{\text{MS}}$ scheme and the iso-scaler quark moment on two different gauge ensembles. Iso-scalar quark moments are taken from Ref. [23] with ${}^{t_s}/_a = 12$. For $\langle x \rangle_g^{\text{bare}}$, only statistical errors are given.

smaller number of steps is quite substantial, one notices a saturation for a larger number of steps. Thus, in order to not overextend the smearing, 10 steps of stout smearing with the parameter $\omega = 0.1315$ are used in this work. The results are shown in Fig. 4.4.

In contrast to the results involving an unsmeared operator, one now obtains a rather distinct signal with a reasonable error. In order to analyze the influence of excited states on the plateau value, results for three different source-sink separations $t_s = t - t'$ are shown. Usually, a strong excited state influence is present if the plateau values differ for different t_s. Such a discrepancy cannot be observed for this setup, since the computed points belonging to the plateau are compatible within errors for different separations. Finally, the lattice value of the gluon moment is extracted from a plateau fit on the ${}^{t_s}/_a = 12$ data and is shown in Tab. 4.2.

The results for the second ensemble with a physical value of the pion mass are presented in Fig. 4.5. Again, one obtains a rather distinct signal. However, the noise is larger than for the previous ensemble, thus smaller source-sink separations are featured in the figure. Still, there is no evidence of a large influence of excited states.

The lattice value of the gluon momentum fraction is extracted from a plateau fit on the ${}^{t_s}/_a = 11$ data and given in Tab. 4.2. The error is rather large in comparison to the previous result. Therefore a larger statistic is certainly necessary here in order to extract a more precise signal. These results differ slightly from the one that was extracted by using the Feynman-Hellmann theorem. However, the two lattice results cannot be compared, since the application of stout smearing certainly alters the way the gluon operator has to be renormalized. As it turns out, the renormalization pattern of this quantity is rather delicate due to the mixing of operators. In the following section, this issue will be explained in some more detail.

4.6 Renormalization

Yet another challenge regarding the computation of the physical value of the gluon momentum fraction is the fact that the lattice result has to be renormalized. Since

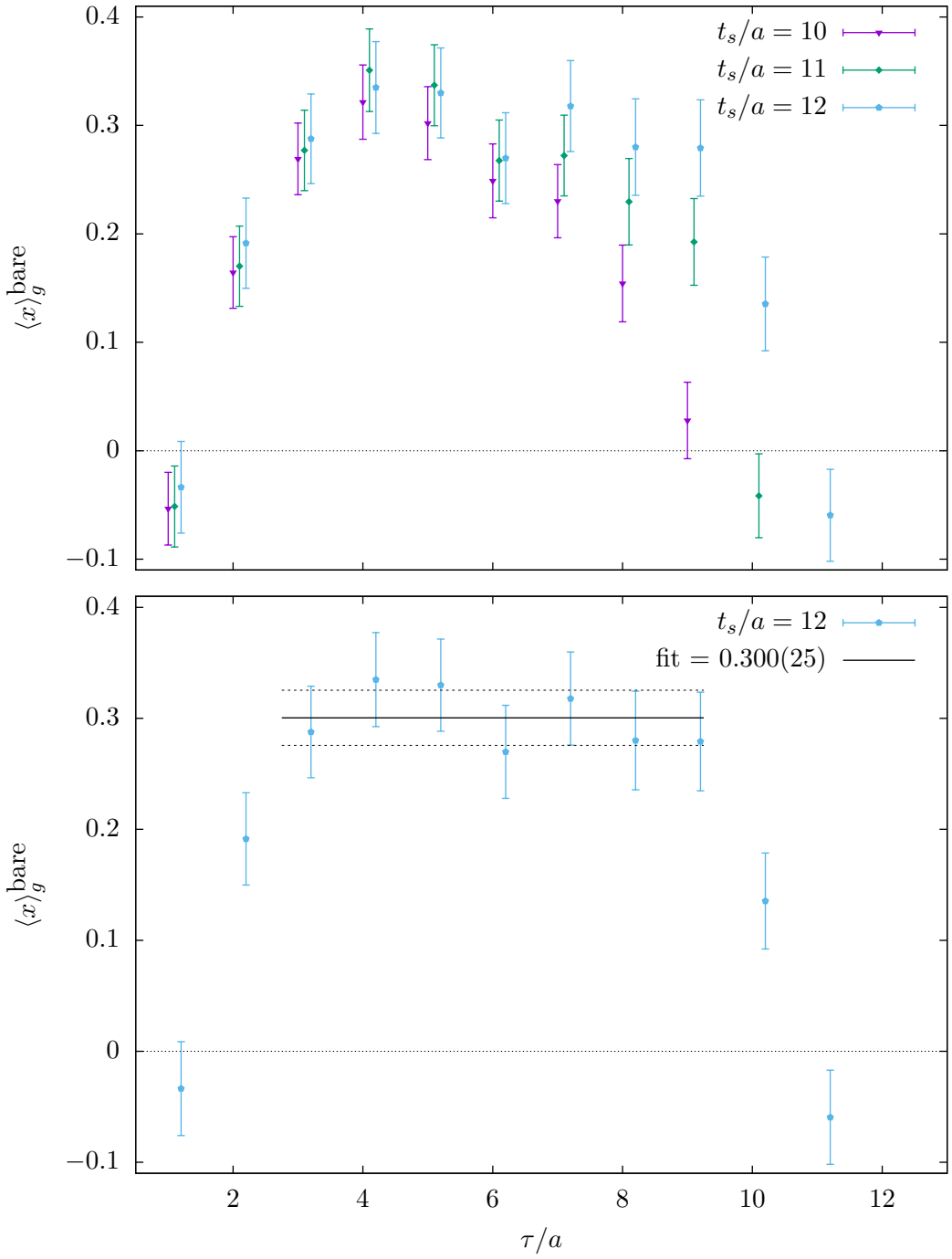

Figure 4.4: top: Results for the effective gluon momentum fraction as a function of the operator insertion and different source-sink separations. 10 steps of stout smearing were applied to the operator. **bottom:** $\langle x \rangle_g^{\text{bare}}$ is extracted from a constant fit to the plateau of $t_s/a = 12$. 34470 measurements on the B55.32 ensemble were used, *cf.* Tab. 4.1.

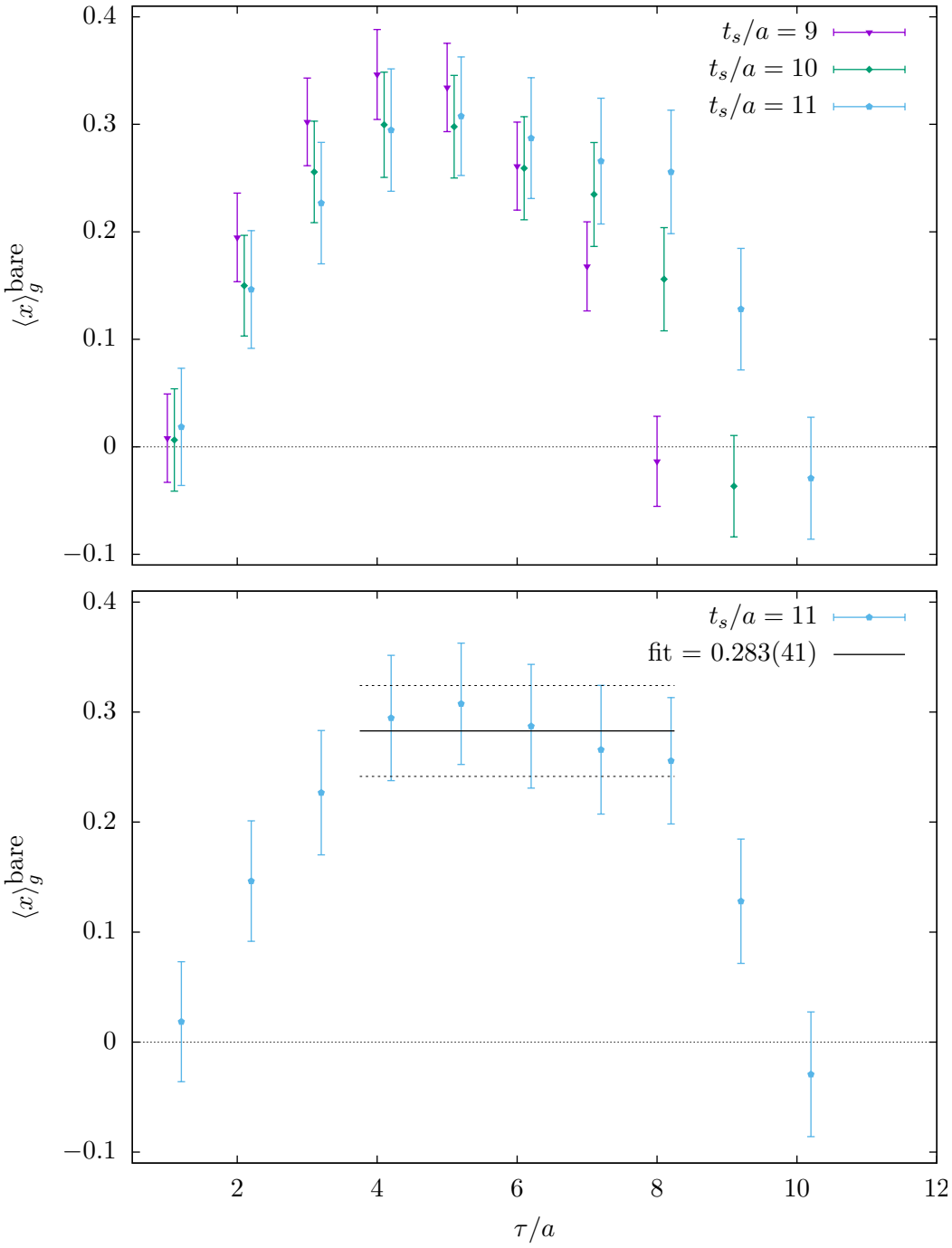

Figure 4.5: top: Results for the effective gluon momentum fraction as a function of the operator insertion and different source-sink separations. 10 steps of stout smearing were applied to the operator. **bottom:** $\langle x \rangle_g^{\text{bare}}$ is extracted from a constant fit to the plateau of $t_s/a = 11$. 155800 measurements on the cA2.09.48 ensemble were used, *cf.* Tab. 4.1.

the gluon operator is a singlet operator, it certainly mixes with other singlet operators, for example the quark operator. Consequently, $\langle x \rangle_g$ mixes with the quark momentum fraction $\langle x \rangle_q$. The mixing of these quantities has been studied in Ref. [65] and can be described by a 2×2 mixing matrix

$$\begin{pmatrix} \langle x \rangle_g \\ \sum_q \langle x \rangle_q \end{pmatrix} = \begin{pmatrix} Z_{gg} & Z_{gq} \\ Z_{qg} & Z_{qq} \end{pmatrix} \begin{pmatrix} \langle x \rangle_g^{\text{bare}} \\ \sum_q \langle x \rangle_q^{\text{bare}} \end{pmatrix}. \tag{4.32}$$

Thus, the physical result of the gluon momentum fraction can be related to the lattice results for $\langle x \rangle_g$ and $\langle x \rangle_q$ by

$$\langle x \rangle_g = Z_{gg} \langle x \rangle_g^{\text{bare}} + Z_{gq} \sum_q \langle x \rangle_q^{\text{bare}}, \tag{4.33}$$

where a certain scheme, *e.g.* $\overline{\text{MS}}$ and an energy scale μ have to be chosen.

In this setup, however, it is not yet known how to define a renormalization condition in order to extract the factors from a non-perturbative lattice calculation, as it has been done for other operators relevant for nucleon structure [66]. Thus, a different approach has to be found.

The initial method of choice is a one-loop perturbative lattice computation. Details of this rather difficult calculation will be published Ref. [67]. Results for the Z factors at a scale of 2 GeV in the $\overline{\text{MS}}$ scheme can be found in Tab. 4.2. These factors were computed for operators with a maximum of two steps of stout smearing, because a larger number of steps is not feasible to compute anymore. Still, a clear saturation in particular for Z_{gg} can be observed when comparing the results for zero, one and two steps of smearing. Consequently, the Z factors for two steps of stout smearing are used to renormalize $\langle x \rangle_g$. The necessary iso-scalar quark moments were taken from Ref. [23]. The resulting gluon momentum fractions can be found in Tab. 4.2 as well.

4.7 Conclusion and outlook

In this chapter, two methods were tested which can potentially be used to obtain an accurate value for the gluon momentum fraction of the nucleon $\langle x \rangle_g$ from a lattice QCD calculation. The first method makes use of the Feynman-Hellman theorem and has the advantage of yielding a statistically significant signal for a rather moderate number of configurations. On the downside, the calculation needs dedicated simulations with different values of λ to establish the linear dependence of the results on λ in an unambiguous way. Furthermore, each simulation has to be tuned to a critical value of κ in order to ensure automatic $\mathcal{O}(a)$ improvement. Therefore, the computational cost associated with this method is too large for it to be feasible, especially when aiming at lattice simulation at a physical value of the pion mass.

The second method directly computes $\langle x \rangle_g$ from a ratio of three- and two-point correlation functions of the nucleon. In this setup, the three-point functions are purely disconnected and thus can be written as the expectation value of a product of a two-point correlator and the gluon operator on each configuration. In order to obtain a non-zero signal, one can apply several steps of stout smearing to the gauge links forming the gluon operator. Admittedly, the amount of nucleon two-point correlation functions that are needed to extract a significant signal is large. However, if existing correlators can be used the overall cost is rather small.

Thus, I employed the direct approach for an extensive study and obtained lattice results for the gluon momentum fraction on two different lattice ensembles, including an ensemble with a physical value of the pion mass. These results could be related to the physical value through a one-loop perturbative lattice calculation of the relevant renormalization and mixing factors.

To compare the results to phenomenological data one can use the PDF data that is provided by several groups and can be accessed via the LHAPDF library [68]. Here, data points for various x and Q^2 are given so that arbitrary x and Q^2 data can be obtained by an interpolation. The moments of PDFs can then be calculated by numerical integration of the data. Using ABM12 data [19] for example, one obtains a value of $\langle x \rangle_g \approx 0.43$ for a scale of $Q^2 = 6.25\,\mathrm{GeV}^2$. Due to the nature of the simplified analysis here employed, this is not a precision results and no error is given, although it will not exceed 5 percent. In the future, it would certainly be helpful to have a better value with a realistic error estimate from some expert groups extracting PDFs. Obviously, the results that were obtained from the lattice are clearly smaller than what the analysis of experimental data suggests. This issue should certainly be addressed in future studies. Note, however, that in the analysis presented here no continuum limit is performed and the systematic errors are not yet included.

Among possible goals for future projects should clearly be the reduction of the error in order to make precise predictions for $\langle x \rangle_g$. Of course, this can be achieved by an increase of statistics, which involves severe computational costs though. An other possibility might be to study the feasibility of using the operator $\mathcal{O}_A$ to extract the relevant form factors. A further interesting project is the computation of the gluon contribution to the nucleon spin. However, the computation of the B^g_{20} form factor that is additionally needed in this case is highly demanding, because it requires the computation of a three-point correlation function with momentum transfer at the operator. It remains to be seen if it is even possible to extract a meaningful signal for this quantity. Since the method that was used in this study can easily be generalized to other hadrons, the computation of the pion's gluon content is another possible project. Here, the existing gluon loops have to be contracted with pion two-point correlation functions. Concerning the renormalization, the possibility to utilize the findings of the perturbative renormalization in order to perform a non-perturbative renormalization should certainly be explored.

5. Quark distributions from lattice QCD

In the last chapter of my work, I will present another lattice study I contributed to, namely the determination of parton distribution functions directly from lattice QCD. This thesis is based on, but also extends a study recently published in Ref. [69].

It has already been stressed in Chapter 2 that parton distribution functions provide an important insight into the structure of hadrons by giving information on the momentum distribution of quarks and gluons in the hadron. In addition, the generalized parton distributions (GDPs) provide access to further quantities such as angular momentum and spin distribution [16].

Consequently, a direct prediction of the parton distributions from quantum chromodynamics would be desirable, because the results could be directly confronted with results from deep inelastic scattering and other experiments and thus used as a rigorous test of QCD. Also, it would provide precious information on the interactions between quarks and gluons in the nucleon.

Since an analytic determination of PDFs from QCD is not possible though, reliable parton distributions can only be obtained through the phenomenological analysis of experimental results, as has been done in Refs. [17, 18, 19], for instance. These groups provide precise PDFs at various values of Q^2, yet the result strongly depends on the choice of experimental data included and the form of the fit that is used, among other factors.

Naturally, lattice QCD methods, which can provide *ab initio* results for a variety of QCD observables would be most suitable for an alternative determination of PDFs and could avoid the intermediate phenomenological step. Yet, such a calculation requires light-cone dynamics or an infinite momentum frame. Both cannot be fulfilled on an Euclidean space-time lattice, because a non-zero and in practice rather large lattice spacing makes it impossible to go to zero distance or employ an infinite momentum. Nevertheless, as already discussed, moments of PDFs can be accessed through lattice QCD calculations, because they can be expressed as matrix elements of local operators. However, the reconstruction of the PDFs from their moments is rather unfeasible on the lattice, since higher moments show a poor signal-to-noise ratio and are very hard to compute.

A possible solution for the calculation of PDFs from lattice QCD is proposed in Ref. [28] and involves the computation of a parton quasi-distribution function which can be accessed on the lattice for finite momenta. This quasi-distribution can be related to the physical distribution through a matching procedure. The necessary matching coefficients have already been computed in one-loop perturbation theory for the iso-vector case in Ref. [70]. In addition, the obtained distribution has to be corrected for a finite nucleon mass, which otherwise can be neglected in the infinite momentum frame. A first test of this approach has been carried out in Ref. [29], using staggered fermions.

This work aims at providing an additional independent study on the feasibility and potential of the proposed method. Thus, the focus will be on the exploration of different methods and parameters, not on a precise determination of the distribution and the estimation of systematic uncertainties. In the following sections, I will at first briefly sketch the necessary framework to compute quasi-distributions on the lattice and relate them to the physical PDFs. In the following, I will present results for the relevant matrix elements using a boosted nucleon with the three lowest lattice momenta, $^{2\pi}/_{L}$, $^{4\pi}/_{L}$ and $^{6\pi}/_{L}$. It is not possible to extract any meaningful signal from larger momenta due to the large noise-to-signal ratio.

Different levels of gauge link smearing in the operator are applied and their influence on the result is studied. This is done to investigate the possible impact of renormalization on the parton distribution. A large variation of the result for different steps of smearing could indicate a significant effect of renormalization, since different levels of smearing lead to different renormalization constants. This is necessary, because the renormalization scheme for the relevant operators is not yet known on the lattice.

Subsequently, after the quasi-distribution is extracted from the matrix elements, the matching conditions and nucleon target mass corrections will be applied in order to relate the quasi-distribution to the physical PDF. These corrections are momentum dependent and the employed momentum is matched to the lattice momentum of the boosted nucleon. I will show results for the obtained PDF using the momenta $^{4\pi}/_{L}$ and $^{6\pi}/_{L}$. In addition, I will present results from a hypothetical setup where the momentum used for the corrections is chosen to be larger than the nucleon boost in order to estimate the behavior of the results for larger momenta.

Finally, I will show first results for the polarized parton distribution from lattice QCD, a computation that has been suggested in Ref. [28] as well. The polarized distribution can be obtained by employing the proposed method and only slightly altering the inserted operator and the corrections given by the matching condition.

5.1 Parton physics on an Euclidean lattice

The relation of the full parton distribution to matrix elements of a local operator can be obtained from the OPE, either directly [71] or from the Mellin transformation of the relation between moments of PDFs and matrix elements of local operators given in Eq. (2.25).

The result, as already stated in Eq. (2.27), is

$$q(x) = \frac{1}{4\pi}\int_{-\infty}^{\infty} d\xi^- \, e^{-ix\xi^- P^+} \langle P|\bar{\psi}(\xi^-)\gamma^+ \exp\left(-ig\int_0^{\xi^-} A^+(\eta^-)\, d\eta^-\right)\psi(0)|P\rangle \,, \tag{5.1}$$

where $|P\rangle$ denotes a nucleon state with momentum P, light-cone coordinates $\xi^{\pm} = {}^1\!/\!_{\sqrt{2}}(\xi^0 - \xi^3)$ and the gauge fields A^μ. Here, the quark distribution is denoted by $q(x)$ instead of $f_q(x)$, matching the notation of the other works on this topic. This expression, however, cannot be computed on an Euclidean lattice. The matrix elements are dominated by an area close to the light-cone $\xi^2 \approx 0$, as shown in Section 3.7.1 of Ref. [31] for example. In Euclidean space-time, the light-cone area is given by $\xi^2 = \mathbf{x}^2 + t^2$. Thus, one needs to consider a separation very close to zero. This cannot be done on a lattice with non-zero lattice spacing.

A new method that was proposed in Ref. [28] employs the computation of a purely spatial distribution in a finite momentum frame. This distribution is called quasi-distribution and can be computed as

$$\tilde{q}(x, \Lambda, P_3) = \int_{-\infty}^{\infty} \frac{dz}{4\pi} e^{-izk_3} \langle P|\bar{\psi}(z)\gamma_3 W_3(z,0)\psi(0)|P\rangle \,, \tag{5.2}$$

where $W_j(z,0)$ is the Wilson line from 0 to z in the spatial j direction. Furthermore, one needs to define $k_3 = xP_3$ and the Euclidean momentum $P = (0,0,P_3,P_4)$. It is required that the Wilson line and the spatial nucleon momentum boost point into the same direction.

Here and in most of the following equations, only the dependence on the relevant space-time index is shown for the spinors ψ and the Wilson line W, while the rest is omitted, *e.g.* $\psi(z) \equiv \psi(0,0,z,0)$. In order to restore the physical quark distribution from this quasi-distribution, a number of corrections have to be applied. To account for the finite momentum frame used on the lattice, one has to perform a computation of the wave function and vertex corrections, which is done perturbatively here

$$\begin{aligned} q(x,\mu_R) = \tilde{q}(x,\Lambda,P_3) &- \frac{\alpha_s}{2\pi}\tilde{q}(x,\Lambda,P_3)\delta Z_F^{(1)}\left(\frac{\mu_R}{P_3},\frac{\Lambda}{P_3}\right) \\ &- \frac{\alpha_s}{2\pi}\int_{-1}^{1}\frac{dy}{|y|} Z^{(1)}\left(\frac{x}{y},\frac{\mu_R}{P_3},\frac{\Lambda}{P_3}\right)\tilde{q}(y,\Lambda,P_3) + \mathcal{O}(\alpha_s^2)\,. \end{aligned} \tag{5.3}$$

The wave function and vertex corrections $\delta Z_F^{(1)}$ and $Z^{(1)}$ were computed up to one loop order for the iso-vector combination in Ref. [70] and can be found in Appendix B.

A further correction that has to be performed is caused by the existence of a finite nucleon mass on the lattice when employing a finite momentum frame, in contrast to the physical distribution, where the infinite momentum frame causes the nucleon mass to vanish. One has to take into account this finite mass on the lattice and correct either the quasi-distribution or the quark distribution for it. Details on how to perform the correction can be found in Ref. [72]. For the quark distribution, one finds

$$\tilde{q}(x, P_3) = \frac{1}{1 + M\xi^2} \tilde{q}^{(0)}(\xi, P_3), \tag{5.4}$$

where $\tilde{q}$ is the distribution with finite nucleon mass, $\tilde{q}^{(0)}$ the distribution without nucleon mass, $M = {}^{m_N^2}/_{4P_3^2}$ and

$$\xi = \frac{2x}{1 + \sqrt{1 + 4Mx^2}}\,, \tag{5.5}$$

which is called the Nachtmann variable. The result is correct to all orders.

5.2 Lattice calculation

After discussing the theoretical setup for the computation of PDFs on the lattice, the first step is to compute the form factors $h(P_3, z)$ of the matrix elements directly on the lattice. These form factors are related to the matrix elements in the following way

$$\langle P|\overline{\psi}(z)\gamma_3 W_3(z, 0)\psi(0)|P\rangle = \bar{u}(P)\gamma_3 h(P_3, z)u(P)\,. \tag{5.6}$$

Consequently, the relevant quasi-distribution can be computed from the form factors as

$$\tilde{q}(x, \Lambda, P_3) = 2P_3 \int_{-\frac{L}{2}}^{\frac{L}{2}} \frac{dz}{4\pi} e^{-izxP_3} h(P_3, z)\,. \tag{5.7}$$

It is important to mention that this form does not just hold for the 3-direction. Due to the spatial rotational symmetry on the lattice, the calculation can be straightforwardly applied to any other spatial directions. Nevertheless, the given notation, in particular for P_3, will be kept throughout this work.

The relevant form factors are extracted as a ratio of suitable three- and two-point functions, *cf.* Section 3.4.3. The three-point functions that are used are constructed in the familiar way with boosted nucleon fields

$$C_\Gamma^{\text{3pt}}(t, \tau, 0; \mathbf{P}) = \Gamma \left\langle N(\mathbf{P}, t)\mathcal{O}(\tau)\overline{N}(\mathbf{P}, 0)\right\rangle, \tag{5.8}$$

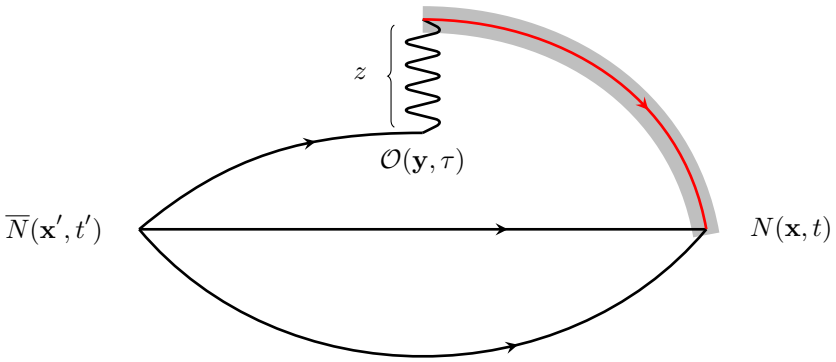

Figure 5.1: Schematic picture of a possible Wick contraction of the quark fields in the three-point function used to extract the matrix elements for the computation of the PDF. Due to the momentum structure, the highlighted propagator is an all-to-all propagator.

where the nucleon interpolating fields are the momentum projected versions of those from Eq. (3.36). For this setup, an appropriate choice for the projector is the parity plus projector $\Gamma_+ = (1+\gamma_4)/2$.

The operator at vanishing momentum transfer $Q^2 = 0$ can be obtained by choosing

$$\mathcal{O}(z,\tau,Q^2=0) = \sum_{\mathbf{y}} \bar{\psi}(y+\hat{e}_3 z)\gamma_3 W_3(y+\hat{e}_3 z, y)\psi(y)\,, \tag{5.9}$$

where $y = (\mathbf{y},\tau)$ and $\hat{e}_j$ denotes one single step in the j direction on the lattice. The Wilson line is computed as a product of gauge links along the according axis, where only the shortest path is considered

$$W_j(y+z\hat{e}_j, y) = U_j(y+(z-1)\hat{e}_j)\dots U_j(y+\hat{e}_j)U_j(y)\,, \tag{5.10}$$

The resulting three-point function can then be expressed by products of quark propagators and gauge links, see Fig. 5.1 for a schematic picture of such a Wick contraction.

Finally, the ratio of this three-point function and the usual nucleon two-point function can be related to the form factors as

$$R_{\Gamma_+}\big(N(P);\mathcal{O};N(P)\big) = \frac{-iP_3}{E_N} h(P_3,z), \tag{5.11}$$

where $E_N = \sqrt{(P_3)^2 + m_N^2}$ is the total energy of the nucleon. A detailed computation of the kinematic factors can be found in Appendix A.

For the operator, the iso-vector quark combination, *i.e.* a τ^3 matrix in flavor space, is considered to avoid operator mixing and disconnected contributions. The resulting form factors are denoted by h_{u-d}.

Due to the symmetric structure of the operator, there is certainly a relation between the form factors in the positive and negative z direction. Indeed, if one applies the gauge link identity $U_{-\mu}(x) = U_\mu(x - \hat{e}_\mu)^\dagger$ to Eq. (5.10), it is possible to show that $W_j(y + \hat{e}_j z, y) = W_j(y, y + \hat{e}_j z)^\dagger$. Thus, one obtains the relation $\mathcal{O}(z, \tau) = -\mathcal{O}(-z, \tau)^\dagger$ for the Euclidean operator defined in Eq. (5.9), due to its translational invariant structure. Taking into account the kinematic factor in Eq. (5.11), one finds the following behavior for the form factors

$$h(P_3, z) = h(P_3, -z)^\dagger \,. \tag{5.12}$$

On the lattice, this relation might only be approximate, depending on how the quark propagators in the three-point function are calculated. This will be further elaborated in the next section. Thus, this relation will not be enforced, but used as a cross-check for the lattice results.

5.2.1 Computing the all-to-all propagator

When computing the necessary three-point functions, there is some flexibility regarding the treatment of the quark propagator connecting the sink position with the operator insertion point. This propagator is highlighted in Fig. 5.1. Due to momentum projection, there is a spatial sum on both ends of the propagator, which naively requires an all-to-all propagator. However, such a computation needs $V = L^3 \times T$ sets of inversions, which is not feasible in this setup due to the large temporal and spatial extension of the lattice.

In principle, there are two different methods that are used to calculate this propagator. The first one is the sequential method [73], where the calculation of the three-point function is divided into two parts. The first step involves the computation and contraction of all the propagators that can be treated as one-to-all propagators. These are represented by the plain black lines in Fig. 5.1. Secondly, the all-to-all propagator is computed by an additional inversion, where the result of the first part is used as the source ξ, *cf.* end of Section 3.4.1. Finally, the result can be contracted together with the operator in order to obtain the three-point correlation function. The drawback of this method is that it requires the sink position and the nucleon momentum at the sink to be fixed.

An alternative method is the stochastic method, where stochastic sources which contain Z^4 noise on one single time-slice are used for the estimation of the all-to-all propagator. For hadron structure calculation, this method was studied in Ref. [74], for instance. The estimation of an all-to-all propagator by using stochastic methods was proposed in Refs. [75, 76] and successfully applied for a variety of lattice computations. The advantage of the stochastic method is its flexibility, allowing to freely choose the momentum at the sink position as well as to vary the time-slice of the current insertion. The drawback is the stochastic noise that is added to the system.

A stochastic source ξ with noise on a single time-slice t_s is constructed in the following way

$$\xi_A^n(x) = \delta_{t\,t_s}(Z_4)_A^n(\mathbf{x})\,, \tag{5.13}$$

where A labels spin and color, and n denotes the stochastic sample. A natural choice for the noise terms are numbers randomly selected from four equidistant entries of the complex unitary circle, *e.g.* $Z_4 \in \{1/\sqrt{2}, -1/\sqrt{2}, i/\sqrt{2}, -i/\sqrt{2}\}$. In principle, other types of noise can be used as well, as long as the following condition holds

$$\sum_{n=1}^{\infty}(\xi_A^n(x))^\dagger \xi_B^n(y) = \delta_{xy}\delta_{AB}\,. \tag{5.14}$$

It is rather simple to show that the Z_4 noise does in fact fulfill this condition. As the next step, a sink spinor ϕ is generated by solving the Dirac equation

$$Q_{A,B}(x,y)\phi_B^n(y) = \xi_A^n(x)\,. \tag{5.15}$$

Finally, the quark propagator can be extracted from the product of the sink spinor with the complex conjugated source

$$Q_{A,C}^{-1}(y,x) = \sum_{n=1}^{\infty}\phi_A^n(y)(\xi_B^n(x))^\dagger\,. \tag{5.16}$$

Thus, one only obtains the unbiased quark propagator when using an infinite number of samples. In practice, there are additional stochastic noise terms which are of the order $O(1/\sqrt{N})$ when computing the propagator for a finite number N of stochastic samples.

The application of the two different methods for the computation of the necessary form factors was explored in a previous study on a smaller gauge ensemble, *cf.* Ref. [77]. It was found that both methods yield comparable errors for the same computational effort. Since this work is intended as an exploratory study which especially focuses on the calculation and comparison of different nucleon momenta, the stochastic method will be used due to its larger flexibility. Consequently, the relation in Eq. (5.12) only holds approximately, due to the different treatment of the propagators on either side of the operator.

5.2.2 Lattice setup and HYP smearing

All results presented in this and the following sections are computed on the B55.32 ETMC ensemble that was already utilized for the computation of the gluon moment, *cf.* Tab. 4.1 and the corresponding section for the relevant parameters.

In an early study, the influence of excited states on the result was explored by comparing two different source-sink separations. The results shown in Fig. 5.2 are

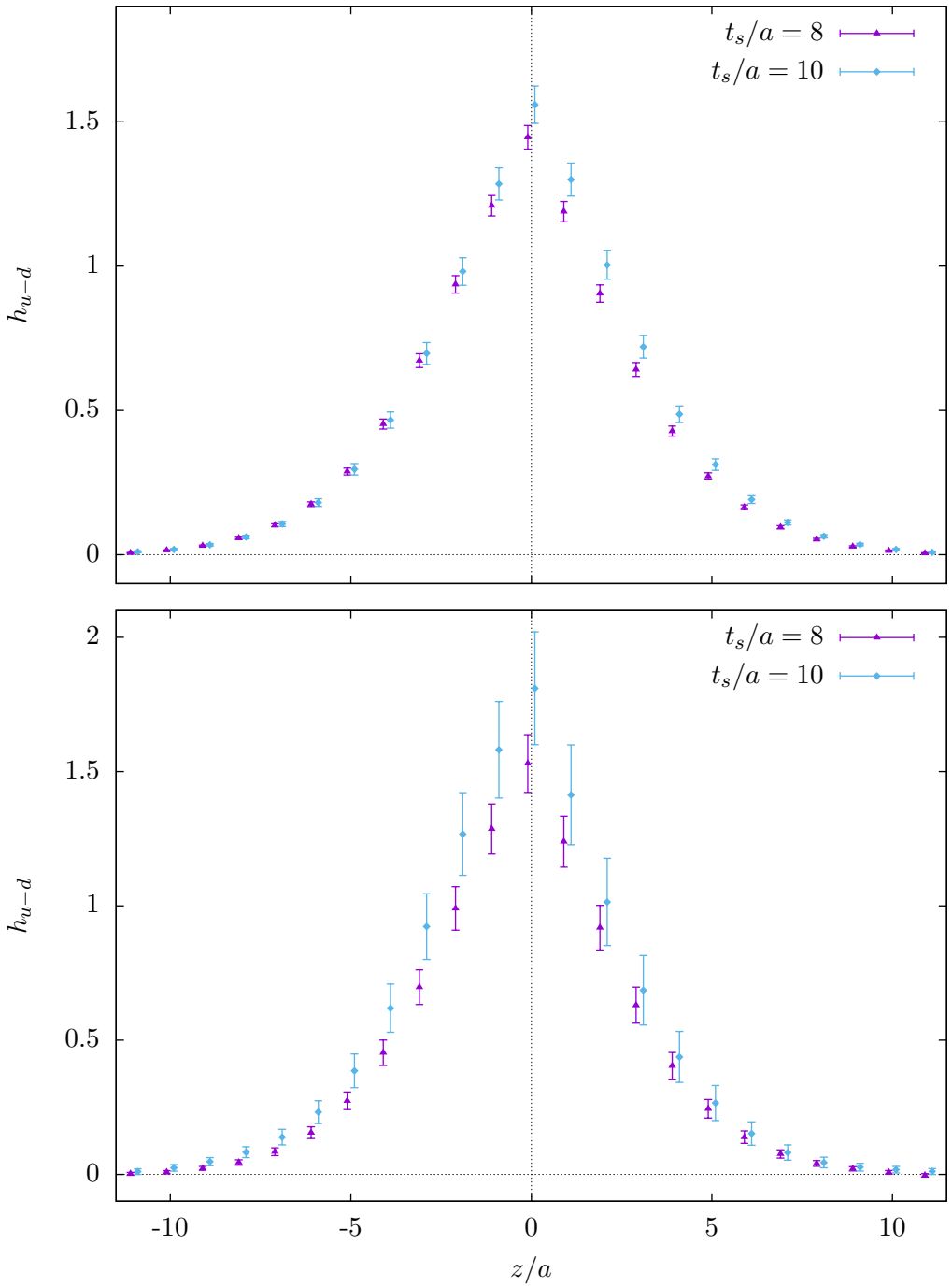

Figure 5.2: Results for the real part of the unrenormalized form factors with different source-sink separations, employing ~ 1000 measurements, **top**: $P_3 = {}^{2\pi}/_{L}$, **bottom**: $P_3 = {}^{4\pi}/_{L}$.

mostly compatible within errors, suggesting only a slight influence of excited states. A further study is certainly necessary in order to discriminate excited state effects in detail. For all following computations, the smaller separation $t_s = t - t' = 8a$ is chosen in order to reduce the resulting noise, which is particularly useful for the computation with larger momenta.

Before presenting any results, another issue needs to be addressed. As for most of the observables used in hadron structure, the form factors need to be renormalized. The computation of the necessary renormalization factors is an ongoing work that will eventually be presented in Ref. [78]. In this work, an alternative approach to obtain an estimate of the importance of renormalization will be used.

In Ref. [29], the authors applied HYP smearing [63] to the gauge links in the inserted operator. This is a lattice technique used to smoothen the gauge links and expected to bring the necessary renormalization factors closer to the corresponding tree-level value. The latter is particularly useful for the current setup, because the renormalization constants for the local quark operators are known. Thus, in order to obtain an estimate on how renormalization could influence the presented results, two and five steps of HYP smearing are applied to the operator and compared with the unsmeared results. For the HYP smearing, the standard parameters $\alpha_{1,2,3} = \{0.75, 0.6, 0.3\}$ suggested in Ref. [63] are used.

The initial tests (Figs. 5.3 and 5.4) are performed with 5430 measurements on 181 gauge field configurations. All other results are computed with 10410 measurements on 694 gauge field configurations.

5.2.3 Lattice results

To compare the results for a different number of HYP smearing steps in the operator, the real and the imaginary part of the form factors for $P_3 = {}^{8\pi}/_{L}$ are shown in Fig. 5.3.

It can be observed that applying HYP smearing to the gauge links in the operator clearly affects the value of the form factors, both the real and the imaginary part. In general, the impact on the imaginary part seems considerably stronger than on the real part. When comparing the different number of smearing steps, the change from zero to two steps appears to be more significant than from two to five steps. This indicates a saturation of the smearing effect. A decrease of the noise-to-signal ratio for the form factors that has been observed for the gluon moment in the previous chapter, respectively Ref. [79], cannot be detected for this setup.

In order to illustrate the effect of HYP smearing on the quasi-distribution, Fig. 5.4 shows the real part of the Fourier transformation of the form factors, *cf.* Eq. (5.7). It should be noted that in all setups studied in this context, the imaginary part of the quasi-distribution vanishes within errors.

Considering the form of Fourier transformation, one expects a strong x asymmetry for the quasi-distribution if the form factors feature a large imaginary part. Indeed, a strong asymmetry can be observed for two and five steps of HYP smearing,

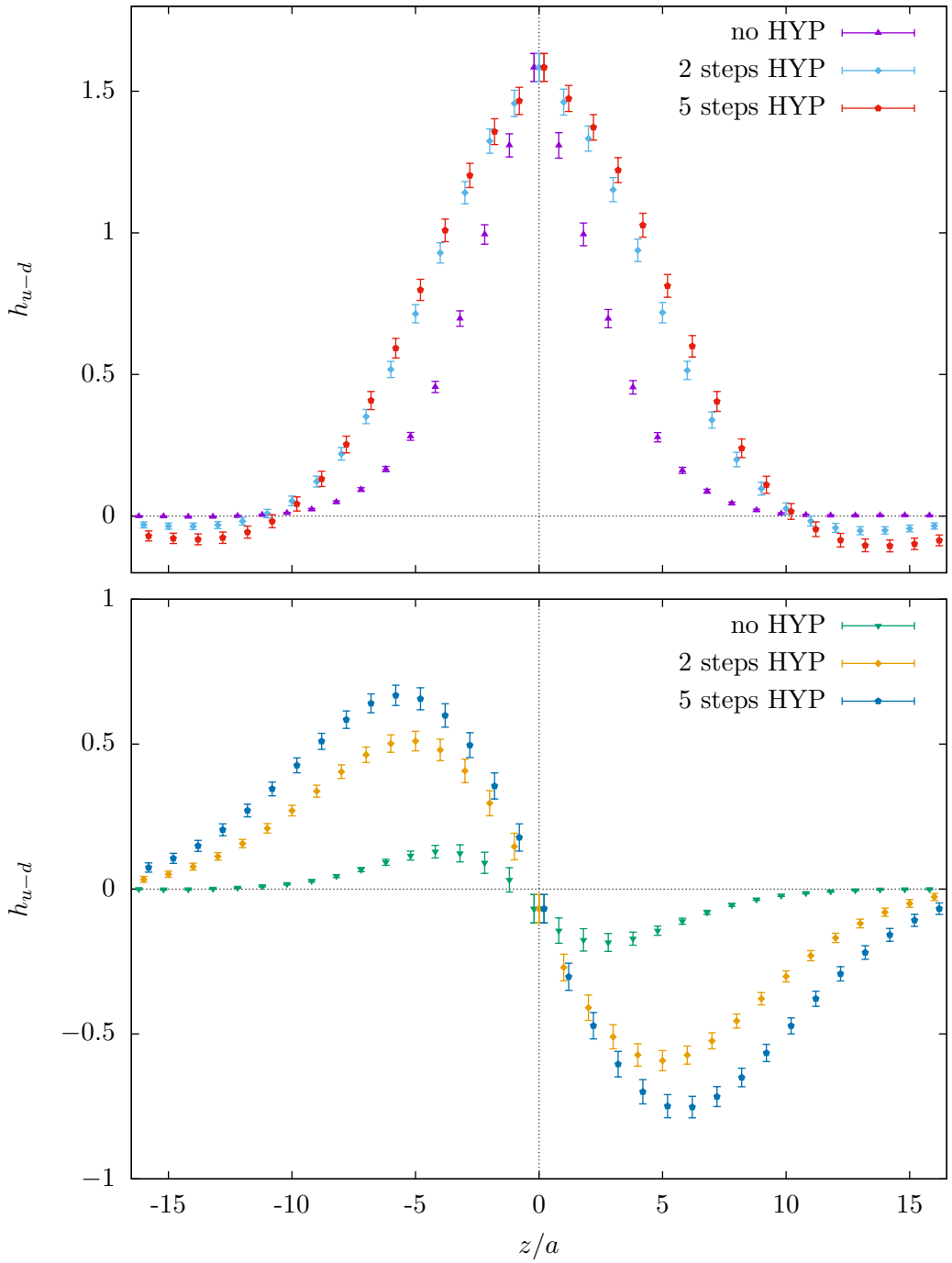

Figure 5.3: Results for the unrenormalized form factors with different steps of HYP smearing and $P_3 = {}^{4\pi}/_{L}$, **top**: real part, **bottom**: imaginary part.

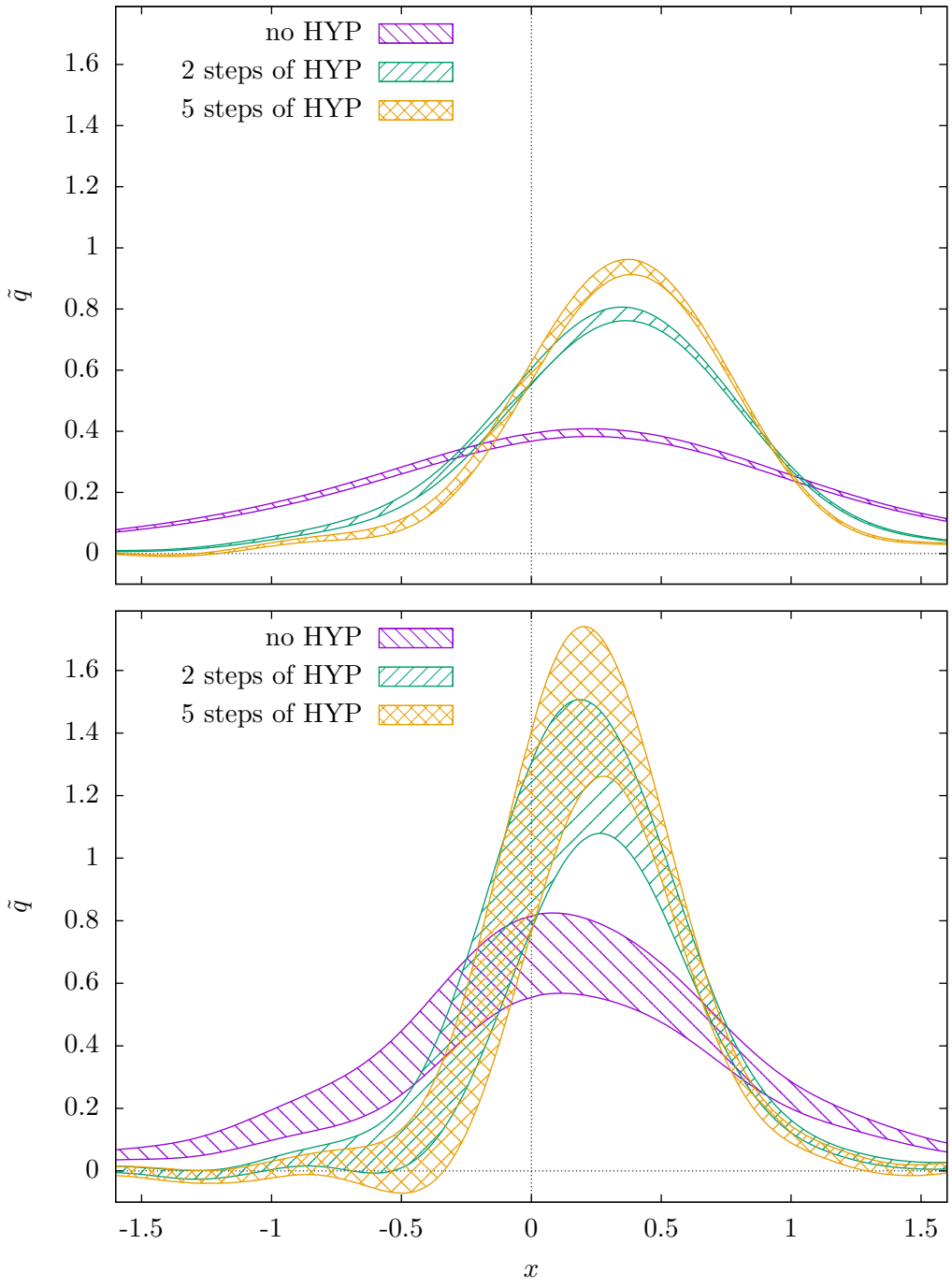

Figure 5.4: Comparison of quasi-distributions $\tilde{q}$, with five, two and no steps of HYP smearing employed, **top:** $P_3 = 4\pi/L$, **bottom:** $P_3 = 6\pi/L$.

which cause an increase of the imaginary part of the form factors. Assuming that the qualitative behavior of the quasi-distribution is already similar to the behavior of the physical PDF, one can conclude that the HYP smearing reveals the expected quark-antiquark asymmetry in the distribution, since antiquarks can be interpreted as quarks in the negative x region, according to the crossing relation [80]

$$\bar{q}(x) = -q(-x)\,. \tag{5.17}$$

This relation also implies that the iso-vector $u - d$ distribution in the negative x region can be interpreted as the $\bar{d} - \bar{u}$ distribution.

The goal of studying the effect of HYP smearing was to estimate the influence of proper renormalization on the PDF. The obtained results clearly point to the fact that renormalization will play an important role when looking at the quark distributions from lattice calculations in the future. Without renormalization, there would barely be an asymmetry between the quark and the antiquark PDF. In the following calculations five steps of HYP smearing will be employed, because the presented results do not indicate any significant impact from a larger number of steps. The corresponding results for $P_3 = {}^{2\pi}/_{L}$, $P_3 = {}^{4\pi}/_{L}$ and $P_3 = {}^{6\pi}/_{L}$ are presented in Fig. 5.5. For $P_3 = {}^{4\pi}/_{L}$, selected results for the effective form factors and the fitted plateau are shown in Fig. 5.6.

The resulting form factors show, within errors, a symmetry in z for the real part and an asymmetry in z for the imaginary part, as was expected from Eq. (5.12). A further valuable cross-check of the obtained results can be done by examining the form factor at $z = 0$. This is the F_1 form factor, which can at $Q^2 = 0$ be identified with the local vector current g_V. Since the local vector current is strictly conserved, it represents the net number of quarks in a hadron. Consequently, $g_V^{u-d} = 1$ should hold for the proton, *cf.* [22]. The corresponding operator is renormalized with the vector current renormalization constant Z_V, which is $Z_V = 0.625(2)$ for the used ensemble, as computed in Ref. [41].

Indeed, one finds $Z_V h_{u-d}(0) = 0.95(17)$ for $P_3 = {}^{6\pi}/_{L}$ and $Z_V h_{u-d}(0) = 0.96(2)$ for $P_3 = {}^{4\pi}/_{L}$. For $P_3 = {}^{2\pi}/_{L}$, one obtains $Z_V h_{u-d}(0) = 0.944(8)$, which is rather low and is probably caused by excited state effects[1].

5.3 Perturbative matching and mass correction

In order to extract the physical PDF from the form factors $h_{u-d}(z, P_3)$, the Fourier transformation in Eq. (5.7) has to be applied. Prior to that, the form factors have to be multiplied by the vector current renormalization constant Z_V.

[1] When using a larger source-sink separation of $10a$, one finds $Z_V h_{u-d}(0) = 0.98(4)$, *cf.* Fig. 5.2, which is compatible with a value of one. The larger error is induced by the larger source-sink separation and the fact that less measurements were used.

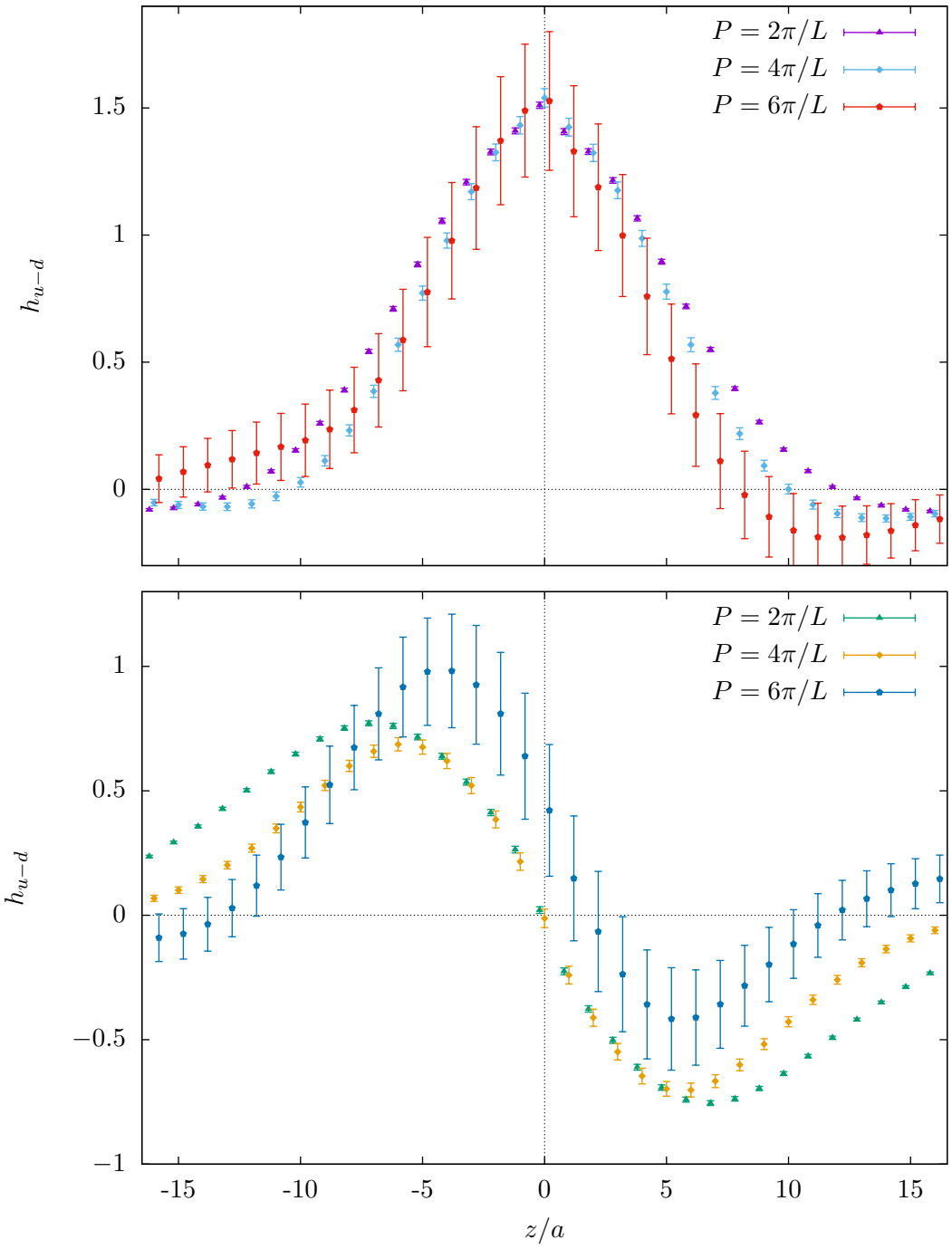

Figure 5.5: Results for the unrenormalized form factors for different momenta and five steps of HYP smearing, **top**: real part, **bottom**: imaginary part.

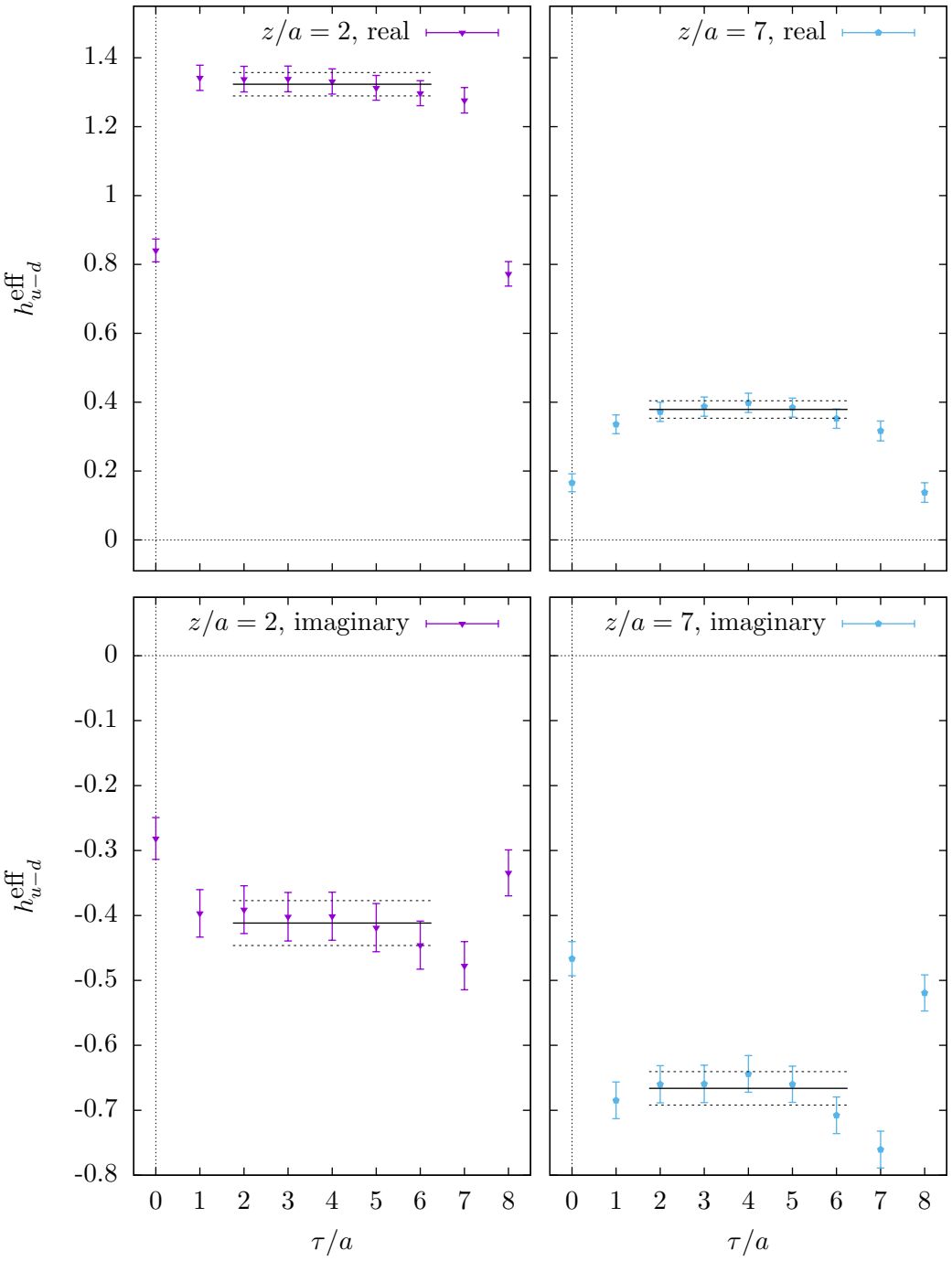

Figure 5.6: Results for the unrenormalized effective form factors for $P_3 = {}^{4\pi}/_{L}$ and five steps of HYP smearing, **top**: real part, **bottom**: imaginary part, **left**: ${}^{z}/_{a} = 2$, **right**: ${}^{z}/_{a} = 7$. The constant fits from which the value for the form factor is extracted are shown as well.

This yields the quasi-distribution $\tilde{q}(x)$. It should be noted that the renormalization with Z_V is correct for $z = 0$ and only approximate for all other form factors if HYP smearing is applied. Once the proper renormalization scheme is known, each form factor will be individually renormalized with the corresponding Z factor.

Subsequently, one can extract the physical quark distribution $q(x)$ from $\tilde{q}(x)$, using Eq. (5.3) and afterwards applying the nucleon target mass corrections in Eq. (5.4). The value of the momentum cut-off in the matching is chosen to be the same as the value of the lattice cut-off itself, which is $\Lambda = {}^{1}/_{a} \cong 2.5\,\mathrm{GeV}$. The renormalization scale μ_R is chosen to be the same. This is a plausible, but only preliminary choice, since the running with μ_R will be known once the renormalization has been performed.

The integrals in the matching procedure have a cut-off at $x_c = {}^{\Lambda}/_{P_3}$ limiting the x region in which the integrands are valid. It is illustrated in more detail in Refs. [70] and [69]. The matching also requires the bare coupling constant as an input parameter. Here, a value corresponding to $\beta = 1.95$ of the lattice calculation $\alpha_s = {}^{6}/_{(4\pi\beta)} \approx 0.245$ is used. The region of $|x| < {}^{1}/_{L}$ will be omitted in the following, because the x resolution is certainly limited by the ratio of the smallest to the largest lattice momentum.

Results for the quasi-distribution $\tilde{q}(x)$, the PDF with finite target mass $q(x)$ and the final PDF $q^{(0)}(x)$ for the momenta $P_3 = {}^{4\pi}/_{L}$ and $P_3 = {}^{6\pi}/_{L}$ are presented in Fig. 5.7. These momenta correspond to physical momenta of 0.98 GeV and 1.47 GeV. The lowest lattice momentum $P_3 = {}^{2\pi}/_{L}$ is not shown in the following, because both matching as well as target mass corrections feature a poor convergence for such a small momentum.

The behavior of the computed parton distributions partly features a qualitative agreement with the distributions extracted from phenomenological analyses [17, 18, 50], which are obtained at $Q^2 = 6.25\,\mathrm{GeV}^2$, matching the lattice scale Λ. For quark as well as antiquark distributions, one finds $q(x) \approx 0$ for $|x| > 1$. The computed $u(x) - d(x)$ distributions show a peak at intermediate values of x, which cannot be observed in the phenomenological distributions. This peak however moves to smaller values of x as the nucleon momentum increases. This behavior will be discussed later in some more detail. For the $\bar{d}(x) - \bar{u}(x)$ distributions, one can observe an increase for the small x region, which is in agreement with phenomenology.

Regarding the nucleon target mass correction, it can be seen that it generates a decrease of the distributions in the large x region. This is in full accordance with expectations from phenomenology and affirms that the nucleon mass corrections are essential to restore the energy-momentum relations, thus ensuring the partonic interpretation of the distributions. With increasing nucleon momentum, the mass corrections decrease, as expected from Eq. (5.4).

For the smaller of the two momenta in particular, one finds a slightly oscillatory behavior in the large x region. It appears to be an effect of changing the Fourier

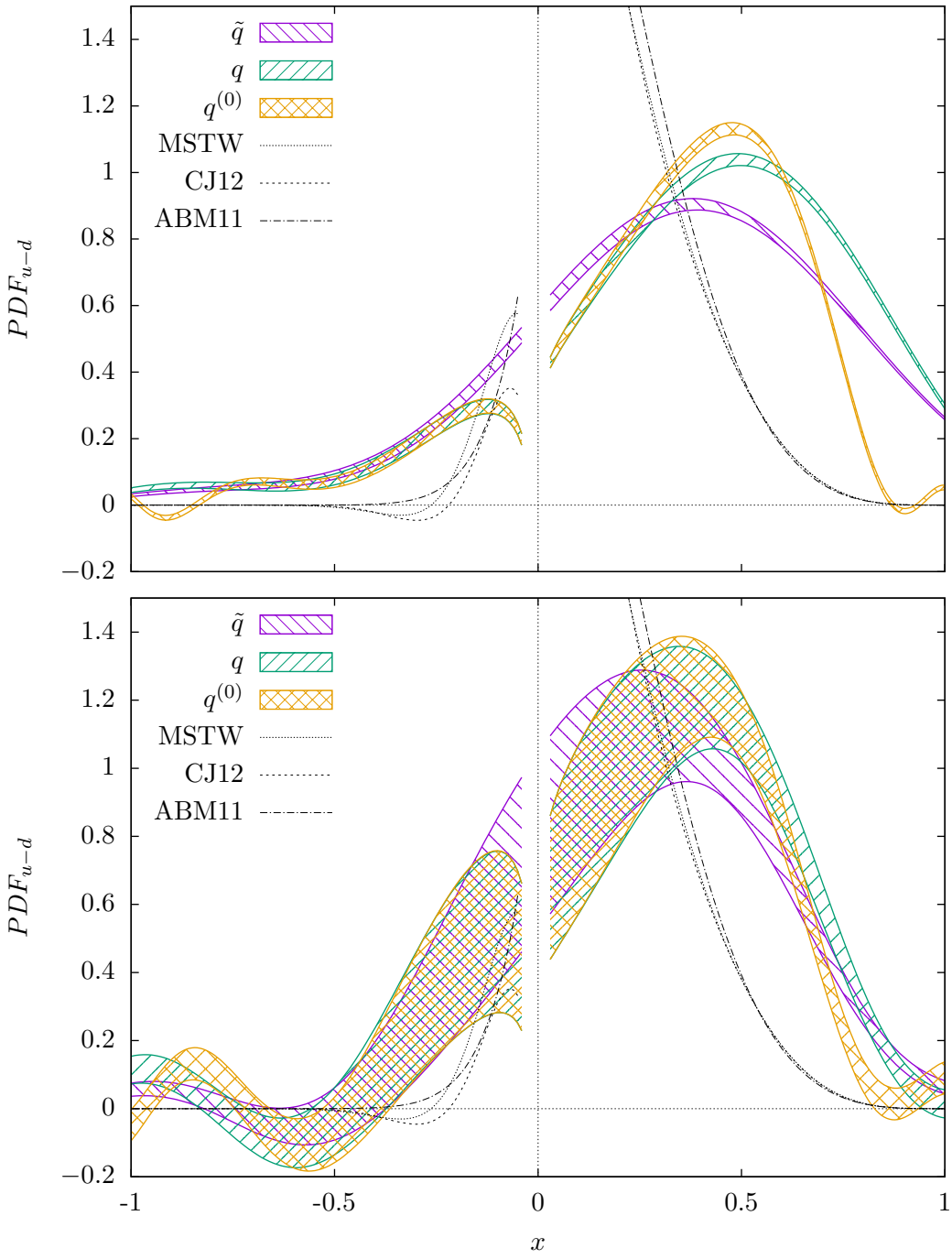

Figure 5.7: Results for the quasi-distribution $\tilde{q}$, the PDF without subtracting the mass correction q, and the final PDF $q^{(0)}$ with 5 steps of HYP smearing, **top**: $P_3 = {}^{4\pi}/_{L}$, **bottom**: $P_3 = {}^{6\pi}/_{L}$, negative region: $\bar{q}(x) = -q(-x)$, comparison with phenomenological $u(x) - d(x)$ curves at $Q^2 = 6.25\,\mathrm{GeV}^2$ (MSTW [17], CJ12 [18], ABM11 [50]).

transformation from an infinite integral to a sum over a finite extension, which in this work is limited by the extension of the used lattice. This can be tested by decreasing the range of summation from $-L/2$ and $L/2$ to smaller values. Here, one observes an increase of the oscillatory behavior for large x. This problem should be addressed in future studies by choosing a lattice with a larger spatial extension.

Although the obtained distributions do not seem to agree with the phenomenological distributions on a quantitative level, there is a clear tendency to converge to the phenomenological parameterizations when P_3 is increased. Consequently, results for larger momenta would be highly desirable, yet, as already mentioned, it is not possible to compute the form factors on the lattice for momenta larger than $P_3 = 6\pi/L$ due to the large uncertainties. At the same time, however, Fig. 5.5 shows that the difference between the form factors for the largest two lattice momenta is only small. Thus, it can be assumed that the difference to results for $P_3 = 8\pi/L$ might be small as well.

Therefore, it might be possible to study the behavior of the distribution for larger momenta by employing a hypothetical setup. In this, the quark distribution will be extracted from an analysis with $P_3 = 8\pi/L$, *i.e.* Fourier transformation, perturbative matching and mass correction. At the same time, the form factors going into this analysis will have a smaller momentum of $P_3 = 4\pi/L$ and $P_3 = 6\pi/L$. If these form factors are similar to the ones extracted from a larger momentum, the resulting distribution will probably be very close to the distribution obtained from a proper analysis. This particular setup will be denoted as the mixed momentum setup. The resulting distributions are shown in Fig. 5.8.

It certainly needs to be stressed that this exercise is only hypothetical and the resulting distributions should only be used to estimate the behavior for momenta larger than the ones currently available. Nevertheless, the observed quark distribution seems to converge to the phenomenological parameterizations of the distributions, especially for the intermediate and large x region. The antiquark distributions even show a decent agreement for the full x region. Altogether, it can be seen that momenta larger than $P_3 = 6\pi/L$ are certainly needed to obtain a quantitative agreement to the phenomenological distributions, at least in certain regions of x. A possible method to gain lattice results for large momenta might be the extrapolation from the available data. However, precise measurements of the form factors for all three momenta and thus substantially higher statistics are necessary to succeed with this approach. Although a big difference to the mixed momentum setup is not expected, a full analysis with real data is of course mandatory and will be presented in a forthcoming work [78].

For the small and positive x region, on the other hand, it seems that increasing the nucleon momentum is not sufficient when it comes to reaching an agreement with phenomenology. In this case, the lattice distributions feature rather small values for small x, which in this particular x region contradicts the phenomenological parameterizations. This discrepancy might be related to the calculation's limitation

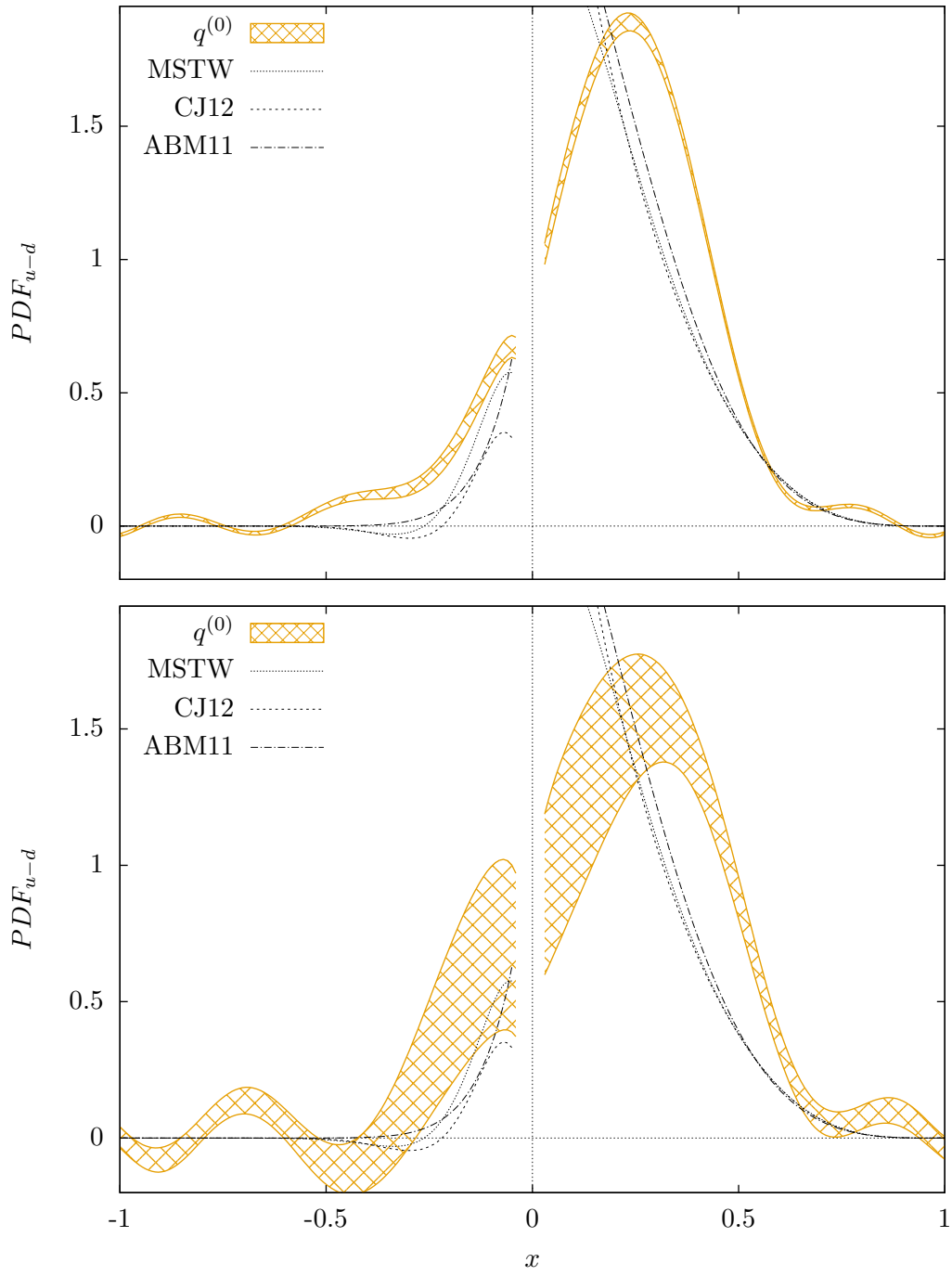

Figure 5.8: Results from a hypothetical mixed momentum analysis using different values of the momentum in the computation of the lattice form factors (**top**: $P_3 = {}^{4\pi}/_{L}$, **bottom**: $P_3 = {}^{6\pi}/_{L}$) than in the Fourier transformation, matching and mass corrections ($P_3 = 8\pi/L$) with five steps of HYP smearing.

in the small x region due to the presence of the infrared $1/L$ and ultra-violet $1/a$ cut-off regulators on a finite lattice. These cut-offs define an x region in which naively a reliable computation of the distributions is expected, yet, the present deviation is well within this range.

Therefore, the x region might also be limited by the employed momentum P_3, which enters into the Fourier transformation Eq. (5.2), where the momentum space is defined as $k_3 = xP_3$. Assuming that k_3 should be larger than the smallest possible lattice momentum, would set a rather strict bound to the x region. For $P_3 = 4\pi/L$, the lattice distribution would only be valid for $x > 1/2$, for $P_3 = 6\pi/L$, it would be $x > 1/3$.

This issue might be clarified when larger lattices and smaller values of the lattice spacing become available and larger momenta can be considered. Furthermore, it should be stressed that the presented results are obtained at only one, non-physical value of the pion mass and the shape of the distribution might as well depend on the quark mass. Here, the calculation of the lattice distribution from an ensemble with a physical pion mass can be used to study the quark mass dependence in the future.

5.4 The polarized parton distribution

As pointed out in Ref. [28], the applied method can easily be extended to compute the quark helicity distribution, which is also called polarized parton distribution. This distribution is defined as the difference between parton distributions with positive and negative helicity as opposed to the unpolarized distribution, which is the sum of the two.

In Euclidean space-time, the polarized distribution can be related to matrix elements of the following operator

$$\Delta\tilde{q}(x,\Lambda,P_3) = \int_{-\infty}^{\infty} \frac{dz}{4\pi} e^{-izk_3} \langle P|\bar{\psi}(z)\gamma_5\gamma_3 W_3(z,0)\psi(0)|P\rangle \,. \tag{5.18}$$

Equivalently to the unpolarized distribution, the polarized distribution can be restored from the quasi-distribution by applying vertex and wave-function corrections

$$\begin{aligned}\Delta q(x,\mu) = \Delta\tilde{q}(x,\Lambda,P_3) &- \frac{\alpha_s}{2\pi}\Delta\tilde{q}(x,\Lambda,P_3)\delta Z_F^{(1)}\left(\frac{\mu}{P_3},\frac{\Lambda}{P_3}\right) \\ &- \frac{\alpha_s}{2\pi}\int_{-1}^{1}\frac{dy}{|y|}\Delta Z^{(1)}\left(\frac{x}{y},\frac{\mu}{P_3},\frac{\Lambda}{P_3}\right)\Delta\tilde{q}(y,\Lambda,P_3) + \mathcal{O}(\alpha_s^2)\,.\end{aligned} \tag{5.19}$$

The corrections computed in Ref. [70] differ only slightly from those of the unpolarized distribution and can also be found in Appendix B.

In order to extract the polarized quark distribution from the lattice, one needs to alter the operator that is inserted into the nucleon correlator. In contrast to the previous operator in Eq. (5.9), it contains an additional γ_5 matrix

$$\mathcal{O}(z,\tau,Q^2=0)=\sum_{\mathbf{y}}\bar{\psi}(y+\hat{e}_3 z)\gamma_5\gamma_3 W_3(y+\hat{e}_3 z,y)\psi(y). \tag{5.20}$$

This, however, will certainly alter the form factor decomposition and thus the calculation of the kinematic factors. Indeed, it is found that a different projector for the three-point function is necessary for this setup in order to obtain a non-zero kinematic factor. Thus, the projector $\Gamma_j = i\gamma_j\gamma_5(1+\gamma_4)/2$ is chosen, equivalently to the computation of g_A, *cf.* Section 3.5, where $j=3$ for the present setup. Again, the calculation can easily be extended to all spatial directions.

With this choice of the projector, the kinematic factor simplifies to 1 and the computed ratio can be related to the necessary form factors as

$$R_{\Gamma_j}\big(N(P);\mathcal{O};N(P)\big)=\Delta h(P_3,z)\,. \tag{5.21}$$

The form factors can be related to the polarized distribution as

$$\Delta\tilde{q}(x,\Lambda,P_3)=2P_3\int_{-\frac{L}{2}}^{\frac{L}{2}}\frac{dz}{4\pi}e^{-izxP_3}\Delta h(P_3,z)\,. \tag{5.22}$$

The following results are computed on the same ensemble as the unpolarized results and similarly five steps of HYP smearing are employed. In Fig. 5.9, the real and the imaginary part of the iso-vector flavor combination for the form factors $\Delta h_{u-d}(P_3,z)$ are shown.

The observed behavior of the matrix elements' form factors looks very similar to that of the unpolarized form factors, only with a few differences. In particular, the imaginary part of the form factors is small for the smallest momentum, yet grows fast for larger values. Here, a more precise determination of the form factors for $P_3 = {}^{6\pi}/_{L}$ is certainly necessary to estimate the behavior for larger momenta.

The form factors at $z=0$ can be identified with the axial charge of the nucleon. After renormalizing with the relevant factor $Z_A = 0.757(3)$ [41], one obtains $Z_A\Delta h_{u-d}(0) = 1.34(15)$ for $P_3 = {}^{6\pi}/_{L}$, $Z_A\Delta h_{u-d}(0) = 1.12(2)$ for $P_3 = {}^{4\pi}/_{L}$ and $Z_A\Delta h_{u-d}(0) = 1.139(6)$ for $P_3 = {}^{2\pi}/_{L}$. These values are compatible within errors with the previously computed lattice value $g_A = 1.141(18)$ on this ensemble, *cf.* Ref. [41].

Similar to the computation of the unpolarized distribution, one can obtain the quasi-distribution from the form factors by applying a Fourier transformation. The matching can then be performed according to Eq. (5.19). The mass correction is identical to the unpolarized setup, *cf.* Eqs. (5.4), (5.5). The resulting distributions for $P_3 = {}^{6\pi}/_{L}$ and $P_3 = {}^{4\pi}/_{L}$ are shown in Fig. 5.10. Here, the relevant parameters

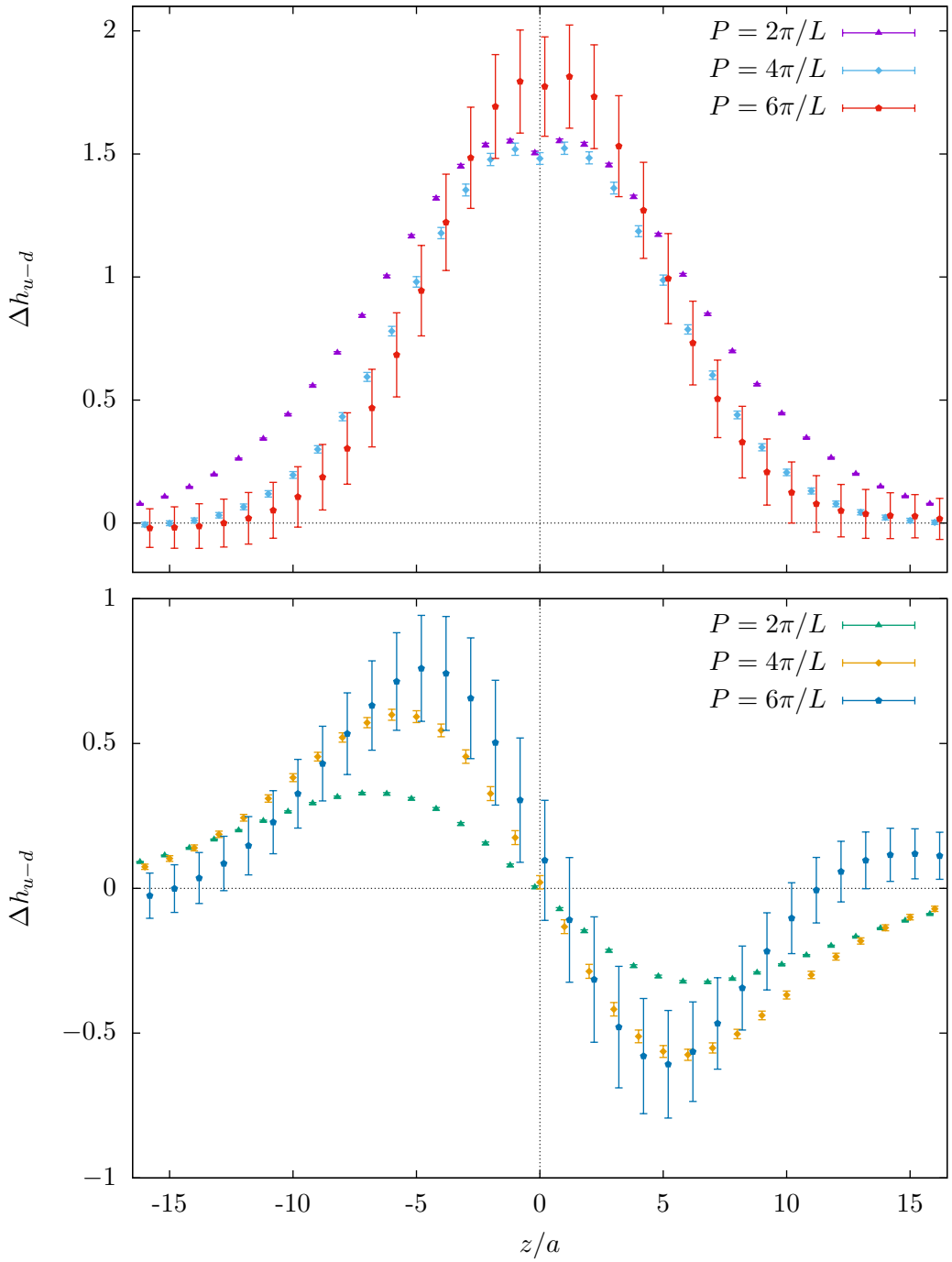

Figure 5.9: Results for the unrenormalized polarized form factors for different momenta with the iso-vector flavor combination, **top**: real part, **bottom**: imaginary part.

α_s, Λ, μ_R and x_c were chosen to be the same as in the unpolarized case given at the beginning of the previous section. The quark distribution in the negative x region can again be related to the antiquark distribution by a crossing relation, which however differs from the unpolarized case [80]

$$\Delta q(-x) = \Delta\bar{q}(x)\,. \tag{5.23}$$

Again, one observes a qualitative, but not quantitative agreement with iso-vector distributions $\Delta u(x) - \Delta d(x)$ and $\Delta\bar{u}(x) - \Delta\bar{d}(x)$, which were obtained from phenomenological analyses [20, 81][2], with the exception of the small x behavior for the quark distribution. Still, the lattice distribution shows a strong quark-antiquark asymmetry and the expected behavior for large $|x|$. The agreement with the phenomenological curves seems to improve for larger momentum. Consequently, the mixed momentum setup employed in the previous section will be studied here as well in order to estimate the effect of larger momenta. The results for a mixed momentum setup with $P_3 = {}^{8\pi}/_{L}$ are shown in Fig. 5.11.

The thus obtained distributions show a decent, partly quantitative agreement to the phenomenological quark distributions for $x > 0.25$. In the antiquark sector, the lattice distribution is much larger than the phenomenological curve. However, the experimental situation for the polarized antiquark distribution is not as good as for the unpolarized one and it thus features a rather large uncertainty.

5.5 Conclusion and outlook

In the last part of my thesis I have presented a first exploratory study for the calculation of the unpolarized and polarized quark distribution from lattice QCD, following the approach proposed in Ref. [28]. Parts of the results were published in Ref. [69]. Together with the work from Ref. [29], these are the first attempts to study the proposed method and acquire results for the parton distribution from lattice QCD. For the polarized distributions, no other published results are available up to now.

The comparison of the form factors and quasi-distributions for different steps of HYP smearing presented in this work clearly emphasizes the importance of a proper renormalization of all relevant form factors, in particular if the corresponding operator contains a spatial Wilson line. Only when doing so one recovers a large quark-antiquark asymmetry, which is expected from phenomenological distributions. The renormalization scheme of the relevant operators is currently studied and will be included in a forthcoming work [78]. It should be noted, however, that it is presently not known if it is possible to find a renormalization scheme that can be straightforwardly applied to the computed data.

[2] In contrast to the unpolarized case, the parametrizations are given with uncertainties, since these are rather large and should not be neglected.

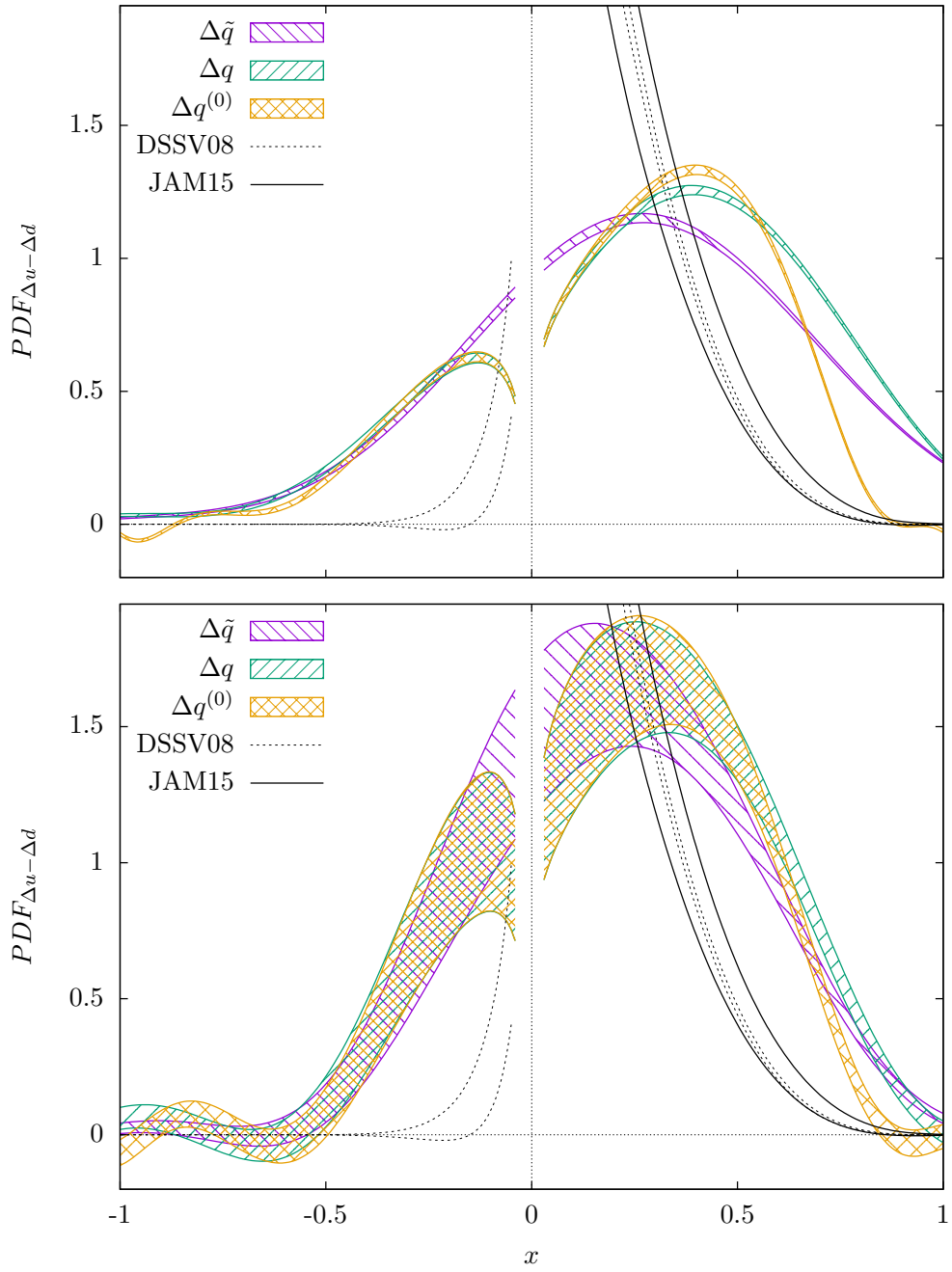

Figure 5.10: Results for the polarized quasi-distribution $\Delta\tilde{q}$, polarized PDF without subtracting the mass correction Δq, and final polarized PDF $\Delta q^{(0)}$ with 5 steps of HYP smearing, **top**: $P_3 = {}^{4\pi}/_{L}$, **bottom**: $P_3 = {}^{6\pi}/_{L}$, comparison with phenomenological parametrizations at $Q^2 = 6.25\,\mathrm{GeV}^2$ (DSSV [20], CJ12 [81]).

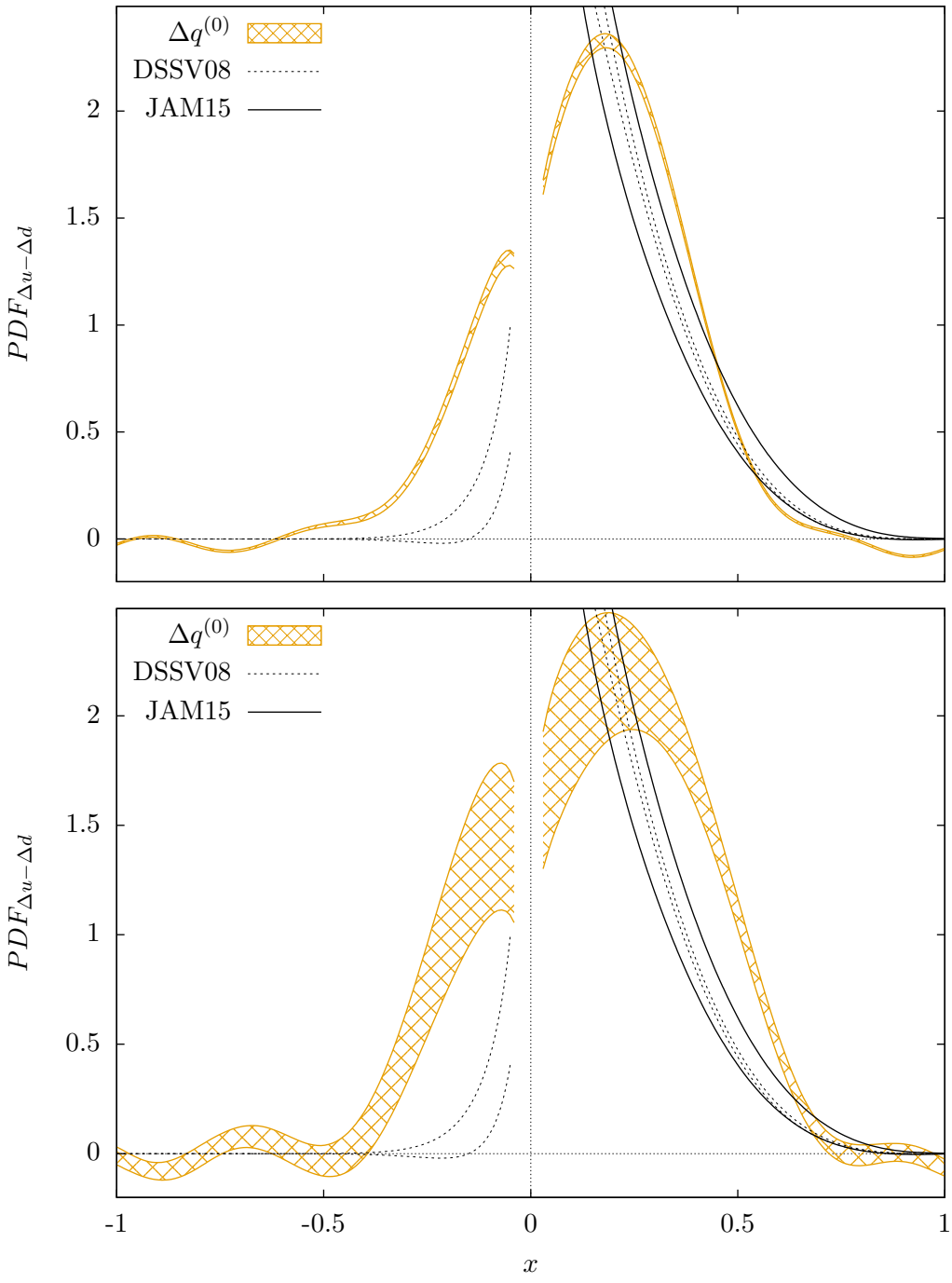

Figure 5.11: Results for the polarized distributions from a hypothetical mixed momentum analysis using different values of the momentum in the computation of the lattice form factors (**top**: $P_3 = {}^{4\pi}/_{L}$, **bottom**: $P_3 = {}^{6\pi}/_{L}$) than in the Fourier transformation, matching and mass corrections ($P_3 = {}^{8\pi}/_{L}$) with 5 steps of HYP smearing.

The results for both the polarized and unpolarized distribution that were shown for $P_3 = {}^{4\pi}/_{L}$ and $P_3 = {}^{6\pi}/_{L}$ indicate a convergence of the lattice distribution towards the phenomenological parametrizations for larger momenta. Nevertheless, the results from the mixed momentum setup indicate that momenta above $P_3 = {}^{6\pi}/_{L}$ are certainly necessary to obtain a decent agreement with phenomenology. A significant increase of the statistics is necessary to have access to larger momenta, which might be extracted by an extrapolation of results for the smaller momenta. The feasibility and form of such an extrapolation have yet to be studied. The problem of strong deviation from the phenomenological quark distribution for small x should be addressed in the future as well. In particular, the question of in which x range the obtained distributions are actually reliable needs to be explored in more detail.

For the results presented here, the utilized gauge ensemble exhibits an unphysical large quark mass, which certainly affects the momentum and spin structure of the nucleon. This potential bias should be excluded by repeating the calculation on the newly acquired gauge ensemble featuring a physical value of the pion mass [61]. In addition, the calculation of the PDF from lattice ensembles with different lattice spacing and extension will certainly provide information on the influence on systematic cut-off and finite-size effects.

Potential extensions of this model have been proposed in Ref. [28] and include for example the computation of the transverse PDF, the gluon PDF and other generalized parton distributions (GPDs). In principle, the computation of the pion PDF seems feasible, too. Yet, a significant amount of work has to be invested into further understanding the method before these challenges can be approached.

To sum up, I successfully demonstrated that it is feasible in principle to extract quark distribution functions from lattice QCD. Certainly, a lot of effort has to be invested into this topic in the future before reliable distributions with realistic systematic uncertainties can be shown. Nevertheless, I have presented promising results for the lattice distributions that might encourage other groups to conquer this new and exciting approach in order to unravel the structure of hadrons from first principle QCD calculations.

6. Summary

In this thesis, I have presented two different studies dealing with aspects of hadron structure calculations from lattice QCD with a special focus on the spin and momentum structure of quarks and gluons in the nucleon. To be more precise, this involves the computation of the gluons' average momentum fraction as well as a direct calculation of the iso-vector momentum and spin distributions of quarks in the nucleon. Up to now, both topics have rarely been studied in the context of lattice QCD, because the associated calculations are either rather cumbersome or conceptually not clear. The aim of this work was to investigate whether such computations are feasible and if significant results can be extracted from lattice QCD computations. This included studying the practicability of available methods and exploring new ideas as well as giving a first estimate for the resulting quantities. A precise study of all systematic uncertainties is beyond the scope of this thesis and has to be subject of future research.

In the first study, I have explored the lattice QCD calculation of gluons' average momentum fraction in the nucleon, which can be interpreted as the first moment of the gluon momentum distribution. This quantity is difficult to study, because only disconnected diagrams contribute to the result and consequently strong gauge field fluctuations induce a poor noise-to-signal ratio. Thus, the main goal for this quantity was to show if a meaningful signal for the necessary form factor can be extracted from recent lattice gauge ensembles featuring dynamical fermions with intermediate to small quark masses, *i.e.* pion masses from 370 MeV to a physical value of 130 MeV.

For this purpose, two different methods were tested which potentially can be used to compute the gluon momentum fraction $\langle x \rangle_g$. In this context, I was able to utilize the Feynman-Hellmann theorem to compute $\langle x \rangle_g$, although only on a rather small lattice with a large quark mass. The feasibility of this method for modern gauge ensembles with a large volume and physical pion masses seems rather unlikely, since the generation of additional sets of gauge field configurations, including the tuning to a maximal twist, is too costly. For the second method, $\langle x \rangle_g$ was extracted from a ratio of a three- and a two-point function, which can be straightforwardly computed on the lattice, yet yields a noisy signal when using the original unaltered gauge field configurations. I was able to show that the large statistical uncertainty of the obtained results can be significantly reduced when applying stout smearing

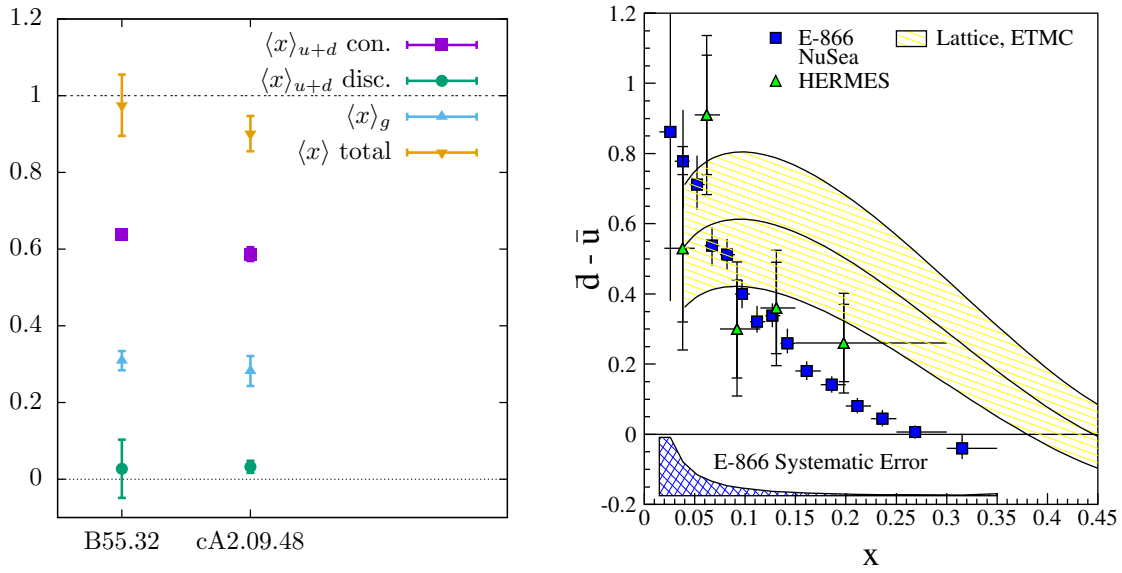

Figure 6.1: Left: lattice results for $\langle x\rangle$ of light quarks, gluons and the resulting total momentum fraction, heavy quarks are not considered. For the quark momentum fraction connected [23] and disconnected [57, 82] contributions are shown. **Right:** comparison of the lattice data for $\bar{d}-\bar{u}$ with experimental data from the E-866 NuSea experiment [83, 84] and the HERMES experiment [85]. Plot provided by Ref. [86].

to the gauge links in the operator. Using the latter method, I was able to give a very first estimate of $\langle x\rangle_g$ on two gauge ensembles with dynamical fermions, one of them featuring a physical value of the quark mass. These lattice values could be related to their physical counterparts by a recently performed one-loop perturbative calculation using an appropriately defined renormalization scheme. All results are shown in Tab. 4.2 with only statistical uncertainties included. Most of the systematic uncertainties, including a continuum limit analysis, have yet to be addressed in follow-up works. Nevertheless, I was able to successfully show that it is possible in principle to access the gluon's momentum fraction using the lattice discretization of QCD. Moreover, the obtained results are in consistency with ETMC lattice results for the quark momentum fraction, *i.e.* the momentum sum rule (4.2) is satisfied within the given uncertainties. A graphical representation of this sum rule is shown on the left-hand side of of Fig. 6.1.

The gluon's average momentum fraction can be identified with the $A^g_{20}(0)$ form factor, which contributes to the total angular momentum of the gluons in the nucleon $J_g = \frac{1}{2}(A^g_{20}(0) + B^g_{20}(0))$. The second form factor B^g_{20} can be extracted from gluon operator matrix elements with non-zero momentum transfer q^2, a calculation that will be attempted in future studies. The total angular momentum J_g is the gluons' contribution to the nucleon spin and can currently not be measured in experiments. Therefore, the results of this work and future lattice QCD studies can provide a

valuable contribution in understanding the structure of the nucleon spin.

A further future focus of research should certainly be the reduction of the still significant statistical error. This might be accomplished by studying other representations of the gluon operator or constructing an improved operator by including higher order Wilson loops. Further noise reduction techniques could be tested, for example the Wilson flow, yet a theoretical concept for its application still needs to be worked out.

The goal of the second part of my thesis was to study the momentum and spin structure of the quarks in the nucleon by directly computing the relevant quark distributions. A direct computation of these distributions from matrix elements of local operators requires light-cone dynamics which cannot be achieved within lattice QCD due to a non-zero lattice spacing. For this reason, I have tested a newly published method which proposes the computation of a spatial quasi-distribution from matrix elements of local operators and the restoration of the physical distribution in the large momentum limit by a perturbative matching and a target mass correction. The main goal of this study was to explore if the necessary matrix elements are feasible to compute within lattice QCD and to investigate whether the proposed method can be used to eventually make a direct contact to the physical quark distributions.

In this context, I have computed the necessary nucleon form factors for three different on-axis momenta and found that a stochastic estimation of the involved all-to-all propagator is preferable in this setup. It allows a greater flexibility concerning the choice of the nucleon momenta, because no additional quark propagator calculations are necessary. I have applied several steps of HYP gauge link smearing to the operator and studied the effect on the resulting form factors and consequently on the quasi-distribution. In this context, the smearing has been used as a tool to investigate the effect of renormalization, since it is supposed to alter the operator renormalization. To be more precise, higher levels of smearing might bring the Z factors closer to a tree-level value. Ultimately, I have used a maximal number of five smearing steps to estimate the influence of renormalization on the final distribution and found a significant increase of the imaginary part of the form factors, which induces a distinct quark-antiquark asymmetry in the quark distribution. I have applied the necessary matching and target mass correction to the computed form factors and presented the resulting unpolarized distributions in Fig. 5.7. In order to study the effect of larger momenta, I have employed a mixed momentum setup and shown the results in Fig. 5.8. All obtained distributions feature a qualitative agreement with distributions obtained from phenomenology, except in the small x region, where the method is not supposed to work well due to the infrared and ultraviolet cut-offs which are present in the lattice calculation. In the mixed momentum setup, the distributions even partly feature a quantitative agreement. Furthermore, this work was able to reproduce crucial non-trivial experimental findings such as the mostly positive $\bar{d}(x) - \bar{u}(x)$ distribution, as can be seen on the right-hand side of Fig. 6.1. In this plot, the lattice result of the $\bar{d}(x) - \bar{u}(x)$ distribution is compared to two

different experimental measurements of this quantity. Although there is no perfect quantitative agreement with these measurements, particularly with the very precise NuSea experiment, the lattice results are able to reproduce the qualitative behavior of the experiments.

I was able to compute first results for the polarized quark distributions, which are shown in Fig. 5.10 and Fig. 5.11 for the mixed momentum setup. For both, a qualitative agreement with phenomenological distributions was found as well. All in all, at least a qualitative agreement with phenomenological predictions could be achieved in all cases, which is a key result of this thesis.

In order to make reliable predictions for the quark distribution within the nucleon there are certainly more tasks that have to be tackled in the future. This includes, among other things, the ideally non-perturbative renormalization of all the form factors and the computation of the quark distribution at a physical value of the pion mass. Nevertheless, it was successfully shown in this thesis that lattice QCD is a capable tool to explore the momentum and spin structure of the quarks and the gluons in the nucleon. Eventually, lattice QCD might be able to venture even further and predict quantities like the transversity distribution or generalized parton distributions.

Altogether, both works discussed in this thesis successfully studied the feasibility of the lattice calculation of two important hadron structure quantities. I tested various methods, applied new ideas and presented exciting results for the involved quantities. Hopefully, these findings will encourage more groups to participate in future efforts to precisely calculate these observables and overcome the challenges that are still present.

Acknowledgements

This thesis is dedicated to my father Friedrich who passed away in December 2014. Despite struggling with a serious illness, he was constantly interested in my work and always one of my strongest supporters. He would have loved to see this thesis completed. I would like to thank my mother Carola and my sister Manuela for standing by my side in these hard times and for being such an amazing family. I also feel incredibly lucky to have a person like Ann-Kathrin, who understands and supports me like no one else, being my companion for over 10 years.

I am grateful to have a supervisor like Karl Jansen, who made this work possible by providing the necessary coordination and resources and being a constant source of precious advice. Moreover, I will of course always remember our Jazz jam sessions and playing together in the band. It was a pleasure to work at DESY in Zeuthen and to meet so many nice colleagues and friends during my time here. They always provided helpful advice, a very pleasant working atmosphere and most of all the necessary diversion from physics. Here, I would like to particularly mention Julia, Attila, Bartek, Elena, Arnd, Felix and Grit.

I would like to give credit to all of my collaborators who contributed to this thesis. In particular, Fernanda Steffens provided great help with her broad knowledge on phenomenology and hadron structure. Moreover, I would like to thank Constantia Alexandrou, Krzysztof Cichy, Martha Constantinou, Simon Dinter, Vincent Drach, Kyriakos Hadjiyiannakou and Giancarlo Rossi for sharing their knowledge with me. I will not forget the countless discussions with everyone, including my colleagues from DESY. Furthermore, I am very thankful that Ulli Wolff agreed on being the formal supervisor for this thesis.

This research was conducted in cooperation with the ETM collaboration which provided the necessary gauge configuration, useful programs and crucial knowledge, thus contributing greatly to the achievements of this thesis. I appreciate the supply of computing resources and support by the John von Neumann Institute for Computing (NIC), the Jülich Supercomputing Center and the DESY Zeuthen Computing Center. This work has been supported in part by the DFG Sonderforschungsbereich/Transregio SFB/TR9-03.

Finally, I would like to pay respect to my dearest mentor and colleague Michael Müller-Preußker, who passed away this fall. I will always remember him as an outstanding scientist and kind-hearted person.

A. Kinematic Factors

The spectral decomposition of the ratio of a three- and a two-point function is given in Eq. (3.49) and can be written using Eq. (3.52) as

$$R_\Gamma\big(N(P);\mathcal{O};N(P)\big) = \frac{\mathrm{Tr}(\Gamma(\not{P}_0+m)\mathcal{O}_{00}(\not{P}_0+m))}{2E\,\mathrm{Tr}(\Gamma(\not{P}_0+m))}\,. \tag{A.1}$$

For the calculation of quark distributions on the lattice, one employs the operator given in Eq. (5.9). The corresponding decomposition of the matrix elements is given in Eq. (5.6). Consequently, one obtains the following relation, where the Euclidean notation is used

$$R_\Gamma\big(N(P);\mathcal{O}(z);N(P)\big) = \frac{\mathrm{Tr}(\Gamma(-i\not{P}+m)\gamma_j h(P_j,z)(-i\not{P}+m))}{2E\,\mathrm{Tr}(\Gamma(-i\not{P}+m))}\,, \tag{A.2}$$

where for matters of convenience the ground state momentum is simply denoted by P. The spatial index j is kept general to account for all possible cases. The parity projector $\Gamma_+ = (1+\gamma_4)/2$ is used for the calculation of the unpolarized quark distribution.

A few trace identities are useful for the following calculation

$$\mathrm{Tr}(\gamma_\mu) = 0 \;\text{ (holds for any odd number of gammas)} \tag{A.3}$$
$$\mathrm{Tr}(\gamma_\mu\gamma_\nu) = 4\delta_{\mu\nu} \tag{A.4}$$
$$\mathrm{Tr}(\gamma_\mu\gamma_\nu\gamma_\rho\gamma_\sigma) = 4(\delta_{\mu\nu}\delta_{\rho\sigma} - \delta_{\mu\rho}\delta_{\nu\sigma} + \delta_{\mu\sigma}\delta_{\nu\rho})\,. \tag{A.5}$$

The following relation between energy and Euclidean momentum will be used as well

$$P_4 = iE\,. \tag{A.6}$$

The trace algebra for the two-point function can be performed and yields

$$\begin{aligned}
&\mathrm{Tr}\left(\frac{1+\gamma_4}{2}(-i\not{P}+m)\right)\\
&\quad=\frac{1}{2}\mathrm{Tr}(-iP_\mu\gamma_\mu+m-iP_\mu\gamma_\mu\gamma_4+m\gamma_4)\\
&\quad=\frac{1}{2}\left(\underbrace{\mathrm{Tr}(-iP_\mu\gamma_\mu)}_{=0}+\mathrm{Tr}(m)+\mathrm{Tr}(-iP_\mu\gamma_\mu\gamma_4)+\underbrace{\mathrm{Tr}(m\gamma_4)}_{=0}\right)\\
&\quad=2m-2iP_\mu\delta_{\mu4}\\
&\quad=2(m+E)\,.
\end{aligned}\tag{A.7}$$

For the three-point function one finds

$$\begin{aligned}
&\mathrm{Tr}\left(\frac{1+\gamma_4}{2}(-i\not{P}+m)\gamma_j h(P_j,z)(-i\not{P}+m)\right)\\
&\quad=\frac{h(P_j,z)}{2}\mathrm{Tr}\left((1+\gamma_4)(-P_\mu\gamma_\mu\gamma_jP_\nu\gamma_\nu-iP_\mu\gamma_\mu\gamma_jm-im\gamma_jP_\mu\gamma_\mu+\gamma_jm^2)\right)\\
&\quad=\frac{h(P_j,z)}{2}\mathrm{Tr}(-P_\mu\gamma_\mu\gamma_jP_\nu\gamma_\nu-iP_\mu\gamma_\mu\gamma_jm-im\gamma_jP_\mu\gamma_\mu+\gamma_jm^2\\
&\qquad-\gamma_4P_\mu\gamma_\mu\gamma_jP_\nu\gamma_\nu-i\gamma_4P_\mu\gamma_\mu\gamma_jm-im\gamma_4\gamma_jP_\mu\gamma_\mu+\gamma_4\gamma_jm^2)\\
&\quad=\frac{h(P_j,z)}{2}\left(\underbrace{\mathrm{Tr}(-P_\mu\gamma_\mu\gamma_jP_\nu\gamma_\nu)}_{=0}-\mathrm{Tr}(iP_\mu\gamma_\mu\gamma_jm)-\mathrm{Tr}(im\gamma_jP_\mu\gamma_\mu)+\underbrace{\mathrm{Tr}(\gamma_jm^2)}_{=0}\right.\\
&\qquad\left.+\mathrm{Tr}(-\gamma_4P_\mu\gamma_\mu\gamma_jP_\nu\gamma_\nu)-\underbrace{\mathrm{Tr}(i\gamma_4P_\mu\gamma_\mu\gamma_jm)}_{=0}-\underbrace{\mathrm{Tr}(im\gamma_4\gamma_jP_\mu\gamma_\mu)}_{=0}+\mathrm{Tr}(\gamma_4\gamma_jm^2)\right)\\
&\quad=\frac{h(P_j,z)}{2}\left(-4iP_\mu m\delta_{\mu j}-4imP_\mu\delta_{j\mu}\right.\\
&\qquad\left.-4P_\mu P_\nu(\delta_{4\mu}\delta_{j\nu}-\delta_{4j}\delta_{\mu\nu}+\delta_{4\nu}\delta_{\mu j})+\underbrace{4m^2\delta_{4j}}_{=0}\right)\\
&\quad=\frac{h(P_j,z)}{2}(-8iP_jm-8P_jP_4)\\
&\quad=-i4P_j(E+m)h(P_j,z)\,.
\end{aligned}\tag{A.8}$$

Combining Eqs. (A.2), (A.7) and (A.8) yields the final result

$$R_{\Gamma_+}\big(N(P);\mathcal{O}(z);N(P)\big)=-i\frac{P_j}{E}h(P_j,z)\,.\tag{A.9}$$

B. Wave function and vertex corrections for PDFs

The wave function and vertex corrections in Eq. (5.3) were calculated in Ref. [70]. The vertex corrections are given by

$$\frac{Z^{(1)}(\xi)}{C_F} = \begin{cases} \dfrac{1+\xi^2}{1-\xi}\ln\dfrac{\xi}{\xi-1} + 1 + \dfrac{1}{(1-\xi)^2}\dfrac{\Lambda}{P_3} & (\xi > 1) \\ \dfrac{1+\xi^2}{1-\xi}\ln\dfrac{(P_3)^2}{\mu_R^2} + \dfrac{1+\xi^2}{1-\xi}\ln 4\xi(1-\xi) & \\ \quad -\dfrac{2\xi}{1-\xi} + 1 + \dfrac{1}{(1-\xi)^2}\dfrac{\Lambda}{P_3} & (0 < \xi < 1) \\ \dfrac{1+\xi^2}{1-\xi}\ln\dfrac{\xi-1}{\xi} - 1 + \dfrac{1}{(1-\xi)^2}\dfrac{\Lambda}{P_3} & (\xi < 0)\,. \end{cases} \tag{B.1}$$

The wave function corrections are given by

$$\delta Z^{(1)} = C_F \int_{-\infty}^{\infty} d\xi\, \delta Z^{(1)}(\xi)\,, \tag{B.2}$$

where

$$\delta Z^{(1)}(\xi) = \begin{cases} -\dfrac{1+\xi^2}{1-\xi}\ln\dfrac{\xi}{\xi-1} - 1 - \dfrac{1}{(1-\xi)^2}\dfrac{\Lambda}{P_3} & (\xi > 1) \\ -\dfrac{1+\xi^2}{1-\xi}\ln\dfrac{(P_3)^2}{\mu_R^2} - \dfrac{1+\xi^2}{1-\xi}\ln 4\xi(1-\xi) & \\ \quad +\dfrac{2\xi(2\xi-1)}{1-\xi} + 1 - \dfrac{1}{(1-\xi)^2}\dfrac{\Lambda}{P_3} & (0 < \xi < 1) \\ -\dfrac{1+\xi^2}{1-\xi}\ln\dfrac{\xi-1}{\xi} + 1 - \dfrac{1}{(1-\xi)^2}\dfrac{\Lambda}{P_3} & (\xi < 0)\,. \end{cases} \tag{B.3}$$

For the polarized PDF the vertex corrections are given by

$$\frac{Z^{(1)}(\xi)}{C_F} = \begin{cases} \dfrac{1+\xi^2}{1-\xi}\ln\dfrac{\xi}{\xi-1} + 1 + \dfrac{1}{(1-\xi)^2}\dfrac{\Lambda}{P_3} & (\xi > 1) \\ \dfrac{1+\xi^2}{1-\xi}\ln\dfrac{(P_3)^2}{\mu_R^2} + \dfrac{1+\xi^2}{1-\xi}\ln 4\xi(1-\xi) & \\ \quad -\dfrac{2}{1-\xi} + 3 + \dfrac{1}{(1-\xi)^2}\dfrac{\Lambda}{P_3} & (0 < \xi < 1) \\ \dfrac{1+\xi^2}{1-\xi}\ln\dfrac{\xi-1}{\xi} - 1 + \dfrac{1}{(1-\xi)^2}\dfrac{\Lambda}{P_3} & (\xi < 0)\,. \end{cases} \tag{B.4}$$

The self-energy correction is identical to the unpolarized case.

Bibliography

[1] E. E. Chambers and R. Hofstadter, "Structure of the Proton," *Phys. Rev.* **103** (1956) 1454–1463.

[2] M. Gell-Mann, "A Schematic Model of Baryons and Mesons," *Phys. Lett.* **8** (1964) 214–215.

[3] G. Zweig, "An SU_3 model for strong interaction symmetry and its breaking; Version 2,". `http://cds.cern.ch/record/570209`. Version 1 is CERN preprint 8182/TH.401, Jan. 17, 1964.

[4] M. Breidenbach, J. I. Friedman, H. W. Kendall, E. D. Bloom, D. Coward, *et al.*, "Observed Behavior of Highly Inelastic electron-Proton Scattering," *Phys.Rev.Lett.* **23** (1969) 935–939.

[5] E. D. Bloom, D. Coward, H. DeStaebler, J. Drees, G. Miller, *et al.*, "High-Energy Inelastic e p Scattering at 6-Degrees and 10-Degrees," *Phys.Rev.Lett.* **23** (1969) 930–934.

[6] H. W. Kendall, "Deep inelastic scattering: Experiments on the proton and the observation," *Rev. Mod. Phys.* **63** (1991) 597–614.

[7] J. Bjorken and E. A. Paschos, "Inelastic Electron Proton and gamma Proton Scattering, and the Structure of the Nucleon," *Phys.Rev.* **185** (1969) 1975–1982.

[8] R. P. Feynman, "Very high-energy collisions of hadrons," *Phys.Rev.Lett.* **23** (1969) 1415–1417.

[9] L. D. Faddeev and V. N. Popov, "Feynman Diagrams for the Yang-Mills Field," *Phys. Lett.* **B25** (1967) 29–30.

[10] H. Fritzsch, M. Gell-Mann, and H. Leutwyler, "Advantages of the Color Octet Gluon Picture," *Phys. Lett.* **B47** (1973) 365–368.

[11] G. 't Hooft, "Renormalization of Massless Yang-Mills Fields," *Nucl. Phys.* **B33** (1971) 173–199.

[12] D. J. Gross and F. Wilczek, "Ultraviolet Behavior of Nonabelian Gauge Theories," *Phys. Rev. Lett.* **30** (1973) 1343–1346.

[13] H. D. Politzer, "Reliable Perturbative Results for Strong Interactions?," *Phys. Rev. Lett.* **30** (1973) 1346–1349.

[14] K. G. Wilson, "Nonlagrangian models of current algebra," *Phys. Rev.* **179** (1969) 1499–1512.

[15] D. Müller, D. Robaschik, B. Geyer, F. M. Dittes, and J. Hořejši, "Wave functions, evolution equations and evolution kernels from light ray operators of QCD," *Fortsch. Phys.* **42** (1994) 101–141, arXiv:hep-ph/9812448 [hep-ph].

[16] X.-D. Ji, "Off forward parton distributions," *J. Phys.* **G24** (1998) 1181–1205, arXiv:hep-ph/9807358 [hep-ph].

[17] A. Martin, W. Stirling, R. Thorne, and G. Watt, "Parton distributions for the LHC," *Eur.Phys.J.* **C63** (2009) 189–285, arXiv:0901.0002 [hep-ph].

[18] J. Owens, A. Accardi, and W. Melnitchouk, "Global parton distributions with nuclear and finite-Q^2 corrections," *Phys.Rev.* **D87** no. 9, (2013) 094012, arXiv:1212.1702 [hep-ph].

[19] S. Alekhin, J. Blümlein, and S. Moch, "The ABM parton distributions tuned to LHC data," *Phys. Rev.* **D89** no. 5, (2014) 054028, arXiv:1310.3059 [hep-ph].

[20] D. de Florian, R. Sassot, M. Stratmann, and W. Vogelsang, "Extraction of Spin-Dependent Parton Densities and Their Uncertainties," *Phys. Rev.* **D80** (2009) 034030, arXiv:0904.3821 [hep-ph].

[21] K. G. Wilson, "Confinement of Quarks," *Phys. Rev.* **D10** (1974) 2445–2459.

[22] P. Hägler, "Hadron structure from lattice quantum chromodynamics," *Phys.Rept.* **490** (2010) 49–175, arXiv:0912.5483 [hep-lat].

[23] A. Abdel-Rehim *et al.*, "Nucleon and pion structure with lattice QCD simulations at physical value of the pion mass," *Phys. Rev.* **D92** no. 11, (2015) 114513, arXiv:1507.04936 [hep-lat].

[24] **European Muon** Collaboration, J. Ashman *et al.*, "An Investigation of the Spin Structure of the Proton in Deep Inelastic Scattering of Polarized Muons on Polarized Protons," *Nucl. Phys.* **B328** (1989) 1.

[25] M. Göckeler, R. Horsley, E.-M. Ilgenfritz, H. Oelrich, H. Perlt, P. E. L. Rakow, G. Schierholz, A. Schiller, and P. Stephenson, "A Preliminary lattice study of the glue in the nucleon," *Nucl. Phys. Proc. Suppl.* **53** (1997) 324–326, arXiv:hep-lat/9608017 [hep-lat].

[26] **QCDSF, UKQCD** Collaboration, R. Horsley *et al.*, "A Lattice Study of the Glue in the Nucleon," *Phys.Lett.* **B714** (2012) 312–316, arXiv:1205.6410 [hep-lat].

[27] M. Deka *et al.*, "Lattice study of quark and glue momenta and angular momenta in the nucleon," *Phys. Rev.* **D91** no. 1, (2015) 014505, arXiv:1312.4816 [hep-lat].

[28] X. Ji, "Parton Physics on a Euclidean Lattice," *Phys.Rev.Lett.* **110** (2013) 262002, arXiv:1305.1539 [hep-ph].

[29] H.-W. Lin, J.-W. Chen, S. D. Cohen, and X. Ji, "Flavor Structure of the Nucleon Sea from Lattice QCD," *Phys. Rev.* **D91** (2015) 054510, arXiv:1402.1462 [hep-ph].

[30] M. E. Peskin and D. V. Schroeder, *An introduction to quantum field theory*. Advanced book program. Westview Press, Boulder CO, 1995.

[31] R. Devenish and A. Cooper-Sarkar, *Deep Inelastic Scattering*. Oxford University Press, Oxford, 2004.

[32] C. Akerlof, R. Hieber, A. Krisch, K. Edwards, L. Ratner, *et al.*, "Elastic Proton-Proton Scattering at 90-degrees and Structure within the Proton," *Phys.Rev.* **159** (1967) 1138–1149.

[33] C. Gattringer and C. Lang, *Quantum Chromodynamics on the Lattice*, vol. 788 of *Lecture Notes in Physics*. Springer-Verlag, Berlin Heidelberg, 2010.

[34] H. J. Rothe, *Lattice gauge theories: an introduction*, vol. 74 of *World Scientific Lecture Notes in Physics*. World Scientific, Singapore, 4th ed., 2012.

[35] Y. Iwasaki, "Renormalization Group Analysis of Lattice Theories and Improved Lattice Action. II. Four-dimensional non-Abelian SU(N) gauge model," arXiv:1111.7054 [hep-lat].

[36] A. Hasenfratz and P. Hasenfratz, "Monte Carlo Simulation Combined With a Hopping Parameter Expansion," *Phys. Lett.* **B104** (1981) 489.

[37] R. Frezzotti and G. Rossi, "Chirally improving Wilson fermions. 1. O(a) improvement," *JHEP* **0408** (2004) 007, arXiv:hep-lat/0306014 [hep-lat].

[38] T. Chiarappa, F. Farchioni, K. Jansen, I. Montvay, E. E. Scholz, L. Scorzato, T. Sudmann, and C. Urbach, "Numerical simulation of QCD with u, d, s and c quarks in the twisted-mass Wilson formulation," *Eur. Phys. J.* **C50** (2007) 373–383, arXiv:hep-lat/0606011 [hep-lat].

[39] C. Urbach, K. Jansen, A. Shindler, and U. Wenger, "HMC algorithm with multiple time scale integration and mass preconditioning," *Comput. Phys. Commun.* **174** (2006) 87–98, arXiv:hep-lat/0506011 [hep-lat].

[40] **ETM Collaboration** Collaboration, C. Alexandrou *et al.*, "Axial Nucleon form factors from lattice QCD," *Phys.Rev.* **D83** (2011) 045010, arXiv:1012.0857 [hep-lat].

[41] C. Alexandrou, M. Constantinou, S. Dinter, V. Drach, K. Jansen, *et al.*, "Nucleon form factors and moments of generalized parton distributions using $N_f = 2 + 1 + 1$ twisted mass fermions," *Phys.Rev.* **D88** no. 1, (2013) 014509, arXiv:1303.5979 [hep-lat].

[42] G. S. Bali, S. Collins, B. Glässle, M. Göckeler, J. Najjar, R. H. Rödl, A. Schäfer, R. W. Schiel, W. Söldner, and A. Sternbeck, "Nucleon isovector couplings from $N_f = 2$ lattice QCD," *Phys. Rev.* **D91** no. 5, (2015) 054501, arXiv:1412.7336 [hep-lat].

[43] T. Bhattacharya, S. D. Cohen, R. Gupta, A. Joseph, H.-W. Lin, *et al.*, "Nucleon Charges and Electromagnetic Form Factors from 2+1+1-Flavor Lattice QCD," *Phys.Rev.* **D89** no. 9, (2014) 094502, arXiv:1306.5435 [hep-lat].

[44] **LHPC** Collaboration, J. D. Bratt *et al.*, "Nucleon structure from mixed action calculations using 2+1 flavors of asqtad sea and domain wall valence fermions," *Phys. Rev.* **D82** (2010) 094502, arXiv:1001.3620 [hep-lat].

[45] J. R. Green, M. Engelhardt, S. Krieg, J. W. Negele, A. V. Pochinsky, and S. N. Syritsyn, "Nucleon Structure from Lattice QCD Using a Nearly Physical Pion Mass," *Phys. Lett.* **B734** (2014) 290–295, arXiv:1209.1687 [hep-lat].

[46] **Particle Data Group** Collaboration, K. A. Olive *et al.*, "Review of Particle Physics," *Chin. Phys.* **C38** (2014) 090001.

[47] Y. Aoki, T. Blum, H.-W. Lin, S. Ohta, S. Sasaki, R. Tweedie, J. Zanotti, and T. Yamazaki, "Nucleon isovector structure functions in (2+1)-flavor QCD with domain wall fermions," *Phys. Rev.* **D82** (2010) 014501, arXiv:1003.3387 [hep-lat].

[48] **QCDSF/UKQCD** Collaboration, D. Pleiter *et al.*, "Nucleon form factors and structure functions from N(f)=2 Clover fermions," *PoS* **LATTICE2010** (2010) 153, arXiv:1101.2326 [hep-lat].

[49] G. S. Bali, S. Collins, M. Deka, B. Glassle, M. Göckeler, J. Najjar, A. Nobile, D. Pleiter, A. Schafer, and A. Sternbeck, "$\langle x \rangle_{u-d}$ from lattice QCD at nearly physical quark masses," *Phys. Rev.* **D86** (2012) 054504, arXiv:1207.1110 [hep-lat].

[50] S. Alekhin, J. Blümlein, and S. Moch, "Parton Distribution Functions and Benchmark Cross Sections at NNLO," *Phys.Rev.* **D86** (2012) 054009, arXiv:1202.2281 [hep-ph].

[51] J. Blümlein and H. Böttcher, "QCD Analysis of Polarized Deep Inelastic Scattering Data," *Nucl. Phys.* **B841** (2010) 205–230, arXiv:1005.3113 [hep-ph].

[52] X.-D. Ji, "Gauge-Invariant Decomposition of Nucleon Spin," *Phys. Rev. Lett.* **78** (1997) 610–613, arXiv:hep-ph/9603249 [hep-ph].

[53] X.-D. Ji, "A QCD analysis of the mass structure of the nucleon," *Phys.Rev.Lett.* **74** (1995) 1071–1074, arXiv:hep-ph/9410274 [hep-ph].

[54] R. P. Feynman, "Forces in molecules," *Phys. Rev.* **56** (Aug, 1939) 340–343. http://link.aps.org/doi/10.1103/PhysRev.56.340.

[55] J. Shigemitsu, "Spectrum calculations in lattice gauge theory using wilson's fermion method," *Phys. Rev. D* **18** (Sep, 1978) 1709–1718. http://link.aps.org/doi/10.1103/PhysRevD.18.1709.

[56] S. Gusken, K. Schilling, R. Sommer, K. H. Mutter, and A. Patel, "Mass Splittings in the Baryon Octet and the Nucleon σ Term in Lattice QCD," *Phys. Lett.* **B212** (1988) 216.

[57] A. Abdel-Rehim, C. Alexandrou, M. Constantinou, V. Drach, K. Hadjiyiannakou, *et al.*, "Disconnected quark loop contributions to nucleon observables in lattice QCD," *Phys.Rev.* **D89** no. 3, (2014) 034501, arXiv:1310.6339 [hep-lat].

[58] **European Twisted Mass** Collaboration, V. Drach, K. Jansen, J. Carbonell, M. Papinutto, and C. Alexandrou, "Low lying baryon spectrum with $N_f = 2 + 1 + 1$ dynamical twisted quarks," *PoS* **LATTICE2010** (2010) 101, arXiv:1012.3861 [hep-lat].

[59] R. Baron, P. Boucaud, J. Carbonell, A. Deuzeman, V. Drach, *et al.*, "Light hadrons from lattice QCD with light (u,d), strange and charm dynamical quarks," *JHEP* **1006** (2010) 111, arXiv:1004.5284 [hep-lat].

[60] C. Alexandrou, V. Drach, K. Jansen, C. Kallidonis, and G. Koutsou, "Baryon spectrum with $N_f = 2 + 1 + 1$ twisted mass fermions," *Phys.Rev.* **D90** no. 7, (2014) 074501, arXiv:1406.4310 [hep-lat].

[61] **ETM** Collaboration, A. Abdel-Rehim *et al.*, "Simulating QCD at the Physical Point with $N_f = 2$ Wilson Twisted Mass Fermions at Maximal Twist," arXiv:1507.05068 [hep-lat].

[62] H. B. Meyer and J. W. Negele, "Gluon contributions to the pion mass and light cone momentum fraction," *Phys. Rev.* **D77** (2008) 037501, arXiv:0707.3225 [hep-lat].

[63] A. Hasenfratz and F. Knechtli, "Flavor symmetry and the static potential with hypercubic blocking," *Phys.Rev.* **D64** (2001) 034504, arXiv:hep-lat/0103029 [hep-lat].

[64] C. Morningstar and M. J. Peardon, "Analytic smearing of SU(3) link variables in lattice QCD," *Phys.Rev.* **D69** (2004) 054501, arXiv:hep-lat/0311018 [hep-lat].

[65] X.-D. Ji, "Breakup of hadron masses and energy - momentum tensor of QCD," *Phys. Rev.* **D52** (1995) 271–281, arXiv:hep-ph/9502213 [hep-ph].

[66] C. Alexandrou, M. Constantinou, T. Korzec, H. Panagopoulos, and F. Stylianou, "Renormalization constants for 2-twist operators in twisted mass QCD," *Phys. Rev.* **D83** (2011) 014503, arXiv:1006.1920 [hep-lat].

[67] C. Alexandrou, M. Constantinou, K. Jansen, H. Panagopoulos, and C. Wiese, "The gluon moment from twisted mass lattice QCD," **to be published** .

[68] A. Buckley, J. Ferrando, S. Lloyd, K. Nordström, B. Page, M. Rüfenacht, M. Schönherr, and G. Watt, "LHAPDF6: parton density access in the LHC precision era," *Eur. Phys. J.* **C75** no. 3, (2015) 132, arXiv:1412.7420 [hep-ph].

[69] C. Alexandrou, K. Cichy, V. Drach, E. Garcia-Ramos, K. Hadjiyiannakou, K. Jansen, F. Steffens, and C. Wiese, "Lattice calculation of parton distributions," *Phys. Rev.* **D92** no. 1, (2015) 014502, arXiv:1504.07455 [hep-lat].

[70] X. Xiong, X. Ji, J.-H. Zhang, and Y. Zhao, "One-loop matching for parton distributions: Nonsinglet case," *Phys.Rev.* **D90** no. 1, (2014) 014051, arXiv:1310.7471 [hep-ph].

[71] R. L. Jaffe, "Deep inelastic scattering with application to nuclear targets," in *Proceedings, Research Program at CEBAF I.* 1985. http://alice.cern.ch/format/showfull?sysnb=0073090.

[72] F. Steffens, M. Brown, W. Melnitchouk, and S. Sanches, "Parton distributions in the presence of target mass corrections," *Phys.Rev.* **C86** (2012) 065208, arXiv:1210.4398 [hep-ph].

[73] G. Martinelli and C. T. Sachrajda, "A Lattice Study of Nucleon Structure," *Nucl. Phys.* **B316** (1989) 355.

[74] **ETM** Collaboration, C. Alexandrou *et al.*, "A Stochastic Method for Computing Hadronic Matrix Elements," *Eur.Phys.J.* **C74** no. 1, (2014) 2692, arXiv:1302.2608 [hep-lat].

[75] S. Bernardson, P. McCarty, and C. Thron, "Monte Carlo methods for estimating linear combinations of inverse matrix entries in lattice QCD," *Comput. Phys. Commun.* **78** (1993) 256–264.

[76] S.-J. Dong and K.-F. Liu, "Stochastic estimation with Z(2) noise," *Phys. Lett.* **B328** (1994) 130–136, arXiv:hep-lat/9308015 [hep-lat].

[77] C. Alexandrou, K. Cichy, V. Drach, E. Garcia-Ramos, K. Hadjiyiannakou, *et al.*, "First results with twisted mass fermions towards the computation of parton distribution functions on the lattice," *PoS* **LATTICE2014** (2014) 135, arXiv:1411.0891 [hep-lat].

[78] C. Alexandrou, M. Constantinou, K. Cichy, K. Jansen, H. Panagopoulos, F. Steffens, and C. Wiese, "Unpolarized and polarized parton distributions from lattice QCD," **to be published** .

[79] C. Alexandrou, V. Drach, K. Hadjiyiannakou, K. Jansen, B. Kostrzewa, *et al.*, "Looking at the gluon moment of the nucleon with dynamical twisted mass fermions," *PoS* **LATTICE2013** (2014) 289, arXiv:1311.3174 [hep-lat].

[80] **Particle Data Group** Collaboration, K. A. Olive *et al.*, "Review of Particle Physics," *Chin. Phys.* **C38** (2014) 090001. In the review about structure functions.

[81] P. Jimenez-Delgado, A. Accardi, and W. Melnitchouk **to be published** .

[82] M. Constantinou. Private communication.

[83] **FNAL E866/NuSea** Collaboration, R. S. Towell *et al.*, "Improved measurement of the anti-d/anti-u asymmetry in the nucleon sea," *Phys. Rev.* **D64** (2001) 052002, `hep-ex/0103030`.

[84] **Fermilab E866/NuSea** Collaboration, E. A. Hawker *et al.*, "Measurement of the light antiquark flavor asymmetry in the nucleon sea," *Phys. Rev. Lett.* **80** (Apr, 1998) 3715–3718.

[85] **HERMES** Collaboration, K. Ackerstaff *et al.*, "Flavor asymmetry of the light quark sea from semi-inclusive deep-inelastic scattering," *Phys. Rev. Lett.* **81** (Dec, 1998) 5519–5523. `http://link.aps.org/doi/10.1103/PhysRevLett.81.5519`.

[86] P. Reimer. Kindly provided by the author.